The influence of point defects on TiO_2(110) surface properties

A scanning tunneling microscopy study

JESPER MATTHIESEN

Interdisciplinary Nanoscience Center (iNANO) and
Department of Physics and Astronomy
University of Aarhus, Denmark

PhD thesis
August 2007

This thesis has been submitted to the Faculty of Science at the University of Aarhus in order to fulfil the requirements for obtaining a PhD degree in physics and nanoscience. The work has been carried out under the supervision of Professor Flemming Besenbacher at the Interdisciplinary Nanoscience Center (iNANO) and the Department of Physics and Astronomy from August 2003 to August 2007.

Printed by the Reprocenter at the Faculty of Science, University of Aarhus, Denmark, 2007.

—

This document was typeset in LaTeX by the author.
2^{nd} version with minor corrections.

Contents

List of publications **vii**

List of abbreviations **ix**

1 Motivation for studying titanium dioxide surfaces **1**
1.1 Metal oxides . . . 2
1.1.1 Applications of TiO_2 . . . 2
1.1.2 What can we learn from STM studies of TiO_2 surfaces . . . 4
1.2 Outline . . . 4

2 Experimental setup and density functional theory basics **5**
2.1 The UHV chamber . . . 6
2.2 Scanning tunneling microscopy . . . 6
2.2.1 Theory of STM . . . 7
2.2.2 The Aarhus STM . . . 9
2.2.3 Parameters for imaging TiO_2(110) with STM . . . 10
2.3 Density functional theory . . . 10
2.3.1 Basic equations used in DFT . . . 11

3 Selected results of the surface science of rutile TiO_2(110) **13**
3.1 Rutile titanium dioxide . . . 14
3.1.1 Bulk rutile TiO_2 . . . 14
3.2 The TiO_2(110) surface . . . 16
3.2.1 Point defects on TiO_2(110) surfaces . . . 17
3.3 Water adsorption on TiO_2(110) surfaces . . . 19
3.3.1 Molecular vs. dissociative adsorption . . . 19
3.3.2 Water diffusion on TiO_2(110) surfaces . . . 20
3.4 CO oxidation catalyzed by supported gold nanoclusters . . . 21
3.4.1 Size effect . . . 22
3.4.2 Effect of choice of support . . . 22
3.4.3 The effect of oxidized gold . . . 22

4 Oxygen vacancies on TiO_2(110) and their interaction with O_2 and H_2O 23
4.1 Introduction . . . 24
4.2 Results . . . 25
4.2.1 Preparation of TiO_2(110) surfaces using various approaches . . 25
4.2.2 Water as a probe molecule . . . 27
4.2.3 Stability of Type-A defects against voltage pulses . . . 29
4.2.4 Tip-related contrast changes . . . 30
4.2.5 Oxygen as a probe molecule . . . 31
4.2.6 DFT calculations . . . 32
4.3 Discussion . . . 35
4.3.1 Identification of the various point defects on TiO_2(110)-(1×1) . 35
4.3.2 Comparison with literature . . . 39
4.4 Conclusion and outlook . . . 42

5 Dynamics of water dissociation on TiO_2(110) 45
5.1 Introduction . . . 46
5.1.1 Experimental and DFT details . . . 46
5.2 STM results . . . 46
5.3 DFT calculations . . . 50
5.4 Conclusions . . . 53

6 Creation and reactions of water dimers on TiO_2(110) surfaces 55
6.1 Introduction . . . 56
6.2 Results and discussion . . . 56
6.2.1 Water dimer and trimer formation on hydroxylated TiO_2(110) surfaces . . . 56
6.2.2 Interaction of water dimers with bridging oxygen rows . . . 59
6.2.3 Comparison with DFT calculations . . . 63
6.3 Conclusions . . . 64

7 Diffusion of water monomers and dimers on TiO_2(110) surfaces 65
7.1 Introduction . . . 66
7.2 Basics of diffusion analysis . . . 66
7.2.1 Extracting diffusion parameters from STM experiments . . . 67
7.3 Results and discussion . . . 69
7.3.1 Diffusion of water monomers . . . 69
7.3.2 Anomalous water dimer diffusion on TiO_2(110) surfaces . . . 71
7.4 Conclusions . . . 76

8 Interaction of oxygen with hydroxylated TiO_2(110) surfaces 77
8.1 Introduction . . . 78
8.2 Results and discussion . . . 79
8.2.1 Initial reaction between O_2 and a bridging hydroxyl . . . 79
8.2.2 Direct observation of the initial reaction between O_2 and a bridging hydroxyl . . . 80

8.2.3 Further steps in the oxidation of hydroxylated TiO_2(110) surfaces 82
8.2.4 Forming almost stoichiometric TiO_2(110) surfaces 85
8.2.5 Energetics for forming stoichiometric TiO_2(110) surfaces . . . 87
8.3 Conclusions 89

9 Bonding of gold nanoparticles on TiO_2(110) surfaces 91
9.1 Introduction 92
9.2 Results and discussion 92
9.2.1 TiO_2(110) surface preparation and Au exposure at RT 92
9.2.2 Influence of sample temperature on Au cluster morphology . . . 94
9.2.3 DFT calculations and comparison with STM measurements . . 96
9.2.4 Charge transfer and bond mechanisms for Au clusters 100
9.3 Conclusions and implications for model studies of supported Au clusters 102

10 Summary and outlook 105

11 Dansk resumé 109

Acknowledgements 115

Bibliography 116

List of publications

[I] *Oxygen vacancies on TiO_2(110) and their interaction with H_2O and O_2: A combined high-resolution STM and DFT study*,
S. Wendt, R. Schaub, J. Matthiesen, E. K. Vestergaard, E. Wahlström, M. D. Rasmussen, P. Thostrup, L. M. Molina, E. Lægsgaard, I. Stensgaard, B. Hammer, and F. Besenbacher, Surf. Sci. **598**, 226 (2005).

[II] *Formation and Splitting of Paired Hydroxyl Groups on Reduced TiO_2(110)*,
S. Wendt, J. Matthiesen, R. Schaub, E. K. Vestergaard, E. Lægsgaard, F. Besenbacher, and B. Hammer, Phys. Rev. Lett. **96**, 066107 (2006).

[III] *Creation and reactions of water dimers on TiO_2(110) surfaces*,
J. Matthiesen, S. Wendt, R. Schaub, E. Lægsgaard, B. Hammer, and F. Besenbacher, In preparation.

[IV] *Anomalous diffusion of water dimers on TiO_2(110)*,
J. Matthiesen, R. Schaub, S. Wendt, E. Lægsgaard, F. Besenbacher, and B. Hammer, In preparation.

[V] *Mechanism for oxidation of the hydroxylated TiO_2(110) surface at the atomic scale*,
J. Matthiesen, S. Wendt, R. Schaub, E. Lægsgaard, B. Hammer, and F. Besenbacher, In preparation.

[VI] *Enhanced Bonding of Gold Nanoparticles on Oxidized TiO_2(110)*,
D. Matthey, J. G. Wang, S. Wendt, J. Matthiesen, R. Schaub, E. Lægsgaard, B. Hammer, and F. Besenbacher, Science **315**, 1692 (2007).

List of abbreviations

AFM	Atomic force microscopy
DFT	Density functional theory
EELS	Electron energy loss spectroscopy
HREELS	High-resolution electron energy loss spectroscopy
L	Langmuir (1 L = 1×10^{-6}Torr·s)
ML	Monolayer
PES	Photoelectron spectroscopy
RT	Room temperature
SPM	Scanning probe microscopy
STM	Scanning tunneling microscopy/microscope
TPD	Temperature-programmed desorption
UHV	Ultrahigh vacuum
UPS	Ultraviolet photoelectron spectroscopy
XPS	X-ray photoelectron spectroscopy

CHAPTER 1

Motivation for studying titanium dioxide surfaces

Metal oxides are a diverse and very interesting class of materials with a wide variety of properties, and for several reasons titanium dioxide (TiO_2) has become the model system of choice for surface science studies on metal oxides. First of all, TiO_2 has many current and possible future applications, and second, TiO_2 surfaces are relatively easy to prepare under ultrahigh vacuum conditions, thus making them suited for many experimental surface science techniques. This chapter will motivate a closer look at the surfaces of TiO_2 and give an outline of the thesis at hand.

1.1 Metal oxides

Metal oxides are a diverse and very interesting class of materials. They have a wide variety of properties and are therefore used in many different applications, e.g. as photocatalysts, support for metal catalysts, gas sensors and biocompatible implants [1,2]. The knowledge of oxides and their surfaces is, however, sparse compared to that of metals. Many oxides are insulators, which inhibits the use of most surface science tools. Furthermore, oxides are very complex materials that can be found in a variety of different phases and with different stoichiometries due to a range of possible oxidation states of the metal part. This makes precise characterization and structural computation much more difficult for oxides than it is the case for metals.

Some metal oxides can be made conducting by introducing defects such as oxygen vacancies or metal interstitials. These defects can be created by annealing the oxide in vacuum, which is routinely done during the preparation of single crystal samples for surface science studies. Therefore, many of the surface science tools can be applied to the reducible oxides. However, the reducibility also adds a dimension to the complexity of the experiments compared to non-reducible oxides, since the electronic structure and therefore many of the chemical and physical properties are controlled by the defect concentration.

Titanium dioxide (TiO_2) has become a model system for surface science on oxides. This is probably due to two reasons. First, TiO_2 has many technological applications, and second, TiO_2 surfaces are relatively easy to reduce and prepare under ultrahigh vacuum conditions, thus making them suited for many experimental surface science techniques.

1.1.1 Applications of TiO_2

The main reason for carrying out studies on TiO_2 stems from the many current and possible future applications and interesting properties of the material. To a very large extent it is used as a pigment in paint, food and candy due to its very high refractive index and non-toxicity, and it is the native oxide surface layer on titanium based biocompatible implants [2]. In photoelectrochemical solar cells TiO_2 nanoparticles are used to form a high surface area film on which dye molecules are adsorbed [3]. This type of solar cell has shown efficiencies above 10 $\%$ [4], and with the prospect of being able to produce this type of solar cell at a lower cost than conventional devices, it might be the solar cell of the future.

A finding that has motivated a lot of studies on TiO_2 is the work by Haruta, in which it is shown that gold nanoclusters supported on TiO_2 are very good catalysts for oxidation of CO even at temperatures below room temperature [5]. This observation is very interesting since today's three-way automobile catalyst only works at elevated temperatures. Because of the latter fact more than 50 $\%$ of the total amount of CO coming from cars is produced during the first five minutes of use while the catalyst is still cold [6].

Many surface scientists have tried to find an explanation for this peculiar behavior of gold nanoparticles on TiO_2 as compared to bulk gold, which is noble and catalytically

Figure 1.1. *Photo of part of a wall in a building in the center of Tokyo. The top part of the shown wall is coated with a self-cleaning coating, while the lower part is not. The difference in cleanliness is very obvious. Of course one has to take into account that the coating on the top part also makes this part hydrophilic, i.e. much of the dirt will simply be washed of this part and will stick on the lower part which is not hydrophilic.*

inactive [7]. Also, many workers have tried to find a solution to the problem of sintering of the nanoparticles, which leads to a dramatic decrease in reactivity [8].

As already mentioned, also the photochemical properties of TiO_2 are an area of focus. TiO_2 is a semiconductor and the electron-hole pairs created upon solar irradiation can be utilized in a number of reactions. Initial work by Fujishima and Honda in 1972 spurred a lot of interest in this area [9]. Fujishima and Honda showed that TiO_2 could be used in a photo-electrochemical cell to split water into hydrogen and oxygen by shining light on a TiO_2 electrode. The largest applied research on TiO_2 today is its use for photo-assisted degradation of organic molecules [10]. Applications utilizing this process are, for example, the purification of waste water, desinfection based on the antibactericidal properties of TiO_2, and self-cleaning coatings used for buildings in urban areas. An example showing the effect of such a self-cleaning coating on a building in Tokyo is shown in Fig. 1.1. Another property of TiO_2 utilized in the self-cleaning coating is the effect that TiO_2 surfaces become hydrophilic when irradiated with UV-light, causing much of the dirt to simply be washed of when it rains. The photo-assisted degradation and photo-induced conversion of the surface from hydrophobic to hydrophilic has also recently been utilized for making self-cleaning windows [11].

1.1.2 What can we learn from STM studies of TiO_2 surfaces

The strength of the scanning tunneling microscope (STM) is its capability to explore surfaces at the atomic level. Where many other surface science techniques acquire signals averaged over thousands of atoms or more, the STM makes us able to watch and manipulate single atoms on a surface, thus, enabling us to detect defects such as single missing oxygen atoms on the TiO_2 surface. Such defects have been presumed to, for example, form nanometer-sized hydrophilic domains on the TiO_2(110) surface after UV-radiation [12], thereby causing the TiO_2(110) surface to become hydrophilic. Oxygen vacancies on TiO_2 have also been suggested as anchor sites for active Au nanoclusters in CO oxidation catalysts. The exact morphology of these small nanoclusters, which is thought to have a large effect on the activity of the nanoclusters, is also difficult to investigate without a local probe like the STM.

An additional forte of the home-built STM used in the investigations presented in this thesis is its fast-scanning capabilities, which enables us to resolve surface processes both in space and time. Because the chemical identification is not possible from static STM images, the STM movies are very useful to compensate this drawback. By following their reactions on the surface, assigning species correctly is indeed possible. By acquiring STM movies we have examined the reactions of oxygen and water molecules with oxygen vacancies, as well as the reaction of oxygen molecules with hydroxyl groups that results from the water dissociation in oxygen vacancies. In addition, we have followed the diffusion of single water molecules and water dimers on differently prepared TiO_2(110) surfaces. Utilizing our knowledge gained on the reactions of the clean TiO_2(110) surface with oxygen and water molecules, we have investigated the binding of Au nanoclusters on differently prepared TiO_2(110) surfaces. Many of the presented STM results are accompanied by density functional theory (DFT) calculations.

1.2 Outline

This thesis consists of a number of TiO_2(110) surface studies conducted using STM, and in many cases accompanied by DFT calculations. The experimental setup is described in chapter 2 along with a brief description of density functional theory (DFT). Chapter 3 presents selected surface science studies of TiO_2(110) surfaces, including some of the conclusions drawn from the studies presented later in this thesis. In chapter 4 we assign by STM the different point defects on the TiO_2(110) surface from their interactions with H_2O and O_2. The assignments are confirmed by DFT calculations. In connection to this we follow the dynamics of water dissociation in an oxygen vacancy in chapter 5. Chapters 6 and 7 concern the diffusion of single water molecules and water dimers on differently prepared TiO_2(110) surfaces. The atomistic details of the interaction of O_2 with the hydroxylated TiO_2(110) surface are described in chapter 8, and it is demonstrated how this knowledge can be used to form an almost defect free TiO_2(110) surface. Chapter 9 describes a study of the adhesion of gold nanoclusters on differently prepared TiO_2(110) surfaces. The results on gold nanoclusters gained from STM measurements are accompanied by extensive DFT calculations. Finally, the results are summarized, and an outlook for future work is given in chapter 10.

CHAPTER 2

Experimental setup and density functional theory basics

The work presented in this thesis has all been carried out in an ultrahigh vacuum (UHV) chamber equipped with different surface science tools. This chapter is devoted to a short description of the UHV chamber and sample preparation as well as a description of our most important tool, the scanning tunneling microscope. In addition a short section on density functional theory (DFT) is included.

2.1 The UHV chamber

The experiments were all performed in one UHV chamber which has a base pressure in the low 10^{-11} Torr range. Inside the chamber the sample is moved around using a long manipulator arm. The sample house at the end of the manipulator is equipped with a filament which is very close to the backside of the sample, enabling us to anneal the crystals up to $\sim$1400 K. A copper braid connects the sample house to a dewar through which we can pump liquid nitrogen, making it possible to cool the crystals to $\sim$100 K. The sample temperature is measured by a K-type thermocouple spot welded on the Ta sample house very close to the crystal.

Cleaning is done using a differentially pumped sputtergun, sputtering the sample with Ar^+ ions. An automated system controls the sputtergun and the filament in the sample house. A typical cleaning cycle for our TiO_2 samples is twenty minutes sputtering at 1 kV followed by twenty minutes annealing at temperatures between 850 K to 950 K, depending on sample history. As discussed in chapter 4 it is necessary to perform an additional short flash of the sample to $\sim$600 K just prior to inspection with the STM to obtain clean, reduced TiO_2(110) surfaces. Such short flashes are additionally used before exposure of a clean, reduced TiO_2(110) surface to gases, or before metal deposition.

After cleaning the sample a number of different surface preparations can be carried out by dosing gases or depositing metals on the surface. O_2 and H_2O are dosed by backfilling the chamber through leak valves, while D_2O is dosed using a directional doser to avoid co-adsorption of H_2O that might be displaced from the chamber walls when backfilling, and exchange reactions between the D_2O and H_2O adsorbed on the chamber walls. Exposures are measured in Langmuir (L), with 1 L = 1×10^{-6}Torr·s. However, because of the particular arrangement of ion gauge, gas inlet, manipulator with sample holder and turbo pump in this UHV chamber, given values of gas exposures are underestimated by about one order of magnitude for H_2O and a factor of 2-3 for oxygen. There is a separate gas line for each gas to avoid intermixing of the different gases. All gases are cleaned before use, oxygen using a liquid nitrogen cooling trap and water using "freeze-pump-thaw" cycles. These cycles remove the gases normally dissolved in the water. For metal deposition an electron beam evaporator (Oxford Applied Research) is used.

For investigation of the different surfaces the chamber is equipped with a home built STM and a differentially pumped quadrupole mass spectrometer which can be used for temperature programmed desorption (TPD).

2.2 Scanning tunneling microscopy

The first STM was developed in 1982 by Gerd Binnig and Heinrich Rohrer [13]. It is a unique and powerful tool in surface science that have made it possible to explore a wide variety of surfaces at the atomic level. The great impact of the technique on surface science was acknowledged already in 1986 when the inventors received the Nobel prize [14]. The basic principle of the STM is rather simple. A sharp metallic tip is brought into

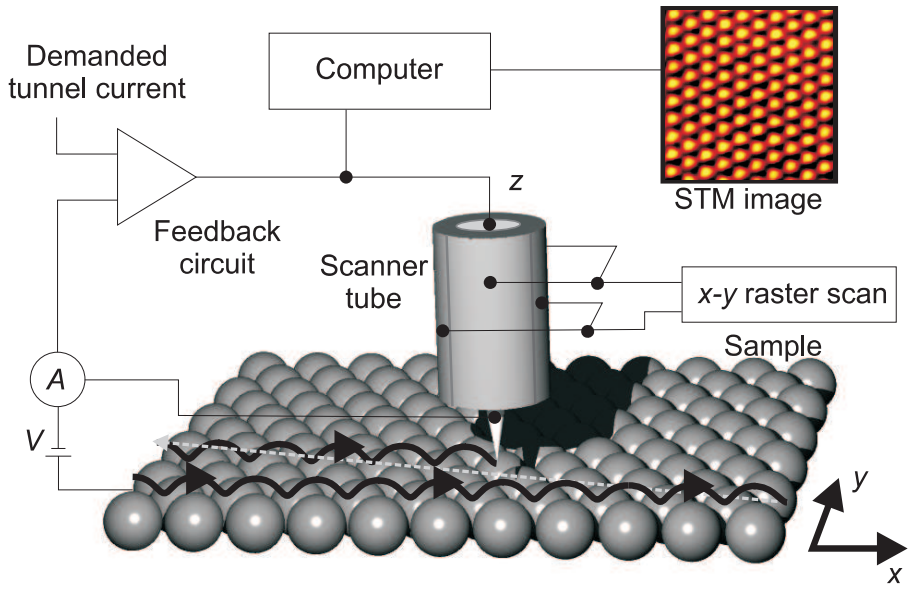

Figure 2.1. *Illustration of the principle of the STM.*

such close proximity of the conducting sample surface that the wave functions of tip and the sample start to overlap. This typically occurs when the distance is ∼5 Å. If a positive bias voltage is applied to the sample, electrons will start to tunnel from the tip to the sample. This tunnel current is in the nanoampere range and strongly dependent on the distance between the tip and the sample as will be shown in section 2.2.1. Imaging the surface is usually done in the so-called constant current mode. In this mode a feedback loop adjusts the distance between the tip and the surface to keep the current constant at a predefined value while the tip is raster scanned across the surface. So when the tip traverses a protrusion the feedback loop will move the tip away from the surface. When the tip has moved across the protrusion the feedback loop will move the tip back towards the surface . The height modulations are recorded and used to make a topographic image of the surface. The operational principle is illustrated in Fig. 2.1.

If the tip is attached to a scanner tube made of piezoelectric material it is in practice possible to control the position of the tip in the sub-Ångstrøm range. This fact combined with the tunnel current being strongly dependent on the distance between tip and sample makes the STM capable of making atomically resolved images of surfaces.

2.2.1 Theory of STM

To be able to interpret the images of different surfaces made with STM, it is necessary to know what determines the tunnel current. This is a very complicated task since knowl-

edge is needed about the quantum mechanical wave functions for both the filled and empty states in the tip and the sample. But in 1983, only one year after the first report on the STM, Tersoff and Hamann [15] developed a method to determine the tunnel current. They assumed the tip and sample to be two non-interacting systems, then in first-order perturbation theory the tunnel current is

$$I = \frac{2\pi e}{\hbar} \sum_{\mu,\nu} f(E_\mu)[1 - f(E_\nu + eV)] \times |M_{\mu\nu}|^2 \delta(E_\mu - E_\nu). \tag{2.1}$$

Here $f(E)$ is the fermi function, $M_{\mu\nu}$ is the tunneling matrix element between the tip states ψ_μ with energy E_μ and the sample states ψ_ν with energy E_ν. V is the bias voltage between the tip and the sample. The fermi functions guarantee that tunneling occurs from filled tip states $f(E_\mu)$ into empty sample states $1 - f(E_\nu + eV)$. Only elastic tunneling is taking into account as can be seen from the delta function. The calculation of the tunneling matrix element is the main problem. Bardeen [16] showed that

$$M_{\mu\nu} = \frac{\hbar^2}{2m} \int d\vec{S} \cdot \vec{j}_{\mu\nu}, \tag{2.2}$$

where $\vec{j}_{\mu\nu}$ is the current density operator and m is the electron mass. The integration is over any surface that lies entirely within the vacuum gap region. Tersoff and Hamann then made the assumption that the end of the tip was spherical and could be described by an s-wave tip wave function. For small bias voltage they found the following simple expression for the tunnel current:

$$I \propto V \sum_{\nu} |\psi_\nu(\vec{r}_0)|^2 \delta(E_\nu - E_F) = V \rho(E_F, \vec{r}_0). \tag{2.3}$$

It shows that the tunnel current is proportional to the bias voltage and to the local density of states (LDOS) of the surface at the Fermi level evaluated at the center of the tip apex ($\vec{r}_0$). So within this approximation, the images made with STM in the constant current mode are images of the contours of LDOS for the surface.

The surface wave functions decay exponentially in the vacuum gap, therefore the tunnel current will depend exponentially on the tip-surface separation

$$I \propto V \exp\Big(- \frac{\sqrt{8m\phi}z}{\hbar} \Big), \tag{2.4}$$

where ϕ is the work function which for simplicity was assumed to be the same for tip and sample. This exponential dependence is what makes the STM capable of obtaining atomic resolution since a change in tip-sample distance of $\sim$1 Å changes the tunnel current by a factor of ten.

STM images of a metal surface can in general be interpreted as a topographic map of the surface, i.e. protrusions can be assigned to single metal atoms. On non-metallic surfaces like oxide surfaces the simple expression Eq. 2.4 derived above is not valid due to the presence of a band gap and rather large bias voltage. The interpretation of STM images is therefore much more complicated. We will return to this subject later on when discussing the TiO_2(110) surface.

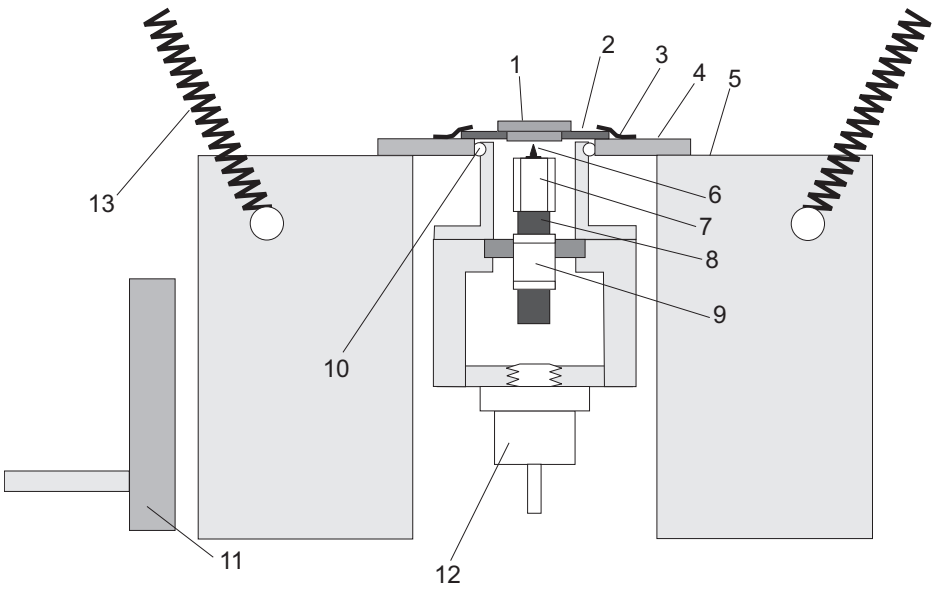

Figure 2.2. *Schematic drawing showing a cross-section of the Aarhus STM. Main features of the STM (see text for details): (1) Sample; (2) sample holder; (3) springs; (4) top plate; (5) aluminium block; (6) tungsten tip; (7) scanner tube; (8) ZrO_2 rod; (9) inchworm; (10) quartz balls; (11) cold finger with LN_2 feedthrough; (12) Zener diode; (13) suspension springs.*

2.2.2 The Aarhus STM

To utilize the principle of the STM one has to be able to position two macroscopic objects, the STM tip and the surface of the single crystal sample with sub-Ångstrøm precision. This is a huge task which has been elegantly overcome in the design of the Aarhus STM [17]. In the following we will shortly look at the design and discuss some of the advantages of the Aarhus STM.

A schematic drawing of the Aarhus STM is shown in Fig. 2.2. The sample (1) is mounted in a tantalum sample holder (2). When a sample is in the STM the sample holder is held by two copper springs (3) which clamp the holder into contact with the top plate (4). The top plate is mounted on a big aluminium block (5) which can be cooled to $\sim$105 K. The cooling is done by pressing the cold finger (11) against the block while pumping liquid nitrogen through the finger. When scanning the cold finger is retracted and the block hangs freely in the the suspension springs (13). Due to the large heat capacity of the block the temperature of the sample only rises $5-10$ K per hour. The scanner part ($6-9$) with the piezoelectric elements is thermally and electrically isolated from the top plate by quartz balls (10). When the block is cold this part is kept at RT by a Zener diode (12), to render the electromechanical respons of the piezoelectric elements

is independent of the sample temperature.

The tip (6) is made by electrochemical etching of a tungsten wire and is mounted in a holder on the end of the scanner tube. The scanner tube (7) is made from a piezoelectric element divided into four equal sections. Each section is coated with a conducting gold layer both on the outside and on the inside. On the outside each segment is isolated from the others, whereas the segments are interconnected on the inside of the tube. By applying a high voltage antisymmetrically to two opposite segments it is possible to bend the tube. This is the principle of the x-y scanning. By applying a voltage to the inner electrode relative to the outer electrodes the length of the tube can be changed. In this way the tip-surface distance can be adjusted in the sub-Ångstrøm scale.

The scanner tube is glued onto a ZrO_2 rod (8) which can be be run up and down by a linear motor called the inchworm (9). The inchworm consists of three sections of piezoelectric material, where the upper and lower sections simply clamp and unclamp the rod while the center section expands or contracts. The upper section is fixed, so the worm-like motion of the inchworm will run the rod up or down. Coarse approach is made using this technique, moving the tip from ca. 1 mm to within a few Ångstrøms of the surface in approximately one minute without crashing into the surface.

Vibrations of the tip relative to the sample can make it impossible to attain images with atomic resolution. Therefore damping vibrations is an important issue in the design of an STM. In the Aarhus STM vibration damping is done very simple. When scanning the block hangs freely in the three suspension springs. This system has a resonance frequency of a few Hertz. In combination with the compact scanner part which has resonance frequencies as high as 8 kHz and 90 kHz this damps external vibrations and additional vibrational damping is not necessary. The compact design of the scanner part also makes fast scanning possible and several constant current images can be recorded per second. This fast scanning capability is utilized when making so called STM movies. These are made by recording successive images of the same area of the sample. By making one image per second we can follow dynamic processes that occur on this time scale, e.g. diffusion of molecules on the surface. To ensure that we keep scanning the same area of the sample, pattern recognition software has been implemented in the scanning software to counteract drift of the sample relative to the tip.

2.2.3 Parameters for imaging TiO_2(110) with STM

Images presented in this thesis were taken in the constant current mode typically using a tunneling voltage (V_T) of $+1.25$ V and a tunneling current (I_T) of $\sim$0.1 nA. Scanning with a high voltage (up to $+10$ V) was used to prepare the STM tip [18].

2.3 Density functional theory

Theoretical calculations have become an increasingly powerful tool for investigating properties of metal oxides, and such calculations can provide insight to atomistic details which are difficult, or even impossible, to probe with experimental techniques. In three of the presented studies in this thesis, density functional theory (DFT) calculations

accompany the experimental results. For this reason a short description of the theory behind DFT will be presented here. It should be pointed out that my own contribution to the theoretical studies has been limited to the level of discussions and suggestions. Therefore, computational details and parameters have, to a large extent, been left out in the forthcoming chapters. However, the computational details can be found in the published papers (see publication list).

2.3.1 Basic equations used in DFT

The foundation of DFT is due to a theorem by Hohenberg and Kohn which, for the ground state of a bound inhomogeneous electron gas with a density, $n(\mathbf{r})$, in an external potential, $v(\mathbf{r})$, states that: "...$v(\mathbf{r})$ is (to within a constant) a unique functional of $n(\mathbf{r})$" [19]. Since $v(\mathbf{r})$ fixes the Hamiltonian, the full many-particle ground state is a unique functional of the electron density. The ground state energy, E, is given by

$$E = \int v(\mathbf{r})n(\mathbf{r})d\mathbf{r} + \frac{1}{2}\iint \frac{n(\mathbf{r})n(\mathbf{r}')}{|\mathbf{r}-\mathbf{r}'|}d\mathbf{r}d\mathbf{r}' + G[n], \tag{2.5}$$

where G is a universal functional of the density independent of $v(\mathbf{r})$.

Kohn and Sham used an approach where they split $G[n]$ into two parts [20]:

$$G[n] \equiv T_s[n] + E_{xc}[n], \tag{2.6}$$

where $T_s[n]$ is the kinetic energy a of non-interacting electron gas with density $n(\mathbf{r})$, and $E_{xc}[n]$ is the exchange and correlation energy of an interacting electron gas with density $n(\mathbf{r})$. By applying the variational principle of quantum mechanics, Kohn and Sham arrived at a set of one-particle Schrödinger equations [20]:

$$\left\{-\frac{1}{2}\nabla^2 + [\phi(\mathbf{r}) + v_{xc}(\mathbf{r})]\right\}\psi_i(\mathbf{r}) = \epsilon_i\psi_i(\mathbf{r}), \tag{2.7}$$

with the corresponding electron density given by

$$\sum_{i=1}^{N} |\psi_i(\mathbf{r})|^2 = n(\mathbf{r}), \tag{2.8}$$

where N is the total number of electrons. The total electrostatic potential $\phi(\mathbf{r})$ is given by

$$\phi(\mathbf{r}) = v(\mathbf{r}) + \int \frac{n(\mathbf{r}')}{|\mathbf{r}-\mathbf{r}'|}d\mathbf{r}' \tag{2.9}$$

and the exchange and correlation contribution to the potential $v_{xc}(\mathbf{r})$ is given by the functional derivative of E_{xc}

$$v_{xc}(\mathbf{r}) = \frac{\delta E_{xc}[n]}{\delta n(\mathbf{r})}. \tag{2.10}$$

Equations 2.7-2.10 have to be solved self-consistently by first choosing a trial $n(\mathbf{r})$ from which $\phi(\mathbf{r})$ and $v_{xc}(\mathbf{r})$ can be calculated. Then a new guess for $n(\mathbf{r})$ can be found from Eq. 2.7 and 2.8. This process is repeated until convergence is reached, i.e. changes in, e.g., forces on atoms and the total energy from one iteration to the next are smaller than a set of preset limits. The total energy of the system is then given by

$$E = \sum_{i=1}^{N} \epsilon_i - \frac{1}{2} \iint \frac{n(\mathbf{r})n(\mathbf{r}')}{|\mathbf{r} - \mathbf{r}'|} d\mathbf{r}d\mathbf{r}' + E_{xc}[n] - \int v_{xc}(\mathbf{r})n(\mathbf{r})d(\mathbf{r}). \tag{2.11}$$

The only intrinsic approximation in DFT lies in the parametrization of the exchange and correlation functional. Kohn and Sham used the local density approximation (LDA) which is a good approximation if the electron density is sufficiently slowly varying [20]. The exchange and correlation energy $E_{xc}[n]$ is given by

$$E_{xc}[n] = \int n(\mathbf{r})\epsilon(n(\mathbf{r}))d(\mathbf{r}), \tag{2.12}$$

i.e., it is a function of $n(\mathbf{r})$ only. However, for binding of adsorbates on surfaces LDA-based DFT calculations overestimate the binding energy. For this reason other approximations for the exchange and correlation functional have been introduced. The generalized gradient approximation (GGA) in which the energy depends both on the electron density and the gradient of the electron density. The typical form of E_{xc} is then

$$E_{xc}[n] = \int f(n(\mathbf{r}), \nabla n(\mathbf{r}))d(\mathbf{r}). \tag{2.13}$$

The DFT calculations presented in this thesis were all carried out using the revised Perdew-Burke-Ernzerhof (RPBE) exchange-correlation functional [21] which is GGA-based.

When DFT calculations are applied to surface science studies such as the binding of an adsorbate to a single-crystal surface, other approximations have to be made. In slab calculations the system is modelled by a super cell with periodic boundary conditions. For TiO_2(110) the super cell consists of a number of so-called tri-layers which are repeated perpendicular to the surface and separated by a vacuum. The number of tri-layers used can have a marked effect on the energy of an adsorbate (e.g. [22]). Also the number of surface unit cells in the super cell can influence the calculated adsorption energies, because if the super cell is too small, adsorbates can interact through the periodic boundary conditions.

CHAPTER 3

Selected results of the surface science of rutile TiO_2(110)

The rutile TiO_2(110) surface is the surface of choice for surface science studies of metal oxides, and it is the surface investigated in the studies presented in this thesis. This chapter will give an introduction to TiO_2 and some of its properties with principal focus on the TiO_2(110) surface. It will also give an overview of selected results from the literature relevant to understand the context in which the results presented in the forthcoming chapters should be viewed.

3.1 Rutile titanium dioxide

Titanium dioxide crystallizes in three major different structures: rutile, anatase and brookite. Only rutile and anatase play a role in the applications of TiO_2 and have been studied with surface science techniques. The work presented in this thesis was performed exclusively on the rutile TiO_2(110) surface, therefore only the bulk structure of rutile TiO_2 and the surface structure of the rutile TiO_2(110) surface will be discussed here.

3.1.1 Bulk rutile TiO_2

The unit cell of rutile TiO_2 is tetragonal with two titanium and four oxygen atoms (Fig. 3.1(a)). Every titanium atom is surrounded by six oxygen atoms in a slightly distorted octahedron. In the crystal, the octahedra are stacked with their long axis alternating by 90 °, resulting in threefold coordinated oxygen atoms. The stacking of the unit cells is shown in Fig. 3.1(b).

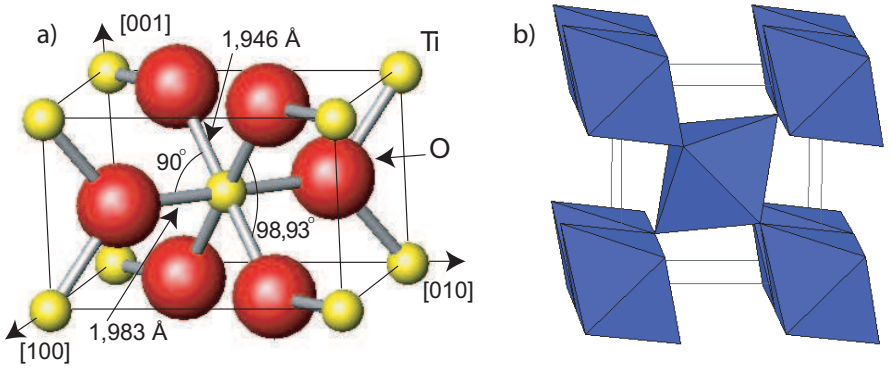

Figure 3.1. *(a) The unit cell of bulk rutile TiO_2. From [10]. (b) Crystal structure of rutile showing the stacking of the unit cells [23].*

Electronically rutile TiO_2 is a wide band gap semiconductor with a band gap of $\sim$3 eV. The valence band is composed of O 2p states, while the conduction band consists mainly of contributions from Ti 3d orbitals [24]. The decomposed density of states can be seen in Fig. 3.2.

3.1.1.1 Bulk defects

TiO_2 is easily reduced by annealing under vacuum conditions. This treatment creates bulk defects and results in a pronounced color change of the TiO_2 crystal from initially transparent to light, and eventually dark blue [25]. The question which defect is the

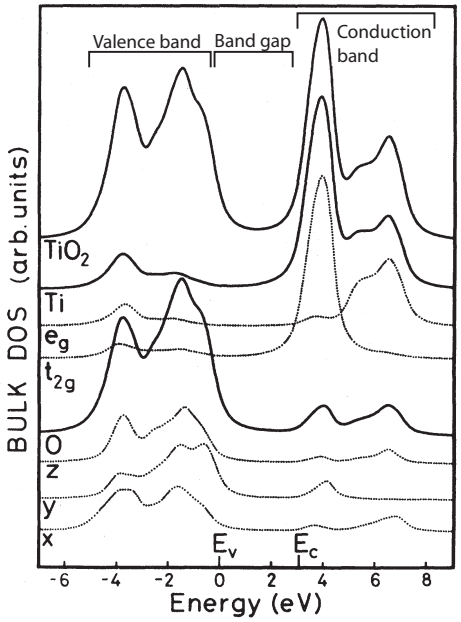

Figure 3.2. *Density of states for bulk rutile TiO_2 decomposed in states derived from Ti and O atoms. The O atoms contribute mainly to the valence band, and Ti atoms contribute mostly to the conduction band. Reproduced from [24].*

dominant is, however, still under debate. In early studies by Cronemeyer it was suggested that the measured defect state ∼0.75 eV below the conduction band was due to bulk oxygen vacancies [26,27]. In more recent studies by Yagi *et al.* [28,29] using electrical resistivity and Hall-coefficient measurements, they reported defect states 0.01 eV below the conduction band minimum and ascribed these defect states to Ti interstitials. This very shallow defect state was found to be thermally excited from around 4 K. Such intrinsic defects result in n-type doping and high conductivity of TiO_2 single crystals even at liquid nitrogen temperatures, which is very important for the applicability of STM and other surface science techniques.

During preparation of a TiO_2 crystal in UHV preferentially oxygen is sputtered away from the surface, leaving a surplus of titanium atoms in the surface region. During the subsequent annealing the Ti atoms have been shown to diffuse into the bulk rather than oxygen anions diffusing from the bulk to the surface [30, 31]. The latter rather points towards Ti interstitials being the dominant defect in TiO_2 crystals prepared by sputtering and annealing as is the case for most surface science experiments.

The diffusion of the Ti interstitials has been suggested to be especially facile through the open channels along the [001] direction [32]. However, recent calculations by Iddir *et al.* have shown that diffusion of Ti interstitials is more favorable in the [110] direction than in the [001] direction, and that diffusion in the [110] direction occurs through the

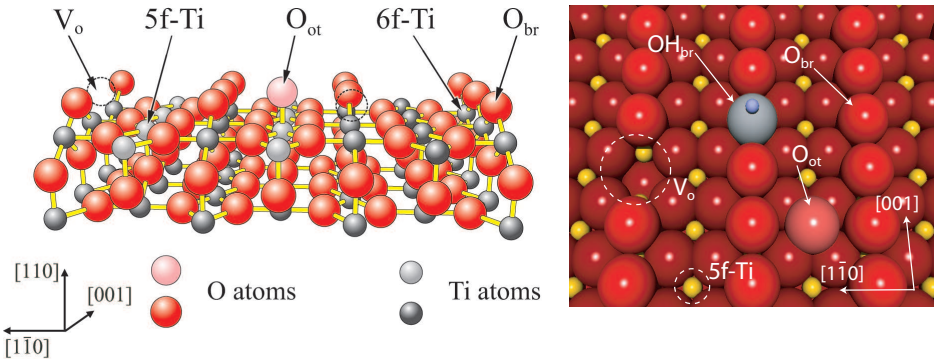

Figure 3.3. *Two models of the $TiO_2(110)$ surface. Both models show different defects and species discussed in the text. Large red balls represent O atoms, and small grey or yellow balls represent Ti atoms. Fivefold (5f-Ti) and sixfold (6f-Ti) coordinated Ti atoms, bridge bonded O species (O_{br}), single oxygen vacancies (V_o), bridging hydroxyl group (OH_{br}), and the on-top bonded O species (O_{ot}) are indicated.*

interstitialcy diffusion (or kick-out) mechanism [33], thus, supporting the mechanism for re-oxidation of the sputtered $TiO_2(110)$ surface suggested by Henderson [30, 31].

3.2 The $TiO_2(110)$ surface

A number of stable rutile TiO_2 surfaces can be formed, with the (110) face being the most stable [34]. Due to the partly covalent nature of the bonds in TiO_2 this is expected, since the (110) surface is the one with the least number of dangling bonds [34]. It is a bulk truncation, i.e. the surface can be imagined as made by cleaving a TiO_2 crystal perpendicular to the [110] direction. However, due to the creation of the surface there are some relaxations in the first few layers of the $TiO_2(110)$-(1×1) surface.

Although the $TiO_2(110)$-(1×1) surface is very stable, it reconstructs at high temperatures under both oxidizing and reducing conditions. In the experiments presented in this thesis only non-reconstructed $TiO_2(110)$-(1×1) surfaces have been used, and therefore only this surface structure will be discussed in the following.

In Fig. 3.3 two $TiO_2(110)$ surface models are shown, including a number of possible defects. The stoichiometric $TiO_2(110)$ surface consists of alternating rows of fivefold-coordinated Ti (5f-Ti) atoms and protruding, twofold coordinated bridging oxygen (O_{br}) atoms. The Ti atoms underneath the bridging oxygen atoms are sixfold coordinated as any other Ti atom in stoichiometric rutile TiO_2. The defects shown in Fig. 3.3 are bridging oxygen vacancies (V_o), a bridging hydroxyl group (OH_{br}), and the on-top 5f-Ti bonded O species (O_{ot}). The (1×1) surface unit cell is 2.96 Å in the [001] direction and 6.49 Å in the $[1\bar{1}0]$ direction.

3.2.1 Point defects on TiO_2(110) surfaces

The single most discussed defect on TiO_2(110) surfaces is the bridging oxygen vacancy. It has been shown that the chemistry of stoichiometric TiO_2(110) surfaces differs markedly from surfaces containing oxygen vacancies [1, 10, 35, 36]. Therefore, oxygen vacancies are considered to be important reactive agents for many adsorbates, and hence many surface reactions are influenced by these point defects. However, other defects on TiO_2(110) surfaces have also been reported to influence adsorbates or the growth of Au nanoclusters.

Averaging spectroscopic techniques have been employed in a number of studies to characterize TiO_2(110) surfaces. From XPS measurements it was found that reduced or defective TiO_2(110) surfaces show a Ti $2p_{3/2}$ feature at slightly lower binding energies, indicating a Ti^{3+} state [37–40], whereas the formal charge of a Ti-ion in TiO_2 is Ti^{4+}. Also UPS [40–42] and EELS [39, 43–46] have contributed to the knowledge of oxygen vacancies on TiO_2(110) surfaces. Kurtz *et al.* showed that the defect state in UPS ascribed to oxygen vacancies was quenched when exposing the reduced TiO_2(110) surface to O_2 at 400 K [42]. Many others annealed their TiO_2(110) samples in an oxygen atmosphere to produce stoichiometric surfaces as measured with XPS, UPS or EELS [1, 37–43]. However, STM studies revealed that the local surface structure depends critically on the exact preparation procedure when exposing TiO_2(110) samples to oxygen at elevated temperatures. Onishi *et al.* observed the formation of added rows ascribed to Ti_2O_3 structures in STM movies acquired during oxidation at 800 K of a reduced TiO_2(110) sample [47]. Li *et al.* performed a comprehensive study of the effect of oxidizing reduced TiO_2(110) samples at different temperatures [48, 49]. The authors found the (1×1) surfaces to reconstruct with structures dependent on both annealing temperature and sample history. For this reason, at present many research groups prepare their TiO_2(110) samples via sputtering and annealing in vacuo, i.e. without annealing in oxygen [10].

A number of theoretical studies have examined the role of oxygen vacancies on TiO_2(110) surfaces [50–58], several of them confirming the importance of oxygen vacancies for surface reactions [52, 55, 56]. We will return to the theoretical studies on different surface reactions and Au nanoclusters on TiO_2(110) in the sections below.

3.2.1.1 Assignment of point defects with STM

As was discussed in chapter 2, the interpretation of constant-current STM images is a priori not straightforward especially for oxide surfaces. There has been some dispute in the past as to whether the bridging oxygen atoms or the fivefold coordinated Ti atoms (Fig. 3.3) are imaged as protruding features in STM images of the TiO_2(110) surface (see Ref. [59], and references therein). In contrast to what one would expect on simple geometric grounds, the protruding bridging oxygen atoms are imaged as dark rows, while the lower lying fivefold coordinated Ti atoms are imaged bright as seen in Fig. 3.4.

Connected to the question as to whether fivefold coordinated Ti atoms or bridging oxygen atoms are imaged as protruding features in STM images is the identification of oxygen vacancies. Diebold *et al.* associated bright spots on the dark rows with bridging

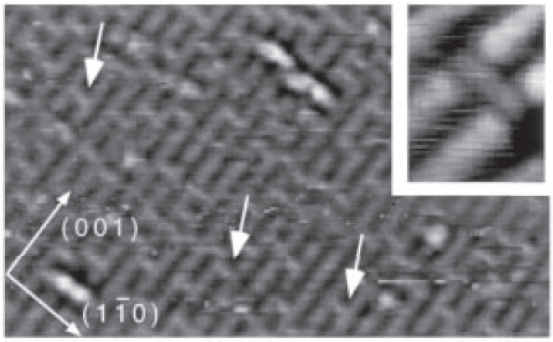

Figure 3.4. *STM image of a reduced $TiO_2(110)$ surface,* 190×120 $\AA^2$. *Bright rows are assigned to fivefold coordinated Ti atoms, while dark rows are assigned to bridging oxygen atoms. The arrows point to features that were assigned to oxygen vacancies, one of which is enlarged in the inset. From [59].*

oxygen vacancies (Fig. 3.4) and introduced the term "Type-A defects" for these point defects [18] (the authors used the term "Type-B defects" for dark spots on bright rows, but this type of defects will not be discussed here). However, also bridging hydroxyl groups, i.e. hydrogen atoms adsorbed on bridging oxygen atoms (Fig. 3.3), are imaged as bright protrusions. This finding was concluded by Suzuki *et al.* using STM and electron-stimulated desorption on $TiO_2(110)$ surfaces exposed to atomic hydrogen [60]. In agreement with the results by Diebold *et al.* [18], Schaub *et al.* assigned bright Type-A defects to oxygen vacancies and assigned less bright Type-A defects to bridging hydroxyl groups [52].

In chapter 4 we assign three different Type-A defects to oxygen vacancies, single bridging hydroxyl groups, and pairs of bridging hydroxyl groups, respectively. The Type-A defects assigned to single bridging hydroxyls in our study, the Type-A defects previously assigned to oxygen vacancies in Refs. [18, 52, 59], and the Type-A defects assigned to bridging hydroxyls by Suzuki *et al.* [60] are all very similar in appearance. We assign faint Type-A defects to oxygen vacancies from their interaction with probe molecules such as H_2O and O_2. We find that both probe molecules dissociate in oxygen vacancies. Water dissociation produces bridging hydroxyls, and O_2 dissociation heals the oxygen vacancy and deposits an oxygen atom on top a fivefold Ti atom. The presence of single oxygen atoms on rows of fivefold Ti atoms resulting from O_2 dissociation at oxygen vacancy sites was also inferred from TPD experiments [44, 45].

Recently, single and paired bridging hydroxyl groups, as well as oxygen vacancies on $TiO_2(110)$ surfaces have also been assigned using non-contact AFM [61]. The authors were able to image the $TiO_2(110)$ surfaces in two different tip modes giving different contrast patterns. In one mode the three Type-A defects were imaged with the same contrast as we found with STM, while in the other mode the contrast was inverted, i.e. Type-A defects were imaged as depressions on bright rows.

3.3 Water adsorption on TiO_2(110) surfaces

The interaction of water with TiO_2(110) surfaces has been studied extensively both experimentally and theoretically. Here we will highlight some of the studies relevant to the results presented in this thesis as well as present some of the conclusions of our work in this context. For a more extensive review on general aspects of water adsorption, see the excellent review article on water adsorption on solid surfaces by Henderson [62].

3.3.1 Molecular vs. dissociative adsorption

From TPD studies of water adsorption by Henderson [63, 64] and Hugenschmidt *et al.* [38] it was concluded that water adsorbs molecularly on the flat stoichiometric TiO_2(110) surface and that water only dissociates at defects. This observation is in agreement with a molecular beam scattering study conducted by Brinkley *et al.* [65], in which it was concluded that very few of the molecules incident on the surface undergo dissociative adsorption, even in the limit of zero coverage. The authors also found a sticking probability of unity at all coverages and temperatures up to 600 K, which helps to explain the very facile hydroxylation of reduced TiO_2(110) surfaces (chapter 4). Kurtz *et al.* reported facile water dissociation at oxygen vacancies, as well as dissociation on TiO_2(110) surfaces exposed to O_2 at 400 K, however, on the latter surfaces only after much larger water exposures as compared to surfaces with oxygen vacancies.

Recent STM studies [52, 66] support the earlier findings that water molecules on clean reduced surfaces only dissociate at oxygen vacancies. However, the two studies do not agree on the temperature at which water dissociates at the oxygen vacancy. Brookes *et al.* [66] report dissociation when heating the water exposed sample to 290 K, while Schaub *et al.* [52] conclude that water will dissociate as soon as molecular water is able to diffuse to the oxygen vacancy at $\sim$160 K.

In contrast to the experimental findings most theoretical studies have predicted dissociative adsorption of water on stoichiometric TiO_2(110) surfaces [67–75], while only a few studies have reported molecular adsorption as the preferred state of adsorption [22, 52, 76–78]. Some studies have found mixed states of molecular and dissociated water molecules to be preferred at monolayer coverage, due to a stabilizing intermolecular hydrogen-bonding interaction [72, 73, 79], and a recent study by Lindan *et al.* concluded that a mixed state is also the most stable for isolated water dimers on perfect TiO_2(110) surfaces [75]. In the same study it was pointed out that, while dissociative adsorption is thermodynamically favored, it might be hindered by a potential barrier. In earlier studies, Lindan and Zhang [71,73] remarked that the dissociated water molecules on stoichiometric TiO_2(110) surfaces cannot be viewed as two separate hydroxyls, one bridging and one terminal hydroxyl, since there is a strong hydrogen bond between the two hydroxyl groups. From the DFT calculations presented in chapter 5 we concluded that the two hydroxyl groups cannot separate, because of a high barrier for diffusion for both the terminal and the bridging hydroxyl, i.e. the dissociated state found in theoretical calculations is only a pseudo-dissociated state, since isolated terminal and bridging hydroxyls are not produced, which at least could explain why dissociation of single water molecules on stoichiometric parts of the TiO_2(110) surface has not been observed with

STM.

In chapter 6 we present the first STM images showing dissociation of water molecules in water dimers on stoichiometric parts of the $TiO_2(110)$ surface in good agreement with theoretical calculations by, for example, Lindan *et al.* [75]. The reason why the water dimer is able to completely separate from the split of proton forming the bridging hydroxyl is the observed mobility of the H_3O_2 species created in the process.

As mentioned in section 3.2.1.1, we have identified bridging hydroxyl group pairs on $TiO_2(110)$ surfaces by STM. Such pairs are expected from the atomistic mechanism for water dissociation in a bridging oxygen vacancy as suggested previously [42,52,66]. In chapter 5 we present a STM movie which represents the first real-space images of this reaction. DFT calculations also presented in chapter 5 confirm the experimental findings, with water dissociation at oxygen vacancies being exothermic with a very low barrier of $\sim$0.2 eV. Other STM results confirming the dissociation model have been published recently by Bikondoa *et al.* [80], and dissociation of a water molecule has also previously been calculated to be exothermic [52]. In connection to the dissociation of a water molecule at an oxygen vacancy, we were also able to follow the splitting of the resulting bridging hydroxyl pair. As mentioned above, we calculated a large barrier for the diffusion of the bridging hydroxyl along the [001] direction ($\sim$1.5 eV). However, we found facile diffusion of the bridging hydroxyls in the $[1\bar{1}0]$ direction mediated by single water molecules. Furthermore, we found that water dimers are able to mediate the diffusion of bridging hydroxyls in both the [001] and the $[1\bar{1}0]$ direction. At odds with the calculated high diffusion barrier along the [001] direction is a recent STM investigation where diffusion of bridging hydroxyls along the [001] direction was observed at RT, however, at very low hopping rates ($\sim 10^{-4}$ s^{-1} OH^{-1}) [81]. The authors estimated the diffusion barrier to be $\sim$1 eV.

3.3.2 Water diffusion on $TiO_2(110)$ surfaces

Henderson remarked in his review article on water adsorption on solid surfaces [62]: "The diffusion of adsorbed water has been one of the more difficult properties of water for experimentalists to study", which is also clear from the relatively few publications concerning diffusion of water on surfaces. The first measurements of kinetics for water were probably the ones by Bryl and co-workers [82–84] using field emission microscopy (FEM). The authors measured on Pt(111)-oriented field emitter tips, as well as Au-covered tungsten tips for monolayer and multilayer water coverages. It is well known that water adsorbed on metal surfaces have a preference for forming clusters [62], i.e., intermolecular water interactions play an important role for water adsorbed on these surfaces. Bryl and co-workers also remarked that the reported energy barriers for water diffusion corresponded roughly to the energy of breaking one hydrogen bond. Therefore, if one wants to investigate the diffusion of isolated water molecules and thereby probe the water-surface interaction, it is necessary to use coverages $\ll$ 1 ML. Such conditions can be investigated using STM, and two recent examples are by Fomin *et al.* [85] and Mitsui *et al.* [86]. In the first case, the authors investigated the influence of tunneling voltage and tunneling current on tip-influenced diffusion of single H_2O and D_2O molecules on Pd(111). In the second case Mitsui *et al.* studied the diffusion and clustering

of H_2O molecules on Pd(111). Interestingly, Mitsui *et al.* found water dimers to have a diffusion coefficient $\sim 10^4$ times higher than for water monomers at the investigated temperature of 40 K. The large mobility of the water dimer was suggested to be due to strong hydrogen bonding between water molecules and a misfit in the O-O distance. A subsequent theoretical paper by Ranea *et al.* [87] suggested a different mechanism explaining the very fast diffusion of water dimers on Pd(111) at 40 K. The suggested mechanism included donor-acceptor tunneling interchange resulting in a very low barrier for water dimer diffusion on Pd(111). Another theoretical paper by Michaelides [88] discusses in more general terms diffusion of water monomers on metal surfaces.

Very little is known about the diffusion of water on oxide surfaces. Akbulut *et al.* [89] investigated the adsorption and decomposition of water on oxidized W(100). Their electron-stimulated desorption measurements showed no evidence of diffusion of water between 25 K and 120 K. Brinkley *et al.* [65] concluded that diffusion of water is not facile on TiO_2(110) based on their molecular beam scattering studies.

As reported in chapter 7 we have conducted extensive experiments employing fast-scanning STM to follow the diffusion of single water molecules and water dimers on hydroxylated and quasi-stoichiometric TiO_2(110) surfaces, i.e., TiO_2(110) surfaces with no or very few point defects on the surface (the bulk crystal is still reduced). We observed diffusion of the water monomers in a temperature range from $\sim$170 K to $\sim$210 K. The energy barrier for diffusion was 0.5 eV, with a prefactor equal to $10^{11.9\pm0.3}$ s^{-1}. Thus, the energy barrier for diffusion is much higher than what was found for Pd(111), where the barrier was reported to be 0.126 eV [86]. As in the case of water on Pd(111), we observed an increased diffusivity of water dimers compared to single water molecules. However, the water dimer hopping rate was only roughly one order of magnitude larger than the water monomer hopping rate. The energy barrier for water dimer diffusion extracted from the data was $\sim$0.2 eV and the prefactor equal to 10^6. An experiment using D_2O instead of H_2O showed no significant isotope effect even though the extracted prefactor indicates that tunneling might be involved in the diffusion process in the investigated temperature range.

3.4 CO oxidation catalyzed by supported gold nanoclusters

The discovery of surprising catalytic properties of dispersed gold nanoparticles on oxide supports [5, 90] have stimulated extensive research activities. A number of excellent reviews focusing on different topics of this area have appeared. Bond and Thompson focused on the oxidation of CO by gold catalysts [91], while Cosandey and Madey have published a review on the growth, interactions, structure, and chemistry of gold deposited on TiO_2(110) surfaces [92]. Catalysis studies have been reviewed by Haruta [93] along with a recent comprehensive review by Meyer *et al.* covering many aspects of gold catalysis [94]. Here we will draw the attention to a few of the aspects concerning CO oxidation catalyzed by gold nanoclusters on metal oxides.

3.4.1 Size effect

It is generally agreed that the size of the gold nanoclusters has a substantial effect on the catalytic activity for CO oxidation. Haruta *et al.* observed a strong size effect for gold nanoparticles supported on TiO_2, Co_3O_4 and α-Fe_2O_3 with the highest activity found for the smallest particles, which had a size of around 2-3 nm [5]. Bamwenda *et al.* [95] tested the effect of preparation method on the catalytic activity of Au-TiO_2 powder catalysts. The most active catalysts were reported to have gold particle sizes of $\sim$2.5-3.5 nm. Studies undertaken under UHV conditions have also shown a clear effect of the size of the gold nanoparticles. Valden *et al.* [8] prepared gold nanoclusters on $TiO_2(110)$ surfaces. The morphology and electronic properties of the gold nanoclusters were probed with STM and STS, respectively. Also the catalytic activity was measured, and the highest activity was reported for particles with a diameter of $\sim$3.5 nm. In a size-selected cluster deposition study, Lee *et al.* found Au_7 clusters deposited on a reduced $TiO_2(110)$ surface to be very catalytically active [96], indicating that even very small gold particles can catalyze the oxidation of CO.

3.4.2 Effect of choice of support

In the seminal study by Haruta *et al.* [90] large differences in the catalytic activity of gold nanoparticles prepared on different supports were reported. However, differences in activity related directly to the support can be difficult to isolate from, for example, the effect the support has on the morphology of the supported gold nanoparticles [94]. Gold nanoparticles of similar size prepared by chemical vapor deposition on Al_2O_3, SiO_2 and TiO_2 were all found to have the same catalytic activity [97], thus indicating that the support has no direct effect on the catalytic activity. On the other hand, Grunwaldt *et al.* reported a significant difference in activity of similarly prepared Au/TiO_2 and Au/ZrO_2 catalysts, with Au/TiO_2 being the most active [98]. In support of this finding Schubert and co-workers reported that reducible oxides are more active than non-reducible ones, because the reducible oxides can work as oxygen reservoirs for the oxidation reaction [99].

3.4.3 The effect of oxidized gold

A number of studies, mainly catalysis work done on high area support materials, have reported on the importance of oxidized or metallic gold, in contrast to reduced gold species, which is found when gold is supported in oxygen vacancies (see chapter 9 and Refs. [100–102]). Guzman *et al.* observed Au^0 and Au^+ on working Au/MgO catalysts [103], and in another study Guzman and co-workers reported a correlation between the concentration of Au^{3+} species and the CO oxidation activity [104]. In a very thorough study, Hutchings *et al.* found Au^+ species to be essential for high CO oxidation activity [105]. A good surface science model for studying Au/TiO_2 CO oxidation catalysts should apparently incorporate metallic or oxidized gold nanoparticles. As we show in chapter 9 cationic gold clusters are found on the oxidized $TiO_2(110)$ surface, due to Au-O adhesion bonds.

CHAPTER 4

Oxygen vacancies on TiO_2(110) and their interaction with O_2 and H_2O

From an interplay between STM and DFT we discuss the origin of various point defects on reduced rutile TiO_2(110)-(1×1) surfaces. By means of adsorption and desorption experiments using water and oxygen as probe molecules we assign the different features observed in STM images to bridging oxygen vacancies, oxygen atoms on surface Ti atoms, and single as well as pairs of hydroxyls on bridging oxygen rows. These experimental results are discussed in comparison to previous STM reports where different assignments of the STM features were suggested. Based on DFT calculations we compare the interaction of water and oxygen with the reduced TiO_2(110) surface with the situation when these molecules encounter a perfect, stoichiometric TiO_2(110) surface. These DFT calculations strongly support the assignments of the features observed experimentally by STM. We report on how to produce clean, reduced TiO_2(110) surfaces and address criteria to ascertain cleanliness by STM.

4.1 Introduction

Defects often play an important role for the properties of bulk materials and surfaces. In heterogenous catalysis defects such as steps or atomic defects often determine the catalytic activity (e.g. [106]). For the TiO_2(110) surface the most discussed defect is the bridging oxygen vacancy. It has been shown that the chemistry of stoichiometric TiO_2(110) surfaces differs markedly from surfaces containing oxygen vacancies [1, 10, 35, 36]. Therefore, oxygen vacancies are considered to be important reactive agents for many adsorbates, and hence many surface reactions are influenced by these point defects. Oxygen vacancies act as direct adsorption sites, but also as electron donor sites thus modifying the surface electronic structure [1, 10, 35, 36]. Furthermore, the oxygen vacancies are nucleation centers for small metal clusters as, for instance, Au particles (see chapter 9). It is therefore highly important to characterize oxygen-related defects on TiO_2(110) surfaces using a variety of surface science techniques.

Averaging spectroscopic techniques like XPS [37–40], UPS [40–42] and EELS [39, 43, 44] have given valuable information on oxygen vacancies on TiO_2(110) surfaces. However, in order to investigate the local structure, the technique of choice is STM. In this respect it is worth mentioning that in many of the earlier UHV studies, the TiO_2(110) samples were characterized with averaging techniques, and mostly TiO_2(110) samples were annealed in an oxygen atmosphere aiming to produce stoichiometric surfaces [1,37,38,40–43,107]. STM studies revealed, however, that the local surface structure depends critically on the exact preparation procedure when exposing TiO_2(110) samples to oxygen at elevated temperatures [10,47,49]. Therefore, at present many research groups prepare their TiO_2(110) samples via sputtering and annealing in vacuo, i.e., without annealing in oxygen [10]. Besides the overall surface morphology, the STM studies have revealed protruding point defects on the TiO_2(110) surface [18, 52, 59, 60, 108–112]. However the assignment of these point defects is not at all a simple task. As mentioned in the introduction of the TiO_2(110) surface (see chapter 3) the interpretation of constant-current STM topographies is a priori not straightforward especially for oxide surfaces. For the TiO_2(110)-(1$\times$1) surface there has been some controversy in the past as to whether the bridging oxygen atoms or the fivefold coordinated Ti atoms (Fig. 3.3) are imaged as bright protrusions in the STM images [10]. In contrast to what one would expect on simple geometric grounds, the $\sim$1.1 Å deeper lying Ti rows are mostly reported to be imaged as the bright rows in the STM images. This means that electronic effects dominate the contrast in the STM images in the case of TiO_2(110) [59].

Closely connected to the question as to whether the Ti or the O atoms are imaged with STM is the identification of oxygen vacancies. According to the finding that Ti atoms are imaged as bright protrusions in the STM images [59], Diebold *et al.* associated bright spots on dark rows with oxygen vacancies and introduced the term "Type-A defects" for these point defects [18]. However, it appears that this issue is even more complex since not only oxygen vacancies, but also hydroxyl groups are imaged as bright protrusions on dark rows [52, 60]. The latter was concluded by Suzuki *et al.* based on experiments where the TiO_2(110) surface was exposed to atomic hydrogen [60]. In agreement with results by Diebold *et al.* [18], Schaub *et al.* assigned relatively bright Type-A defects to oxygen vacancies and associated Type-A defects of smaller appear-

ance with hydroxyl groups [52]. It is worth mentioning that the bright Type-A defects of Refs. [18, 52, 110], which have been ascribed to oxygen vacancies, and the Type-A defects assigned to hydroxyls in the work of Suzuki *et al.* [60] are very similar in appearance.

The role of oxygen vacancies on TiO_2(110)-(1×1) has also been examined in a number of theoretical studies [50–56], although many other theoretical studies focused on perfect, stoichiometric TiO_2(110) surfaces [10, 22, 70, 73, 74, 77, 78]. In several examples the importance of oxygen vacancies for surface reactions has been theoretically confirmed [52, 54–56]. However, in the past it was quite challenging to properly model the interaction of small molecules with oxide semiconductor surfaces. To achieve good convergence of adsorption energies, large unit cells and several layers must be considered [22, 55, 70, 73].

In this chapter, new and improved STM results addressing TiO_2(110)-(1×1) surfaces that have been sputtered and annealed up to temperatures as high as 950 K in UHV are reported. Oxygen vacancies are identified as faint protrusions on the dark rows as predicted previously. However, unlike previously reported [52], the protrusions associated with oxygen vacancies are imaged clearly less bright than hydroxyl groups. A comparison to previous STM studies addressing this issue indicates that TiO_2(110)-(1×1) surfaces inspected so far were mostly hydroxylated. It appears that surface oxygen vacancies quickly react with residual water even under excellent UHV conditions and therefore the time frame for the detection of vacancies is limited. By means of adsorption and desorption experiments using water and oxygen molecules we assign the different features observed in the STM images to bridging oxygen vacancies, single oxygen atoms on 5f-Ti atoms, and single as well as pairs of hydroxyls on the rows of bridging oxygen atoms, respectively. Both probe molecules, water and oxygen, dissociate at oxygen vacancies. DFT calculations support the interpretation of the experimental data, including the paired bridging hydroxyls which turn out to be a quite stable configuration on the TiO_2(110) surface. With respect to oxygen adsorption on the reduced TiO_2(110) surface, we find that each O_2 dissociation event causes the annihilation of one oxygen vacancy and the deposition of an O atom on 5f-Ti atoms. Paired hydroxyls are typical features at virtually clean, reduced TiO_2(110) surfaces, whereas frequent contrast changes indicate hydroxylated surfaces. Finally, we provide a comprehensive data set which allows us to estimate the vacancy concentration on a TiO_2(110) surface based on sample preparation parameters, annealing time and annealing temperature.

4.2 Results

4.2.1 Preparation of TiO_2(110) surfaces using various approaches

In Fig. 4.1, STM images of TiO_2(110)-(1×1) surfaces corresponding to samples with different reduction states are compared. The image in Fig. 4.1(a) was obtained from a slightly reduced sample prepared by 9 sputter/annealing cycles, while 32 of such cycles were applied to achieve a stronger reduced sample from which we took the image shown in Fig. 4.1(b). In addition to sputtering and annealing, samples were shortly flashed to

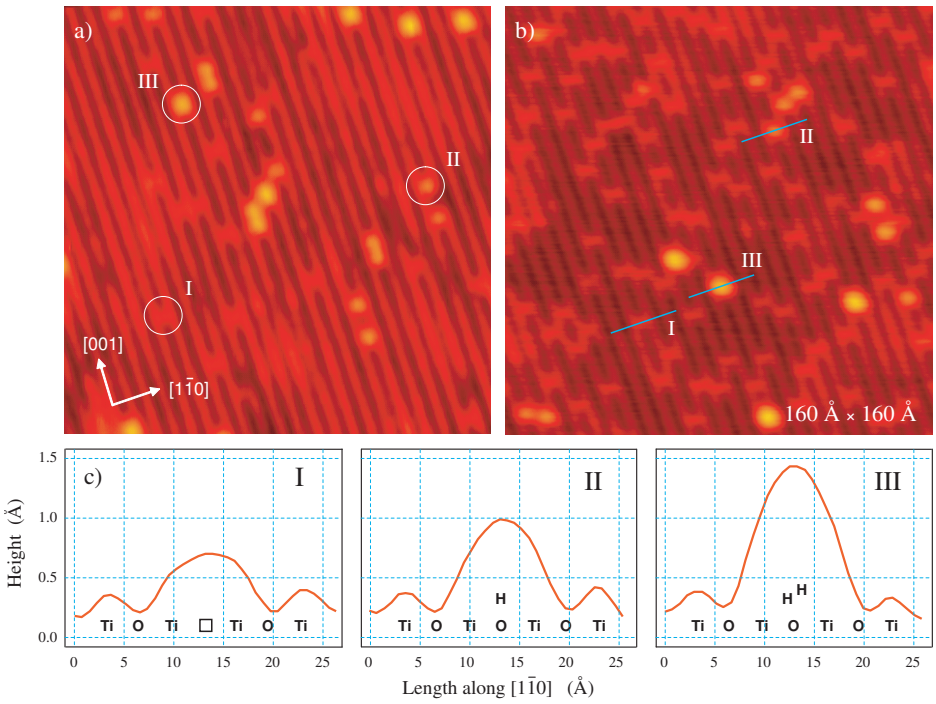

Figure 4.1. *STM images* 160×160 *Å*^{2} *of clean, reduced* TiO_2*(110) samples showing three sorts of Type-A defects referenced by Roman numerals. The sample in (a) was prepared by 9 sputter/annealing cycles while 32 such cycles were applied to achieve a stronger reduced sample in (b). Prior to inspection with STM, samples were shortly flashed to 600 K. (c) STM height-profiles along the* $[1\bar{1}0]$ *direction of the Type-A defects that are indicated in (b).*

600 K prior to inspection at RT. Point defects located on the bridging oxygen rows (see Fig. 3.3) appear in the STM images as protrusions on dark rows (Type-A defects) which connect the bright lines. For both of the two TiO_2(110) samples (Fig. 4.1(a,b)) three different sorts of Type-A defects are clearly resolved which we labeled with Roman numerals (I, II, III) for reference, respectively. Obviously the faint Type-A defects (I) are more numerous for the stronger, reduced crystal; estimated values of their densities based on total areas of $\sim$3000 nm^2 are 2.5$\pm$0.1 % ML (a) and 6.1$\pm$0.1 % ML (b), respectively, where 1 ML (monolayer) is defined as the density of the (1$\times$1) units, 5.2×10^{14} cm^{-2}. In contrast, the densities of the medium bright Type-A defects (II) and the brightest Type-A defects (III) are similar for both samples. Below, we will assign these three Type-A defects to vacancies (I), bridging hydroxyls (II), and pairs of bridging hydroxyls (III), respectively. To facilitate the reading of the manuscript we write in the following A-I (vac), A-II (OH), and A-III (2OH) defects instead of the longwinded

terms Type-A defects (I), (II) and (III), respectively.

The effect of the short flash to 600 K prior to surface inspection by STM is obvious from Fig. 4.2(a) where we show an image of the stronger reduced TiO_2(110) sample acquired directly after sputtering/annealing. Clearly, the densities of the A-II (OH) and the A-III (2OH) defects are markedly higher while the density of the A-I (vac) is lower than on the flash-treated surface (see Fig. 4.1(b)). For comparison a second STM image is presented which has been acquired 24 h later from the same sample (Fig. 4.2(b)). In this case no cleaning procedure at all was performed directly prior to acquisition. While A-I (vac) defects are visible at the STM image shown in Fig. 4.2(a), no such defects were detected 24 h later. The surface that has been exposed for 24 h to the background pressure of the UHV chamber is dominated by A-II (OH) defects, i.e. also no A-III (2OH) defects are observed. It should be noted, however, that we observed TiO_2(110) surfaces as shown in Fig. 4.2(b) already after much shorter storage time under UHV conditions. Keeping the sample at RT in the manipulator after sputtering/annealing, we typically obtained TiO_2(110) surfaces with the A-II (OH) defects being dominant after 30-60 min. The latter holds for our best pressure conditions at $\sim 3\times 10^{-11}$ Torr. In another chamber in our laboratory, which has a vacuum in the 10^{-10} Torr range, it is difficult to obtain TiO_2(110) surfaces with A-I (vac) defects, whereas A-II (OH) defects are usually found. These findings suggest that the density of A-II (OH) defects increases with exposure of the sample to residual gases in the UHV chamber. The faint A-I (vac) defects dominate exclusively when the surface was freshly prepared including a flash to 600 K. The A-III (2OH) defects seem to be an intermediate since they are not present for TiO_2(110) surfaces that have been exposed to the background pressure for longer than 60 min. In the following we use the designation "clean TiO_2(110)" only for those surfaces which show comparably low densities of A-II (OH) and A-III (2OH) defects, and for which the defects are mainly A-I (vac) as exemplified in Fig. 4.1.

In Fig. 4.2 (c) and (d), we zoom in on the indicated areas in Fig. 4.2 (a) and (b), respectively, for a more detailed analysis. By means of the superimposed lattice grids we checked the positions of the various Type-A defects in the [001] direction on these images. Aligning the grid at A-I (vac) and A-II (OH) defects, respectively, yields that the A-III (2OH) defects appear to lie exactly between two intersection points of the lattice (Fig. 4.2 (c)). This finding suggests that the A-III (2OH) defects are composed of two point defects, most likely of two A-II (OH) defects. The superimposed grid also helps to identify A-II (OH) defects which are separated in the [001] direction by two lattice spacings. The finding that two A-II (OH) defects which are next-nearest neighbors (Fig. 4.2 (d)) appear brighter in the STM images than isolated A-II (OH) defects supports the assignment of the A-III (2OH) defects being composed of two nearest-neighbor A-II (OH) defects.

4.2.2 Water as a probe molecule

To check whether there is a correlation between the density and appearance of Type-A defects and water adsorption, we exposed clean TiO_2(110) surfaces to small amounts of water. Prior to the STM inspection we quenched the sample as fast as possible to avoid unwanted water adsorption from the residual gas. It is worth mentioning that it is

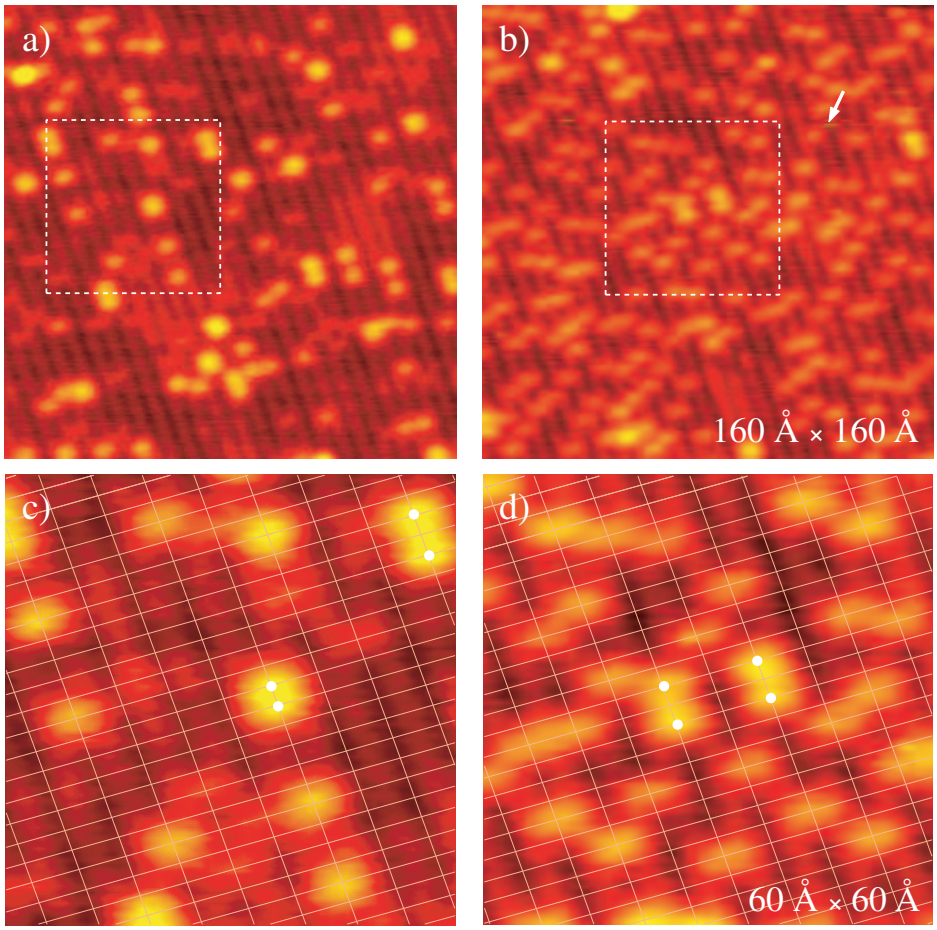

Figure 4.2. *STM images* 160×160 $Å^2$ *exemplifying* TiO_2*(110) surfaces inspected directly after sputtering and annealing, i.e. without an additional flash to 600 K (a), and 24 h later (b), respectively. The indicated areas* 60×60 $Å^2$ *in (a) and (b) are shown enlarged in (c) and (d), respectively. Grids are superimposed to unravel the positions of the various Type-A defects in the [001] direction. White dots indicate specific Type-A defects which are discussed in the text. One of the small streaks in image (b) is indicated by an arrow.*

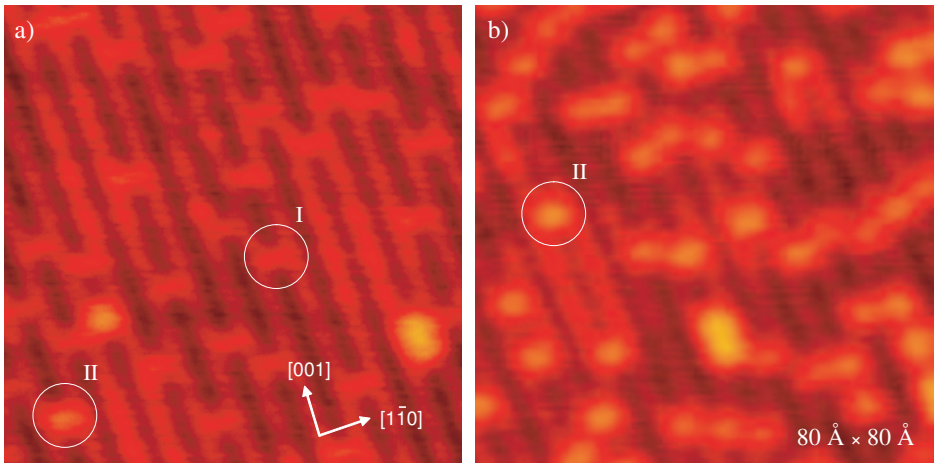

Figure 4.3. *Clean, reduced TiO_2(110) surface 80×80 Å^2 at 120 K prior to (a) and after water exposure of 0.01 L followed by a short flash to 400 K (b).*

noticeably easier to obtain clean TiO_2(110) surfaces, i.e. those which dominantly show A-I (vac) defects in STM images, if the sample is quenched using liquid N_2, which allows us to reach the desired sample temperature faster. The clean surface, as characterized by the image shown in Fig. 4.3 (a), was exposed to 0.01 L water at 120 K. Subsequently, the sample was flashed to 400 K to facilitate water dissociation at oxygen vacancies [42,52,66] and to free the sample from residual molecular water [38,46,63,65,66]. As can be seen from the image presented in Fig. 4.3 (b), this recipe leads to a surface with A-II (OH) defects as in the case shown in Fig. 4.2 (d). Note that the density of A-II (OH) defects after water exposure is twice the density of A-I (vac) defects on the clean TiO_2(110) surface.

4.2.3 Stability of Type-A defects against voltage pulses

In turn we also probed whether the Type-A defects can be removed from the surface. To facilitate such an experiment with the STM, we applied voltage pulses with $U_{pulse} \geq 2.5$ V (feedback loop open) individually on the various Type-A defects while scanning. To follow the development during this experiment, we recorded an STM movie, i.e. a series of time-lapsed sequential images on the same region on the surface [113]. Three selected images of movie 'pulses_oh' are shown in Fig. 4.4, illustrating that A-II (OH) and A-III (2OH) defects disappear upon voltage pulsing. The A-I (vac) defects, however, do not disappear when subjected to the voltage pulses.[1] Furthermore, we observed, in line with the reports by Diebold *et al.* [18] and Suzuki *et al.* [60], that defect-free areas can be produced by scanning the surface with A-II (OH) defects using a tunneling

[1]The STM movie 'pulses_oh' can be accessed at www.phys.au.dk/spm/movies/pulses_oh.mpg. The acquisition time is 2.34 s/frame.

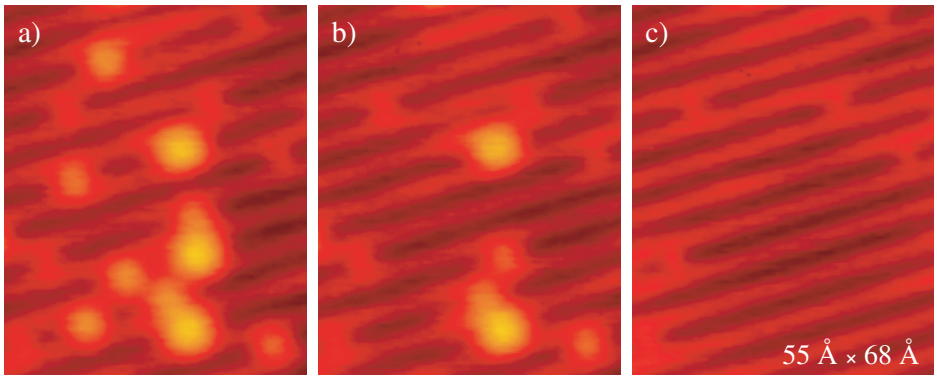

Figure 4.4. *Three selected STM images (a)-(c) acquired while applying voltage pulses with $U_{pulse} \leq +2.5$ V onto the various Type-A defects on a TiO_2(110) sample at RT (see movie 'pulses_oh').*

voltage of $V_T \leq 2.5$ V.

4.2.4 Tip-related contrast changes

For TiO_2(110) surfaces with A-II (OH) defects we occasionally observed pronounced changes of the STM contrast. An example of the most frequent contrast change is presented in Fig. 4.5 where we show two consecutive STM images of the same TiO_2(110) surface (different scan areas). We are certain that neither A-I (vac) nor A-III (2OH) defects are present at this surface, since the sample was exposed to the background pressure of the chamber for 24 h prior to data acquisition. As can be seen in Fig. 4.5 (a), we first imaged the A-II (OH) defects as bright, relatively broad protrusions as usual. However, within a data set of 15 images, and correlated with a tip change, we also collected an image in which the A-II (OH) defects appear as narrow protrusions of considerably smaller height (Fig. 4.5 (b)). In the images measured subsequently (not shown), the A-II (OH) defects again appear as usual, bright and relatively broad protrusions. It is noteworthy that changes in the STM contrast of this kind are often observed on water-exposed TiO_2(110) surfaces.

We observed other kinds of tip-induced contrast changes for TiO_2(110) surfaces with A-II (OH) defects. However, most of these contrast changes are less dramatic than that exemplified above. In some cases we collected images showing the A-II (OH) defects with an asymmetrical shape; these images are very similar to those presented in Ref. [111]. Furthermore, it is noticeable that bright streaks in the scanning direction occur in some images (see arrow in Fig. 4.2 (b)). For water-exposed TiO_2(110) surfaces we observed this phenomenon frequently. Also noteworthy, we did not succeed in imaging clean TiO_2(110) surfaces with the STM contrast mode exemplified in Fig. 4.5.

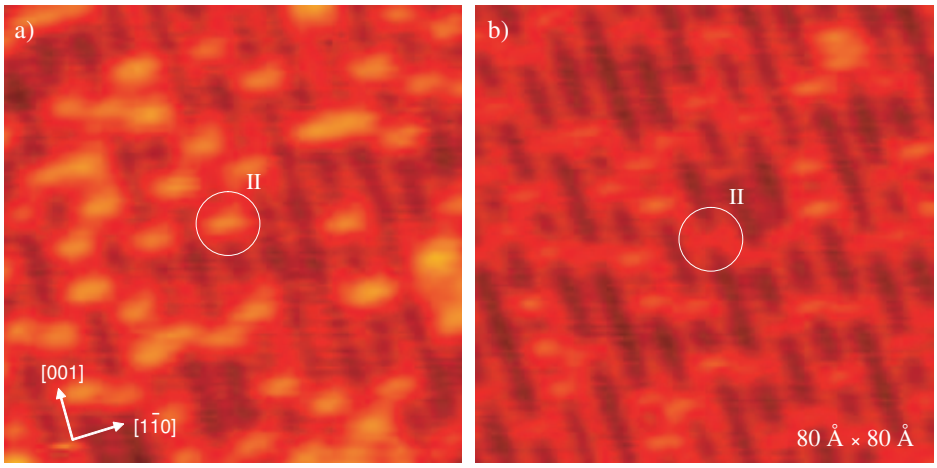

Figure 4.5. *Two consecutively measured STM images of a TiO_2(110) surface with A-II (OH) defects* 80×80 *Å*^{2}*. In (a) A-II (OH) defects are imaged as usual whereas in (b) A-II (OH) defects are imaged narrower and clearly less bright than usual.*

4.2.5 Oxygen as a probe molecule

To assess the nature of the various Type-A defects, the interaction of oxygen with these defects was studied at cryogenic temperature (Fig. 4.6). In a first experiment, a clean, reduced TiO_2(110) surface was exposed to 5 L oxygen at 120 K (Fig. 4.6 (a)). In this case the A-I (vac) defects disappeared and new protrusions on the Ti rows appeared (Fig. 4.6 (b)). We find a ratio of 1:1 between the A-I (vac) defects on the clean TiO_2(110) surface and the new protrusions on Ti atoms after oxygen exposure. In a second experiment, we exposed a TiO_2(110) sample with the A-II (OH) defects present at the surface to 5 L O_2 (Fig. 4.6 (c)). This experiment was also carried out at 120 K. In this case A-II (OH) defects reside on the surface in spite of the oxygen exposure (Fig. 4.6 (d)). In addition, a few new protrusions appear on Ti rows with at least two distinguishable types (marked with dotted and dashed circles in Fig. 4.6 (d)). One of the protrusions appears to be identical to those in the first O_2 adsorption experiment, whereas the second type of protrusions appears as greater protrusions. Obviously the second oxygen adsorption experiment shows a more complex surface chemistry, thus supporting our assignment of A-I (vac) defects to oxygen vacancies and A-II (OH) to OH groups, as will be discussed below.

To gain further insight into the interaction of O_2 with the clean, reduced TiO_2(110) surface, we recorded an STM movie, while dosing O_2 at 135 K. Based on three selected STM images from this movie it is evident that the new protrusions on Ti rows sit next to those locations on the surface where originally A-I (vac) defects resided (Fig. 4.7). This is an important result since it allows us to draw conclusions addressing the atomistic mechanism of the interaction of O_2 molecules with the clean, reduced TiO_2(110) surface

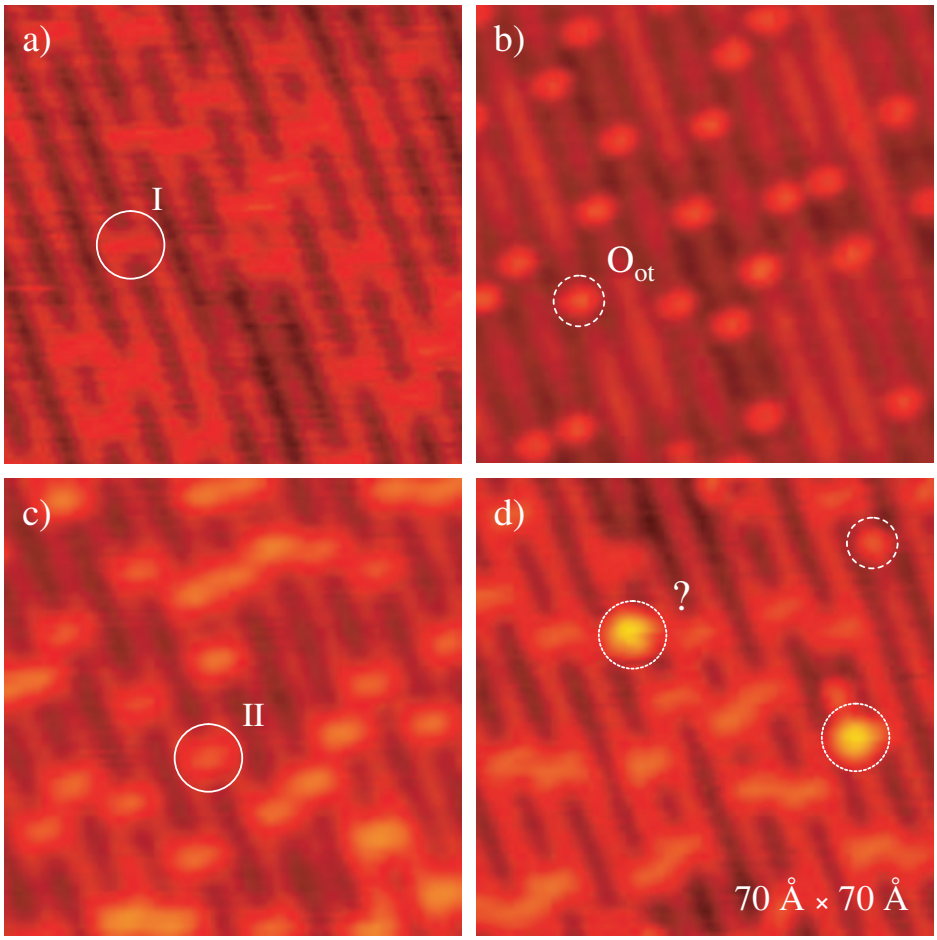

Figure 4.6. *Low-temperature experiments using oxygen as a probe molecule: (a) clean, reduced TiO_2(110) surface (A-I (vac) defects). (b) Clean, reduced TiO_2(110) surface exposed to 5 L O_2 at 120 K. (c) TiO_2(110) surface with A-II (OH) defects. (d) Surface as shown in (c) exposed to 5 L O_2 at 120 K.*

at low temperatures; we will address this issue using the density functional theory (DFT) approach below.

4.2.6 DFT calculations

Here we present results of a thorough set of DFT calculations dealing with the interaction of water and oxygen with perfect, stoichiometric and reduced TiO_2(110) surfaces. As will be apparent in the following, these calculations model the atomistic mechanisms un-

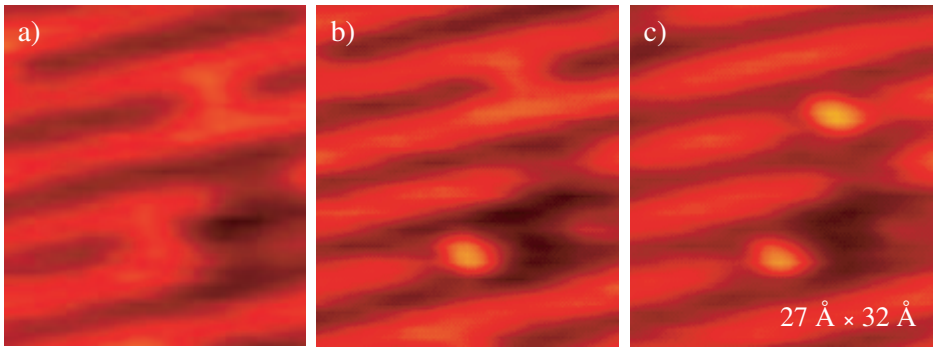

Figure 4.7. *Series of three STM images (a) - (c) illustrating the interaction of O_2 molecules with A-I (vac) defects at 135 K. The same surface area is inspected in these images.*

derlying the main reactions corresponding to the experimental findings presented above. For water adsorption we find H_2O dissociation at bridging oxygen vacancies energetically more favorable than H_2O adsorption on the 5f-Ti atoms. For the oxygen adsorption on the reduced TiO_2(110) surface, we find that O_2 molecules dissociate with great energy release at oxygen vacancies provided that excess electrons originating from other oxygen vacancies are available in the near-surface region of the sample.

4.2.6.1 Water on the TiO_2(110) surface

Fig. 4.8 summarizes the results obtained using DFT calculations addressing water adsorption on perfect, stoichiometric and reduced TiO_2(110) surfaces. For these calculations we introduced only one water molecule per (3×2) surface unit cell since we aim at modeling the water adsorption at low H_2O partial pressure. On the stoichiometric TiO_2(110) surface the molecular adsorption of water is exothermic by ∼0.66 eV (Fig. 4.8 (a)). Once adsorbed on a 5f-Ti atom, the water may dissociate by transfer of one or two protons to adjacent bridging oxygen atoms. The proton transfer leads to formation of bridging hydroxyls and either terminal hydroxyl groups (Fig. 4.8 (b)) or on-top O atoms (O_{ot}) on the Ti row (Fig. 4.8 (c)). Only for the transfer of one proton of the water molecule we find an energy gain (∼0.13 eV) whereas the transfer of both protons is unfavorable. Our result regarding water dissociation on the stoichiometric TiO_2(110) surface (Fig. 4.8 (a,b)) is in good accordance with the prediction by Lindan and Zhang [77]; it differs, however, from the conclusion reached by Harris and Quong [22]. Since we used the RPBE exchange-correlation functional also used by Lindan and Zhang [77], the presented results are consistent with the supposition reached through recent dispute in the literature, where the exchange-correlation functional is discussed as being a possible explanation for the discrepancy among the most recently published computational results [77, 78].

Regardless of this long-standing dispute, adsorption of a water molecule in a bridging oxygen vacancy (Fig. 4.8 (d)) is energetically comparable with respect to water

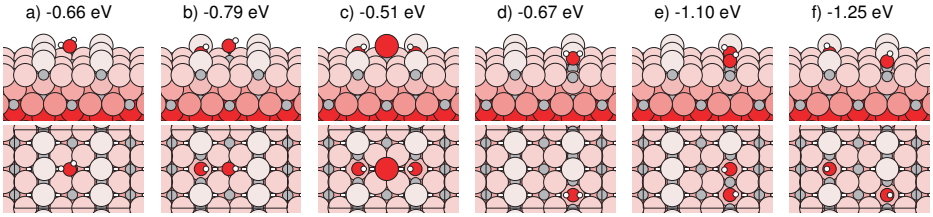

Figure 4.8. *Water/TiO_2(110) configurations calculated using DFT considering a perfect, stoichiometric TiO_2(110) surface (a)-(c) and a reduced TiO_2(110) surface (d) - (f). The potential energies with respect to H_2O in the gas phase and the two considered TiO_2(110) surfaces are given. Large, light red balls represent oxygen atoms, medium size, grey balls Ti atoms, and small white balls protons. For clarity, oxygen atoms of water and terminal hydroxyl groups are drawn dark red and smaller than lattice oxygen atoms.*

adsorption on 5f-Ti atoms in case of the stoichiometric TiO_2(110) surface (Fig. 4.8 (a)). However, $\sim$0.43 eV is gained through proton transfer to an adjacent bridging oxygen atom (Fig. 4.8 (e)), indicating that a water molecule in the vacancy is thermodynamically unstable. Whereas an energy difference of only $\sim$0.13 eV (Fig. 4.8 (a,b)) is too small to be out of dispute, an energy gain of $\sim$0.43 eV is surely large enough, i.e. we trust that DFT reliably predicts water dissociation at bridging oxygen vacancies. The situation in which the paired bridging hydroxyls have separated into single hydroxyls is even more stable by $\sim$0.15 eV (Fig. 4.8 (f)).

4.2.6.2 Oxygen on the TiO_2(110) surface

In Fig. 4.9 we present the calculated structures and energies for various configurations considering O_2 adsorption on a reduced TiO_2(110) surface. While according to previous calculations, O_2 does not bind to a perfect, stoichiometric TiO_2(110) surface [55], it binds with several electron volt to a reduced TiO_2(110) surface with two vacancies in the rows of bridging oxygen atoms (Fig. 4.9 (a)). In Ref. [55] the details of O_2 dissociation at vacancy sites are given, although in that work different calculational parameters have been used. In line with Ref. [55] we find that two oxygen vacancies per O_2 molecule are required in order for the dissociation of O_2 to become exothermic. With the present approach, $\sim$3.54 eV is gained when one of the two oxygen atoms fills a vacancy and the other oxygen sits on a 5f-Ti atom nearby (Fig. 4.9 (b)). We calculate an energy barrier of $\sim$1.14 eV for the diffusion of this O_{ot} atom when comparing the situation shown in Fig. 4.9 (b) with the one where the O_{ot} atom resides midway between two 5f-Ti atoms (Fig. 4.9 (c)). Because of this high diffusion barrier the O_{ot} atoms appear to be immobile. In the unexpected case that the O_{ot} atom would somehow reach the second vacancy (Fig. 4.9 (d)), a final potential energy would be gained which amounts

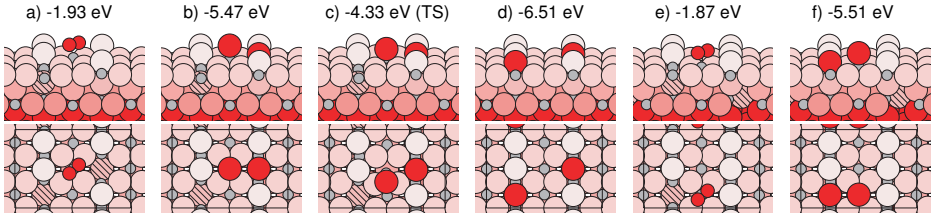

Figure 4.9. *Oxygen/TiO_2(110) configurations calculated using DFT modeling the interaction of O_2 molecules with reduced TiO_2(110) surfaces, either with a surface vacancy concentration of 1/3 (a) - (d) or with vacancy concentrations of 1/6 at the surface and 1/6 in the near-surface region (e, f). The potential energies with respect to O_2 in the gas phase and the two TiO_2(110) surfaces considered are given. Balls indicate various species as ascribed in Fig. 4.8. For clarity, oxygen atoms of O_2 molecules are drawn dark red and smaller than lattice oxygen atoms. Near-surface vacancies are highlighted by hatching oxygen atoms behind the vacancies.*

to (minus) twice the vacancy formation energy.

In addition to the case with both vacancies residing in the first layer, we also considered the case of a reduced TiO_2(110) surface with one vacancy in the rows of bridging oxygen atoms and another one in the bulk (Fig. 4.9 (e,f)). For this situation the energy gain upon O_2 dissociation is $\sim$3.64 eV, i.e. virtually identical to the case with both vacancies residing in the first layer.

4.3 Discussion

4.3.1 Identification of the various point defects on TiO_2(110)-(1$\times$1)

4.3.1.1 Type-A defects

The results presented above can be understood when assigning the A-I (vac) defects in the STM images to bridging oxygen vacancies and the other two Type-A defects, A-II (OH) and A-III (2OH) to single and paired hydroxyls, respectively. The fact that a short flash to 600 K is required to prepare clean, reduced TiO_2(110) surfaces already suggests this assignment (Fig. 4.1 and 4.2); the reason being that hydroxyl groups desorb recombinatively at $\sim$500 K on the TiO_2(110) surface [38,46,63]. In addition, TiO_2(110) surfaces with A-II (OH) defects can be produced via water exposure (Fig. 4.3), in line with this assignment. Furthermore the A-II (OH) and A-III (2OH) defects but not A-I (vac) defects can be removed from the surface using voltage pulses (Fig. 4.4). As shown in previous work, the same sort of Type-A defects can be removed either when scanning with $V_T\sim$3 V, which is consistent with the voltage pulses used here, or when exposing the TiO_2(110) surfaces to electrons with $\sim$20 eV kinetic energy [60]. In addition, it is

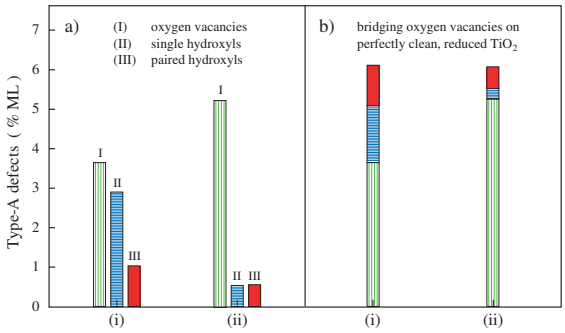

Figure 4.10. *(a) Densities of the various Type-A defects on the (110) plane of a TiO_2 sample which was sputtered/annealed (i), and additionally flashed to 600 K (ii), respectively. The distributions rely on a set of STM images acquired at RT whereby total areas of 3000 nm^2 have been examined. Images exemplifying surfaces (i) and (ii) are shown above in Fig. 4.2(a) and 4.1(b), respectively. (b) Surface oxygen densities extracted from the defect distributions in part (a) of the figure. In order to determine the vacancy concentration two single hydroxyls (A-II (OH) defects) and each A-III (2OH) defects, respectively, were counted for one vacancy.*

known that the desorption threshold of H^+ lies at this kinetic energy and furthermore that the threshold of O^+ desorption is higher than that of H^+ [114]. Therefore, it seems plausible that protons can be removed from the surface, converting the OH-groups in the vacancies to bridging oxygen atoms.

The detection of features in the STM images which can be assigned to paired hydroxyls on reduced TiO_2(110) surfaces (Fig. 4.1, 4.2 and 4.4) strongly supports that water dissociation at oxygen vacancies is responsible for the transformation of the A-I (vac) defects (vacancies) into A-III (2OH) defects (paired hydroxyls) and finally into twice the number of A-II (OH) defects (single hydroxyls). The set of DFT calculations summarized in Fig. 4.8 shows that this atomistic mechanism, which was previously proposed in Refs. [42, 52, 66], is a very likely route to explain the experimental findings. Note that paired bridging hydroxyls are quite stable on the surface (Fig. 4.8 (e)). A thorough analysis of the images collected directly after sputtering/annealing and after an additional flash to 600 K further substantiates that water dissociation at vacancies leads to a hydroxylation of the originally clean, reduced TiO_2(110) surfaces (Fig. 4.10). The two distributions of Type-A defects shown in Fig. 4.10 (a) reflect the cleaning effect of the additional flash to $\sim$600 K. Moreover, if counting two A-II (OH) defects and one A-III (2OH) defect as one vacancy, respectively, we trace back to the original vacancy concentration for a perfectly clean TiO_2(110) surface (Fig. 4.10 (b)). The fact that we find equal values of the original vacancy concentration for both distributions of Type-A defects is strong evidence for the suggested atomistic mechanism.

Using the same approach to determine the vacancy concentration on partly hydroxylated TiO_2(110) surfaces, as illustrated in Fig. 4.10, we evaluated data sets collected

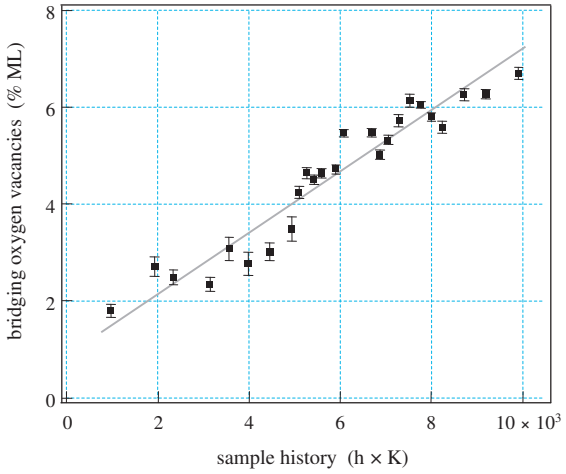

Figure 4.11. *Surface vacancies concentration of one TiO_2(110) sample as a function of the sample history. Since we slightly increased the temperature during annealing the longer the crystal was in use, we define the product of annealing temperature in Kelvin (K) and annealing time in hours (h) as 'sample history'. The Ar^+ sputtering conditions were identical throughout all measurements used for this plot (20 min; 1 keV; RT). Data points in this plot rest upon STM data covering surface areas of at least 2000 nm^2 each. The densities of oxygen vacancies were extracted as exemplified in Fig. 4.10. Similar analyses were done for two other TiO_2(110) samples (not shown). The concentrations of oxygen vacancies on these three samples agree within 0.4 % ML.*

from three samples addressing the correlation between the vacancy concentration and the "sample history". We define the product of annealing temperature in Kelvin (K) and annealing time in hours (h) as 'sample history' since the annealing temperature was slightly increased the longer the crystals were in use. Vacancy concentrations on the surface corresponding to data for one of the three TiO_2(110) samples are shown in Fig. 4.11 (data for the two other samples are identical within experimental uncertainties). We find an approximately linear correlation between the sample history and the vacancy concentration. The fact that the spanned range of vacancy concentrations is in good agreement with values derived from spectroscopic techniques [10] also supports the assignment of the A-I (vac) defects to single oxygen vacancies. Note that the highest densities of A-I (vac) defects on (1×1) terraces observed were ∼10 % ML. This implies that the concentration of single hydroxyls (A-II (OH) defects) amounts to ∼20 % ML. Such a high density, which we indeed observed for A-II (OH) defects, is too high to account for oxygen vacancies. We found that the highest oxygen vacancy density reported in the literature amounts to ∼14 % ML [46]. Typical values throughout the literature are, however, with ∼5 % ML clearly lower [10]. For vacancy concentrations higher than ∼10 % ML we observed that the morphology of the TiO_2(110) surface changes: Besides (1×1) terraces, also (1×2) strands evolve on the surface ([10] and Refs. herein).

Samples exhibiting (1×2) strands are discarded, and we thus did not attempt to monitor vacancy concentrations for more reduced samples. In summary, we assign with certainty the A-I (vac) defects to single oxygen vacancies in the rows of bridging oxygen atoms and the A-II (OH) and A-III (2OH) defects to single and paired bridging hydroxyls, respectively.

4.3.1.2 On-top O atoms on 5f-Ti sites

The observations using O_2 as a probe molecule also strongly support the assignment of the A-I (vac) defects to oxygen vacancies (Fig. 4.6 and 4.7). Experimentally we find exclusively single oxygen vacancies, a result which can be explained by repulsion between negative charges associated to vacancies [54, 55]. Thus, upon O_2 dissociation at vacancies, one O atom heals the vacancy and one O atom is left over. Therefore, the new protrusions on the Ti rows are likely to arise from single oxygen atoms, O_{ot}. This assignment is supported by the fact that the density of the new protrusions on the Ti rows is as high as the density of vacancies prior to O_2 exposure. Furthermore, this assignment is strongly supported by the DFT calculations summarized in Fig. 4.9. According to these and previous calculations [55], two vacancies per surface unit cell are required for the O_2 dissociation to become favorable. Experimentally we find that vacancies at the surface can be healed through O_2 exposure to the clean, reduced $TiO_2(110)$ surface at 120 K (Fig. 4.6 (a,b)). When comparing with the computational results, we conclude that the oxygen vacancies in the near-surface region provide the electrons to make the O_2 dissociation favorable. Hence, the configuration shown in Fig. 4.9 (e,f) is a more realistic model than the one sketched in Fig. 4.9 (a,b). Once the O_{ot} atoms have been deposited on the 5f-Ti atoms next to sites where vacancies resided prior to the O_2 exposure (Fig. 4.7), the O_{ot} atoms do not diffuse along the Ti rows. The latter we infer from time-lapsed STM movies. This observation holds also for higher temperatures, for instance RT, which is consistent with the calculated high diffusion barrier of ∼1.14 eV. Moreover, the presented results are largely consistent with previous reports where the presence of O_{ot} atoms on the $TiO_2(110)$ surface has been inferred from temperature programmed desorption (TPD) experiments [44, 45]. In agreement with Ref. [44], we find that O_{ot} atoms still reside on the $TiO_2(110)$ surface when water is coadsorbed at cryogenic temperatures followed by a flash to 375 K (data not shown). Furthermore, the presented data support the dissociative adsorption channel of O_2 molecules as previously reported in Refs. [44, 45]. However, our STM results indicate that dissociation of O_2 molecules is feasible even at ∼120 K (Fig. 4.6 (b)), whereas in Ref. [45] it has been concluded that O_2 molecules do not dissociate on the reduced $TiO_2(110)$ surface at temperatures lower than ∼150 K. The finding that O_2 dissociation is feasible even at ∼120 K suggests that O_2 molecules which desorb at ∼410 K [45] are stabilized on the surface because of other defects than bridging oxygen vacancies. The ability of the $TiO_2(110)$ surface to stabilize O_2 molecules at ∼120 K is presumably to a large extend caused by oxygen vacancies in the near-surface region which cannot be healed at this low temperature. Interestingly, an O_{ot} atom species adsorbed on five-fold coordinated metal atoms has also been found on the (110) face of RuO_2 [115, 116], an oxide surface which is isomorphous to the $TiO_2(110)$ surface. However, in contrast to the $TiO_2(110)$

surface where vacancies are a prerequisite to make dissociation of O_2 favorable, O_2 dissociation is feasible on the stoichiometric $RuO_2(110)$ surface, i.e. no vacancies are required [115]. This comparison reflects nicely that the ability to dissociate O_2 is determined by the electronic properties, since RuO_2 is a good conductor whereas TiO_2 is semiconducting.

In comparison to the O_2 adsorption experiment just discussed, the O_2 exposure at 120 K to a $TiO_2(110)$ surface with A-II (OH) defects (Fig. 4.6 (c)) leads to a completely different situation (Fig. 4.6 (d)). The fact that A-II (OH) defects still reside on the surface in spite of the O_2 exposure confirms our interpretation of these defects as being due to hydroxyls on bridging positions. The latter finds strong support when comparing with HREELS data reported by Henderson *et al.* [46]. These HREELS data (Fig. 4.6 of Ref. [46]) were collected from $TiO_2(110)$ surfaces which have been prepared using virtually the same recipe as we did in the second experiment using O_2 as a probe molecule (Fig. 4.6 (c,d)). With HREELS it was observed that the feature corresponding to bridging hydroxyls at $\sim$3665 cm^{-1} is broadened and slightly less intense after O_2 exposure at 120 K [46]. According to this finding, Henderson *et al.* concluded that bridging hydroxyls interact at 120 K with O_2 molecules, but also stated that a reaction does not take place [46]. Both techniques, STM and HREELS, point to a low reactivity of the bridging hydroxyls with O_2 molecules at this low temperature. However, something is puzzling regarding this experimental result since we observe a few new, unidentified protrusions on 5f-Ti sites and other protrusions which are likely to have arisen from the O_{ot} atoms. Thus, it appears that the O_2 molecules to some extend interact with the hydroxylated $TiO_2(110)$ surface already at 120 K, although the nature of this interaction is not understood in detail. Nevertheless, in view on the HREELS data, the comparison of the experiment with A-II (OH) defects being present on the surface (Fig. 4.6 (c,d)) with the one in which A-I (vac) defects dominate prior to O_2 exposure (Fig. 4.6(a,b)) also points to the assignments with the A-I (vac) and A-II (OH) defects corresponding to bridging oxygen vacancies and hydroxyls on bridging positions, respectively.

4.3.2 Comparison with literature

4.3.2.1 STM data

For a thorough discussion with respect to the nature of the observed Type-A defects in various STM studies addressing the $TiO_2(110)$ surface we find the following three criteria to be important. Our first criterion is the presence of paired hydroxyls on the surface (Fig. 4.2 (c)). According to Fig. 4.1 and 4.10, paired hydroxyls are characteristic for freshly prepared, reduced $TiO_2(110)$ surfaces. At first glance this statement might be irritating since one would expect that freshly prepared, reduced $TiO_2(110)$ surfaces are totally clean. This, however, is very hard to reach experimentally. Instead, a few water molecules have already reached the surface and have dissociated at oxygen vacancies prior to imaging of the sample. Therefore, we can take the presence of paired hydroxyls as a measure whether oxygen vacancies can be expected to be present at the surface. Note that the features arising from paired hydroxyls are easier to resolve than the faint features corresponding to vacancies. To the best of our knowledge, paired hydroxyls

on TiO_2(110) have not been reported so far using the STM technique. This we account as strong indication that the TiO_2(110) surfaces inspected previously with STM were probably in many cases hydroxylated.

The second criterion rests on the observation that defect-free areas on the nanometer scale can be produced on the TiO_2(110) surface by scanning at high tunneling voltages [18, 60]. The latter we also observed, although in Fig. 4.4 we solely show images in which voltage pulses have been successfully used for the same purpose. Furthermore, the initial configuration in the experiment illustrated in Fig. 4.4 was a TiO_2(110) surface which was only partly hydroxylated. This is the reason why in this particular case we did not end up with a perfect, stoichiometric TiO_2(110) surface, i.e., without any vacancies. The fact that Diebold *et al.* [18] and Suzuki *et al.* [60] succeeded to produce defect-free areas on the TiO_2(110) surface points to the view that in both these studies the initial configuration was a fully hydroxylated surfaces. Thus, there is full agreement on the observed production of defect-free areas on the TiO_2(110) surface between the reports by Diebold *et al.* [18], Suzuki *et al.* [60] and the present work. However, the suggestions to explain this result in Refs. [18, 60] differ markedly. A tip-induced re-oxidation of the TiO_2(110) surface, as proposed by Diebold *et al.* [18], is debatable. On the other hand, based on the results presented in Fig. 4.4 we agree with Suzuki *et al.* that protons originating from bridging hydroxyls are removed from the surface when scanning with high tunneling voltage [60]. Since the removal of protons is feasible at voltages as low as $\sim$2.5 V, the protons might be transferred to the STM tip rather than desorbed into the gas phase.

The third criterion we want to stress is connected to the contrast changes obtained while scanning TiO_2(110) surfaces with various degrees of hydroxylation. Frequent contrast changes have been reported by Diebold *et al.* [18] and also by Xu *et al.* [108]. Since we find contrast changes preferentially for fully hydroxylated TiO_2(110) surfaces, a link is very likely to exist between the state of the surface (with vacancies or with hydroxyls) and the likeliness of tip-changes resulting in STM contrast changes. Possibly, thereby also water molecules play a role, since the changes of the STM image contrast, such as shown in Fig. 4.5, often occur when the sample is exposed to water. The latter observation has previously led to the idea that faint spots, as shown in Fig. 4.5 (b), correspond to hydroxyls and bright, relatively broad protrusions (Fig. 4.5 (a)) to oxygen vacancies [52]. According to the presented results we now know that this assignment is not correct. Based on the results addressing tip-related phenomena for TiO_2(110) surfaces with predominantly single hydroxyls on one hand, and vacancies (and few single and paired hydroxyls) on the other, we propose that changes in the STM contrast are triggered by a proton transfer to the tip apex or alternatively, but less likely, by the adsorption of a water molecule on the tip apex. Thus, our observations related to tip-induced contrast changes are an additional indication that the TiO_2(110) surfaces previously studied with STM may in many cases have been hydroxylated.

How is it possible for clean, reduced TiO_2(110) surfaces on a short time scale to convert into hydroxylated surfaces even under excellent UHV conditions? First, the density of oxygen vacancies on the TiO_2(110) surface is usually only a few percent of a ML. This implies that already trace amounts of water in the rest gas are sufficient for the conversion of a clean, reduced TiO_2(110) surface to its hydroxylated state. In this respect it

is noteworthy that the sticking coefficient of water on the TiO_2(110) surface is high, not only for cryogenic temperatures [65]. Once the water molecules have been adsorbed, their mobility is expected to be very high at temperatures around RT. Thus, a high fraction of the water molecules will reach vacancies and dissociate. For these reasons, it is crucial to lower the water partial pressure in the low 10^{-11} Torr range and to cut down on the period of time between sample preparation and data acquisition. In addition to the time to reach a sample temperature close to RT after the sample was flashed, the STM technique requires a sample transfer and tip preparation prior to the data acquisition. Within this delay, an originally clean, reduced TiO_2(110) surface can easily be partially or in some cases completely converted to a hydroxylated surface. When starting with our best conditions at $\sim 3\times 10^{-11}$ Torr base pressure, a freshly prepared TiO_2(110) surface with $\sim$5 % ML oxygen vacancies is fully hydroxylated at RT typically after 30-60 min. Note that the partial pressure of water at the sample rises during annealing of the sample and part of the desorbed water may readsorb on the sample surface while cooling down to temperatures $\leq$300 K. For vacuum conditions of approximately 2×10^{-10} Torr, which are typical of many previous studies, this implies that a surface with 5 % ML vacancies can be fully hydroxylated within a few minutes. This may to a large extent explain why previously mainly hydroxyls have been imaged with STM instead of oxygen vacancies. However, the partial pressure of water and the portion of readsorption do not solely depend on the base pressure of the chamber, but also on the particular sample holder design and the pumping speed of the vacuum system.

It is reasonable to assume that the TiO_2(110) surfaces studied in various laboratories were originally free of hydroxyls since in most studies cited here, it is explicitly mentioned that the samples were flashed to elevated temperatures prior to scanning with STM. However, in some laboratories the samples have been flashed to very high temperatures. We believe that a short flash up to 600 K to free the surface from hydroxyls is more efficient than a flash to very high temperatures, since the delay time required when approaching RT is clearly shorter in the first case where the sample holder heats up to a lesser extent.

Finally, we would like to point out that in our experimental setup the partial water background pressure can be markedly lowered via cooling of the STM and the sample holder at the manipulator using liquid N_2. We have found out that in this way it is easier to achieve TiO_2(110) surfaces with clean vacancies for low-temperature experiments, because the cooling of the STM and the sample house works as an efficient water trap, which significantly lowers the H_2O partial pressure.

4.3.2.2 Spectroscopic data

According to the presented results clean, reduced TiO_2(110) surfaces quickly convert into hydroxylated surfaces even under very good UHV conditions. This result is in line with HREELS and UPS data reported previously. Using HREELS, a feature at 3665-3690 cm^{-1} has been observed, not only for water exposed surfaces, but also for "clean, nearly defect-free surfaces" [63]. In accordance with the present work, this feature has been associated to hydroxyls on bridging positions [46, 66]. Furthermore, UPS data support that the H_2O dissociation occurs quite easily on freshly annealed sur-

faces [42]. However, one should take into consideration that in Ref. [63] and also partly in Ref. [42], the surface was oxidized after sputtering and annealing to prepare stoichiometric surfaces. Therefore, it is more appropriate to compare our STM data with HREELS and UPS data taken from sputtered and vacuum-annealed surfaces. Since reduced TiO_2(110) surfaces are certainly more reactive than oxidized surfaces, the features derived by hydroxyls are expected to appear more intense than what was found previously in Ref. [63] and Ref. [42]. In fact, in case of HREELS, such data have been published recently [46]. A sharp and relatively intense feature at 3665 cm^{-1} has been found for a reduced TiO_2(110) surface which was exposed to water at low temperature followed by a flash to 375 K (Fig. 4.6 in Ref. [46], spectrum "b").

If the sample is kept at RT one might think that no water is present on the surface since the first-layer desorption feature in water TPD spectra occurs at $\sim$270 K [38, 46, 63, 65]. However, it is difficult to determine based on TPD results the net coverage of water on the TiO_2(110) surface at RT. To date, no conclusive model is available which explains the TPD results comprehensively [65, 73]. In addition, the tail of the first layer feature spans temperatures higher than 300 K (Fig. 1 in Ref. [46]). Thus, trace amounts of water cannot be ruled out based on TPD results. Note that for the thermal equilibrium, Brinkley *et al.* reported a water coverage of 0.01 ML (upper limit) at 350 K [65], and Pan *et al.* 0.07 ML (lower limit) at 300 K [37], respectively. These values are based on studies using modulated molecular beam scattering [65] and low-energy ion scattering [37], respectively. Even if these values overestimate the real water coverages under UHV conditions, all the vacancies at the surface can successively react with water molecules, and thus be converted to hydroxyls.

4.4 Conclusion and outlook

Based on high-resolution STM experiments in conjunction with DFT calculations addressing vacuum-annealed TiO_2-(1$\times$1) surfaces we reach the following conclusion:

1. Bridging oxygen vacancies show up in the STM images as faint spots on dark rows, but hydroxyls on bridging positions appear as protrusions on these rows as well. At typical scanning conditions, hydroxyls appear brighter in the STM images than vacancies, i.e. it is indeed possible to distinguish the two point defects from each other in high-resolution STM images. The ability to distinguish oxygen vacancies and hydroxyls allows us to determine the vacancy concentrations on the TiO_2(110)-(1$\times$1) surface very accurately. Even at our best conditions, part of the vacancies already reacted with water molecules, and thus being converted to hydroxyls prior to imaging with STM. Therefore, in order to trace back to the real vacancy concentration for a perfectly clean TiO_2(110) surface, it is necessary to divide the hydroxyl density by two and to add this value to the density of vacancies. We find that the vacancy concentration on a TiO_2(110)-(1$\times$1) surface increases approximately linearly as a function of annealing time and annealing temperature of the sample. Typical values for vacancy concentrations on the TiO_2(110)-(1$\times$1) surface lie between 2 and 8 % ML. Because of the quick hydroxylation of freshly prepared, reduced TiO_2(110) surfaces, the presented STM

images are certainly among the first to indeed show oxygen vacancies. From a thorough comparison to previous STM studies we surmise that the TiO_2(110) surfaces which have been studied so far were mostly hydroxylated.

2. Besides single hydroxyls also paired hydroxyls reside on TiO_2(110) surfaces, particularly in the case of freshly prepared, reduced samples. We can easily resolve the paired hydroxyls in high-resolution STM images since they appear as even brighter spots than single hydroxyls. The presence of paired hydroxyls indicates that the quick hydroxylation of the reduced TiO_2(110) surfaces is caused by water dissociation at vacancies, a mechanism which has been proposed previously [42, 52, 66]. DFT calculations confirm that the paired bridging hydroxyls are a very stable configuration on the TiO_2(110) surface.

3. Besides the presence of paired bridging hydroxyls, two further criteria exists to ascertain with STM whether TiO_2(110) surfaces are partly or fully hydroxylated. A clear indication of hydroxylated TiO_2(110) surfaces is the removal of Type-A defects when scanning with high tunneling voltage ($V_T \geq 2.5$ V). Using this methodology, exclusively the protons of the hydroxyls on bridging positions can be removed from the surface whereas vacancies cannot be removed. Thus, if defect-free areas on the TiO_2(110) surface can be produced the initial configuration was a fully hydroxylated surfaces. A second indication of hydroxylated TiO_2(110) surfaces is frequent contrast changes during scanning. These phenomena are tentatively explained as being triggered by proton transfer reactions between the surface and the tip apex.

4. Oxygen vacancies can be healed by dissociation of O_2 molecules. The dissociation of O_2 molecules was found for temperatures as low as 120 K. The dissociative O_2 adsorption is not only evident by the healing of vacancies but also by appearance of O atoms adsorbed on-top at 5f-Ti atoms. Such oxygen species has been inferred previously using spectroscopic data [44, 45]. The diffusion of on-top O atoms is inhibited by a large diffusion barrier as found computationally and confirmed experimentally. For temperatures $\leq$ RT this oxygen species does not diffuse at all.

5. A temperature as low as 120 K is too low for an efficient reaction between O_2 molecules and hydroxyls on the TiO_2(110) surface, i.e. hydroxyls still reside on the surface in spite of exposing the fully hydroxylated TiO_2(110) surface to O_2 at this temperature. However, upon O_2 exposure few new species appear on 5f-Ti atoms, indicating that the O_2 molecules to some extent interact with the hydroxylated TiO_2(110) surface even at 120 K. The experiments using O_2 as a probe molecule strengthen the assignments of the different features observed in the STM images.

With respect to previous publications from our group, several issues remain to be considered more in-depth. First, the enhanced density of hydroxyls after exposing the TiO_2(110) surface to high doses of water (Fig. 5 in Ref. [52]) is currently being studied more in detail. In addition, it is not clear from the presented results how the paired

hydroxyls undergo splitting into single hydroxyls. Furthermore, the conflict between the STM results addressing the oxygen chemistry on the $TiO_2(110)$ surface as reported here with respect to the findings presented in Ref. [110] should be reconciled.

Finally, it is worth mentioning that the quick hydroxylation of reduced $TiO_2(110)$-(1×1) surfaces even under very good UHV conditions might be a phenomenon of general relevance with respect to reducible oxide surfaces. This possibility is by far not devious since it is well-known that water molecules dissociate at oxygen vacancies for many oxide surfaces [62, 117]. Thus, for scanning techniques as well as for many other surface science techniques which rest on fairly long data acquisition times, special care is required in order to identify problems arising from hydroxylation of the oxide surfaces considered.

CHAPTER 5

Dynamics of water dissociation on TiO_2(110)

A combination of high-resolution scanning tunneling microscopy and density functional theory is utilized to study the interaction of water with the reduced TiO_2(110)-(1×1) surface. As the direct product of water dissociation in oxygen vacancies, paired hydroxyl groups are formed. These pairs are immobile and stable unless they interact with adsorbed water molecules. As a result of these interactions, protons are transferred to adjacent oxygen rows, thereby forming single hydroxyl groups. Additionally, we show that hydroxyl groups facilitate the diffusion of water molecules over the oxygen rows.

5.1 Introduction

Many previous studies addressing TiO_2(110) have assumed perfectly clean surfaces with bridging oxygen vacancies. However, as we showed in chapter 4 this assumption is not always justified. The reason is twofold: first, even in UHV, a small water background cannot be completely avoided, and second, water reacts very efficiently with bridging oxygen vacancies in a wide temperature range. The knowledge of how an oxide surface undergoes hydroxylation helps in characterizing the state of the oxide more precisely. Furthermore, the hydroxylation process itself is of broad interest for a better understanding of the chemistry on oxide surfaces. Note that in many applications the natural state of an oxide is such that hydroxyls are present at the surface [118].

In this chapter, the hydroxylation of the reduced TiO_2(110)-(1×1) surface is described by means of STM movies [113] and DFT calculations. We present the first STM images showing the dissociation of a single water molecule in an oxygen vacancy on an oxide surface. As a result, stable pairs of hydroxyl groups are formed in the bridging oxygen rows. Spontaneous splitting of the bridging hydroxyl pairs is not observed at any investigated temperature. However, the interaction with water molecules provides a path for the splitting of the bridging hydroxyl pairs into two single bridging hydroxyls that reside in adjacent bridging oxygen rows. Utilizing DFT calculations, we explain the splitting of a bridging hydroxyl pair as a sequence of proton transfers in the $[1\bar{1}0]$ direction. Finally, we show that water diffusion in the $[1\bar{1}0]$ direction is facilitated by bridging hydroxyl groups in the bridging oxygen rows. Based on these results, a previous STM study is reinterpreted (Ref. [110]).

5.1.1 Experimental and DFT details

The TiO_2(110) crystal used for the experiments presented in the following was dark blue, indicating an oxygen deficient, bulk-reduced sample. Using the STM, the bridging oxygen vacancy concentration was estimated to be 5.1 ± 0.2 % ML. The STM images presented here were all acquired in the constant current mode using a tunneling voltage of +1.25 V and a tunneling current of ∼0.1 nA.

The DFT calculations were done using the DACAPO package. We employed ultrasoft pseudopotentials, a plane wave basis (orbital cutoff: 25 Ry, density cutoff: 35 Ry), and the RPBE exchange-correlation functional [21]. The TiO_2(110) surface was modeled using (3×2) periodic slabs of four tri-layers, half of which were relaxed. Theoretically derived lattice constants (a = 4.69 Å, c = 2.99 Å, and u = 0.305) were used and estimates of the energy barriers were obtained by constrained relaxation.

5.2 STM results

Fig. 5.1 shows snapshots from a STM movie ("dissociation")[1] recorded after dosing ∼0.1 ML water on a freshly prepared TiO_2(110) sample at ∼110 K. Subsequently,

[1] Both movies "dissociation" and "splitting" (2.7 s/image) are acquired within the same experiment at ∼187 K (see additional information at www.phys.au.dk/spm).

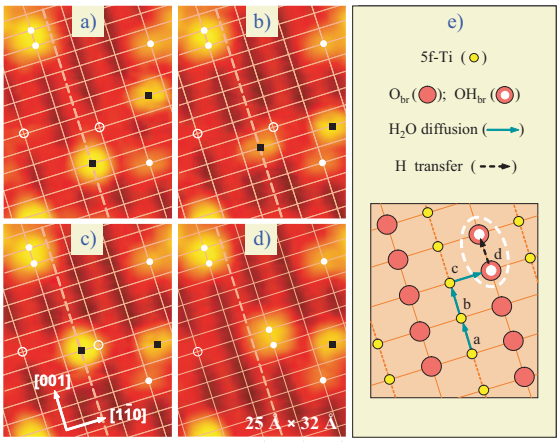

Figure 5.1. *(a)-(d) Dissociation of water in a bridging oxygen (O_{br}) vacancy on TiO_2(110) at ∼187 K (STM movie "dissociation"). Protrusions are labeled as follows: Bridging oxygen vacancies (open white circles), bridging hydroxyl (OH_{br}) groups (filled white circles), water on 5f-Ti sites (filled black squares). (e) Schematic: letters (a)-(d) mark oxygen positions of the water.*

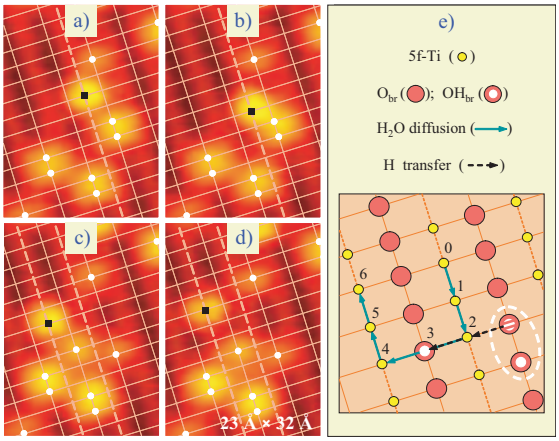

Figure 5.2. *(a)-(d) Splitting of a bridging hydroxyl pair mediated by a water molecule at ∼187 K (STM movie "splitting"). Protrusions are labeled as in [Fig. 5.1(e)]. Schematic: numerals 0-6 mark oxygen positions of the water for selected configurations that we will discuss in the DFT section. The hatched white disk indicates the proton of the pair that is transferred.*

the sample was slowly warmed up while recording STM movies. When imaging the $TiO_2(110)$ surface with the STM, dark rows correspond to geometrically protruding bridging oxygen atoms, whereas Ti atoms in the troughs appear bright [10]. In Fig. 5.1 various kinds of bright features on the dark rows, so-called type A defects, are discernible. Among the type A defects, bridging oxygen vacancies show up as faint spots, single bridging hydroxyls are imaged brighter, and bridging hydroxyl pairs are seen with even brighter contrast than single bridging hydroxyls (chapter 4). Besides the type A defects on the dark bridging oxygen rows, a protruding species is seen in Fig. 5.1(a) on the bright Ti troughs. Its identity is revealed when tracking the dynamics of this species. Focusing on the Ti trough marked by a dashed line, it is evident that this species is adsorbed on 5f-Ti sites, and diffuses along the Ti trough [Fig. 5.1(a)-(c)]. When this species reaches a 5f-Ti site next to a bridging oxygen vacancy [Fig. 5.1(c)], both the species on the Ti trough as well as the vacancy in the bridging oxygen row disappear, and are replaced by a bridging hydroxyl pair [Fig. 5.1(d)]. The reaction monitored in movie "dissociation" (Fig. 5.1) is explained straightforwardly when ascribing the species in the Ti trough to an isolated water molecule that dissociates in the vacancy [Fig. 5.1(e)]. This interpretation is consistent with temperature programmed desorption data in the literature [46, 62], since the species in the Ti troughs is absent after flashing the sample to 350 K. In addition, our DFT calculations presented below strongly support this interpretation.

The atomistic mechanism of water dissociation in bridging oxygen vacancies, which explains the formation of bridging hydroxyl pairs, has been suggested previously [42, 52, 66], but movie "dissociation" (Fig. 5.1) represents the first real-space images of this reaction. We observe water dissociation in bridging oxygen vacancies at $\sim$180 K, which is in line with recent vibrational data [46]. The bridging hydroxyl pairs are stable under the given experimental conditions, as, e.g., illustrated by the static appearance of the pair in the upper left corner of all images in Fig. 5.1. At temperatures of 300 K and above the bridging hydroxyls have been found to be able to diffuse along the [001] direction. The hopping rate at 300 K was found to be $\sim 10^{-4}$ OH^{-1} s^{-1}, meaning that diffusion events happen on the timescale of hours [81].

However, the bridging hydroxyl pairs split into two single bridging hydroxyl groups when interacting with water. Fig. 5.2 shows snapshots from STM movie "splitting", which was recorded in the same experiment as STM movie "dissociation". After a water molecule has diffused to a 5f-Ti site next to a bridging hydroxyl pair [Fig. 5.2(a) and (b)], several changes are discernible when comparing with the subsequent image [Fig. 5.2(c)]. Instead of the bridging hydroxyl pair in the center of Fig. 5.2(a) and (b), two single bridging hydroxyl groups are now seen, one residing at the same place as in Fig. 5.2(b), but the other in the adjacent bridging oxygen row on the left. In addition, the water molecule also appears on a different adsorption site, namely, shifted one Ti trough to the left. The changes seen in STM movie "splitting" suggest that water molecules mediate proton transfer from one bridging oxygen row to another, and further that water molecules can easily diffuse over the bridging hydroxyl groups in the bridging oxygen rows. The latter suggestion is supported by the STM images shown in Fig. 5.4. Here a water molecule is seen to jump to an adjacent Ti through when passing a single bridging hydroxyl. In Fig. 5.2(e) we show a schematic denoting likely intermediate

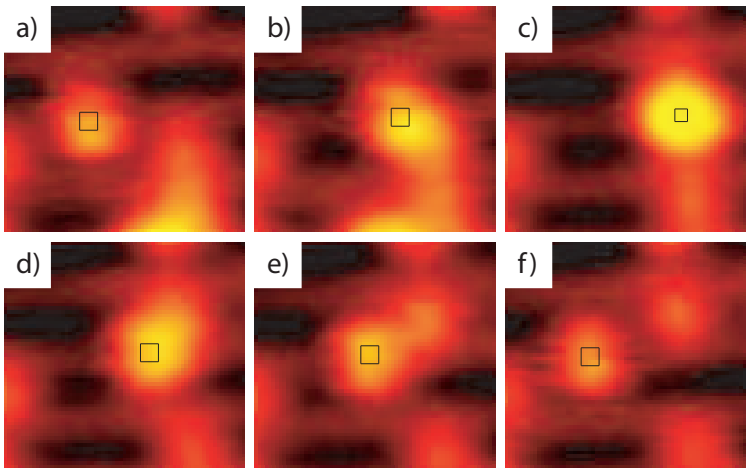

Figure 5.3. *Snapshots from a STM movie made at ∼186 K. The images show diffusion of a single bridging hydroxyl in the* $[1\bar{1}0]$ *direction. The diffusion process occurs as a single water molecule (black square) interacts with the bridging hydroxyl.*

configurations corresponding to STM movie "splitting".

We also observe diffusion of single bridging hydroxyls mediated by water molecules (see Fig. 5.3). However, the reverse reaction as compared to Fig. 5.2, i.e., the formation of bridging hydroxyl pairs from two single bridging hydroxyls, is found very rarely and only for high bridging hydroxyl coverages. This result indicates that water dissociation in bridging oxygen vacancies is the major channel for producing the bridging hydroxyl pairs. Also notably, we observe water diffusion over the ∼1.1 Å protruding bridging oxygen atoms at bridging hydroxyl groups (Fig. 5.4), but not at regular bridging oxygen atoms.

The series of STM images showing the diffusion of a single bridging hydroxyl in

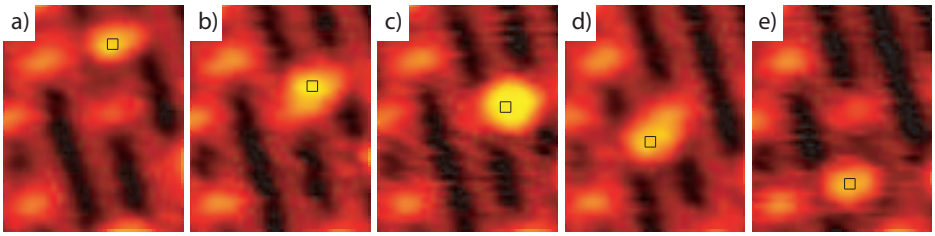

Figure 5.4. *Images from STM movie made at ∼187 K. A single water molecule (black square) diffuses along the [001] direction. As it passes by a single bridging hydroxyl it jumps to the adjacent Ti row.*

the $[1\bar{1}0]$ direction (Fig. 5.3) is indistinguishable from the STM movies previously published [110]. In Ref. [110], the dynamics of the $TiO_2(110)$ surface after oxygen exposure is described, and the STM movies have been interpreted as diffusion of O_2 molecules on a surface with bridging oxygen vacancies. However, according to our recent results discussed in chapter 4, it is evident that the type A defects in Ref. [110] were single bridging hydroxyls and not vacancies. The species diffusing in the Ti troughs in Ref. [110] is therefore reassigned to water molecules. Accordingly, also the proposed mechanism of "O_2 diffusion through bridging oxygen vacancies" must be corrected to "H_2O diffusion over bridging hydroxyl groups".

5.3 DFT calculations

We now turn to our DFT calculations, starting with the case of an isolated water molecule on the stoichiometric $TiO_2(110)$ surface. Previous calculations addressing this issue indicate that the adsorption energies for water being adsorbed either molecularly or dissociatively depend critically on the water coverage [10, 62, 75]. In accordance with Ref. [75], our calculations predict dissociation of an isolated water molecule on the stoichiometric $TiO_2(110)$ surface at low coverages to be preferred by 0.13 eV (Section 4.2.6.1). In the dissociated configuration, a terminal hydroxyl group resides in the Ti trough, and an adjacent bridging hydroxyl is formed. The dissociation reaction would be completed if these two OH groups were able to separate from each other. However, high barriers for the diffusion processes in the [001] direction inhibit the separation of the two OH groups. For the diffusion of the terminal hydroxyl group, the barrier is 1.17 eV, while the diffusion of the proton along the bridging oxygen rows is hindered by a barrier as high as $\sim$1.5 eV. Therefore, the state of an isolated water molecule on the stoichiometric $TiO_2(110)$ surface is "pseudo-dissociated", since the two OH groups remain neighbors. As we calculate only a small barrier ($\sim$0.4 eV) for the transition from the pseudodissociated to the molecular state of adsorbed water, we anticipate rapid dynamics of the protons. At the time scale of the STM experiments, the bridging hydroxyl may thus be formed many times at the bridging oxygen rows on alternating sides of the 5f-Ti site. Therefore, pseudo-dissociated water molecules appear in STM images as features which are symmetrical about the Ti troughs.

With the aim of modeling the reduced $TiO_2(110)$ surface, we calculate the energy profile for a water molecule diffusing from the Ti trough (Fig. 5.5, $s = 0$ Å; $s \sim 2.7$ Å) into an adjacent bridging oxygen vacancy ($s \sim 10.6$ Å), where it dissociates ($s \sim 14.3$ Å). In agreement with our STM results, we find low barriers for all diffusion and transfer processes (Fig. 5.5). The pseudo-dissociated water absorbed in the Ti trough ($s = 0$ Å) is comparable in energy to molecular adsorption of water in the bridging oxygen vacancy ($s \sim 10.6$ Å). However, upon dissociation in the bridging oxygen vacancy, more than 0.4 eV is gained. In addition, the barrier for this proton transfer is only 0.2 eV ($s \sim 12.4$ Å). As a result of the dissociation, a bridging hydroxyl pair is created, which is exactly what we observe with STM (Fig. 5.1).

Guided by our STM results in Fig. 5.2, we further use the DFT approach to study the splitting of bridging hydroxyl pairs mediated by an adsorbed water molecule. In

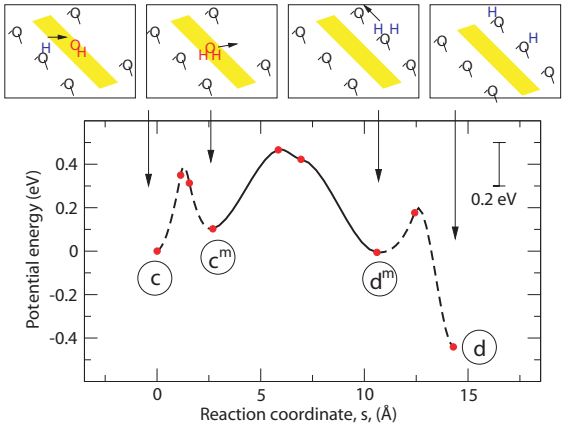

Figure 5.5. *Potential energy profile for water diffusion into a bridging oxygen vacancy and subsequent dissociation. Dashed lines are used for proton transfers and solid lines for water diffusion. Encircled characters refer to the positions as indicated in Fig. 5.1(e). The superscript "m" indicates that the water is in its molecular state. The reaction coordinate, s, is defined as $s_j = \sum_{i=1}^{j-1} \sqrt{|\Delta\vec{R}_{i,i+1}|^2}$, where $\Delta\vec{R}_{i,i+1}$ connects the $i'th$ and the $i+i'th$ configurations in $3N$ space, N being the number of atoms.*

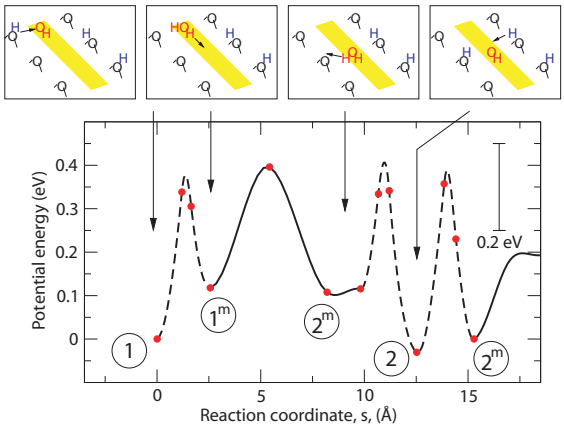

Figure 5.6. *Potential energy profile for the water mediated splitting of a bridging hydroxyl pair. As in Fig. 5.5, dashed lines indicate proton transfers and solid lines water diffusion. Encircled numbers refer to the positions that are labeled in Fig. 5.2(e). At $s \sim 15.3$ Å, the terminal hydroxyl group in the Ti trough has taken one of the protons from the bridging hydroxyl pair.*

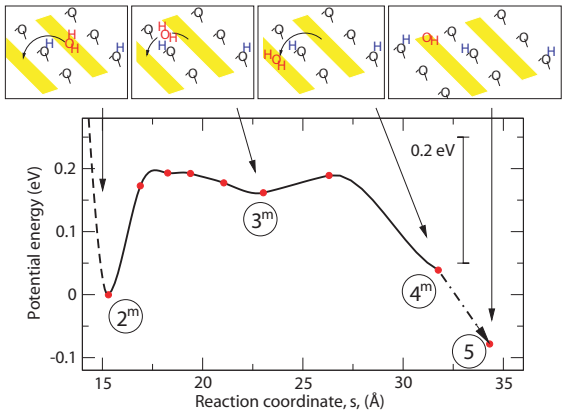

Figure 5.7. *Potential energy profile for the water diffusion in the* $[1\bar{1}0]$ *direction over the bridging oxygen row at a bridging hydroxyl group. Labels as in Fig. 5.6. The reaction coordinate of Fig. 5.6 is continued. To avoid falsifications through interaction of species over the periodic boundaries, the configurations* ④ *to* ⑤ *are calculated in a (3* $\times$ *3) supercell.*

Fig. 5.6, the energy profile and selected configurations are shown for the case when a water molecule diffuses to a position in the trough right next to a bridging hydroxyl pair. As in the case of the stoichiometric surface, the pseudo-dissociated state ($s = 0$ Å) is slightly preferred (here by 0.12 eV). After diffusion of the water in its molecular state to the Ti site next to one of the two bridging hydroxyl in a pair ($s \sim 9.8$ Å), one proton of the water molecule is transferred to the adjacent, bare bridging oxygen row; i.e., the water molecule pseudo-dissociates. In this configuration ($s \sim 12.5$ Å), the terminal hydroxyl group left behind in the Ti trough is surrounded by bridging hydroxyl groups on both sides. The diffusion of the water molecule may proceed when the terminal hydroxyl group takes a proton from either of the surrounding bridging hydroxyl. Splitting of the bridging hydroxyl pair occurs, because transferring a proton from a bridging hydroxyl pair is favored by 0.12 eV compared to the case where a proton is taken from the single bridging hydroxyl. Thus, in total a proton is transferred to the adjacent bridging oxygen row ($s \sim 15.3$ Å). Such a sequence of proton transfers is calculated to be possible also when a water molecule passes a single bridging hydroxyl. Accordingly, water molecules mediate the splitting of bridging hydroxyl pairs as well as the net bridging hydroxyl diffusion in the $[1\bar{1}0]$ direction.

Finally, we utilize DFT to study the diffusion in the $[1\bar{1}0]$ direction (from one Ti trough to another) of the water molecule left after the splitting of the bridging hydroxyl pair. The diffusion energy profile is shown in Fig. 5.7 for the direction, where the water passes over the adjacent bridging hydroxyl group and ultimately pseudo-dissociates at some distance to the bridging hydroxyl. The diffusion event is surprisingly facile, the barrier being only 0.19 eV, which we attribute to the formation of a strong hydrogen

bond between the proton of the bridging hydroxyl group and the oxygen of the water molecule (bond length: 1.79 Å at $s \sim 23.0$ Å). In the absence of the bridging hydroxyl group, we calculate a barrier as high as 0.6 eV (profile not shown) for the diffusion of water across the bridging oxygen row. This barrier is almost as high as the desorption energy on the stoichiometric surface, which amounts to 0.79 eV. In this hypothetical configuration where a water molecule diffuses over a bare bridging oxygen atom, only a weak hydrogen bond can be formed (length: 2.07 Å).

5.4 Conclusions

In summary, the hydroxylation process of the reduced $TiO_2(110)$ surface is elucidated by STM and DFT on the atomic scale. As a result of water dissociation in bridging oxygen vacancies, stable pairs of bridging hydroxyl groups are formed. However, the bridging hydroxyl pairs split into single bridging hydroxyl groups when interacting with adsorbed water molecules. The splitting reaction consists of several proton transfers with the result of net bridging hydroxyl diffusion in the $[1\bar{1}0]$ direction. In analogy, also the diffusion of single bridging hydroxyl groups is mediated by water molecules. Furthermore, it is shown that bridging hydroxyl groups facilitate the diffusion of isolated water molecules in the $[1\bar{1}0]$ direction.

CHAPTER 6

Creation and reactions of water dimers on TiO_2(110) surfaces

By means of high-resolution STM movies we have been able to observe the formation of stable water dimers and trimers on the rows of fivefold coordinated Ti atoms on TiO_2(110) surfaces. The trimers have a lifetime of a few minutes before they split again, while the dimers were not observed to split in the investigated temperature range from 176 K to 194 K. On a hydroxylated surface the water dimers are observed to readily interact with bridging hydroxyls to form a species assigned to $H_5O_2{}^+$ or H_5O_2. Through this interaction we show that water dimers are able to mediate the diffusion of bridging hydroxyls along both the [001] and $[1\bar{1}0]$ direction. On a quasi-stoichiometric surface the water dimers are observed to interact directly with the bare bridging oxygen rows to form a bridging hydroxyl and a H_3O_2 species in good agreement with recent DFT calculations.

6.1 Introduction

Water is perhaps the most important and pervasive chemical on our planet and is probably the most important adsorbate at TiO_2 surfaces [10, 62]. Many of the applications involving TiO_2 are performed in an aqueous environment, for example, almost all photocatalytic processes. And, as it was shown in chapter 4 even under UHV conditions the water vapor in the residual gas plays an important role for the state of the TiO_2(110) surface.

The interactions between water molecules and both the stoichiometric and reduced TiO_2(110) surfaces have been investigated using a variety of experimental techniques, e.g. PES [38,40,42], TPD [38,63,65] and STM [52,66,80], as well as DFT calculations [22, 75]. The focus has mainly been on the adsorption of H_2O and the interaction of H_2O with the bridging oxygen vacancies, although Lindan *et al.* [75] also performed calculations on water dimers on the stoichiometric TiO_2(110) surface thereby probing intermolecular water interaction. From water TPD one can also gain information on the intermolecular water interaction. Henderson found that the peak temperature of the first layer water TPD peak changes from ∼270 K at a full monolayer to ∼300 K at ∼1/10 of a monolayer [63], suggesting that the water molecules repel each other slightly at high compared to low coverages. However, it can be very difficult to gain specific information on a molecular level from measurements using averaging techniques like TPD.

Here we will show that water at low coverages will form water dimers and trimers. The dimers are completely stable at the investigated temperatures and have not been observed to split into single water molecules, while the trimers split reversibly into a water dimer and a single water molecule on a timescale of minutes. The water dimers were observed to interact readily with the bridging hydroxyls on the hydroxylated TiO_2(110) surface. On the a quasi-stoichiometric surface the water dimers were found to be able to transfer one proton to an adjacent bridging oxygen row to form a bridging hydroxyl and a H_3O_2 species. From these observations possible explanations for the discrepancy between theoretical calculations and experiments on water adsorption on the TiO_2(110) surface are suggested.

6.2 Results and discussion

6.2.1 Water dimer and trimer formation on hydroxylated TiO_2(110) surfaces

In Fig. 6.1 four snapshots from an STM movie are shown. The STM movie was recorded on a hydroxylated TiO_2(110) surface with a water coverage of ∼6.0 % ML at ∼179 K. In image (a) two protrusions arising from the same species are adsorbed on a bright row of fivefold coordinated Ti atoms. By fixing a grid (not shown) using the surrounding bridging hydroxyls the two protrusions are observed to be adsorbed on-top fivefold Ti atoms. The same species was observed in chapter 5 where it was assigned to a single water molecule on the basis of its dissociation in an oxygen vacancy forming a pair of bridging hydroxyls (Fig. 5.1). Between image (a) and (b) the two single water mole-

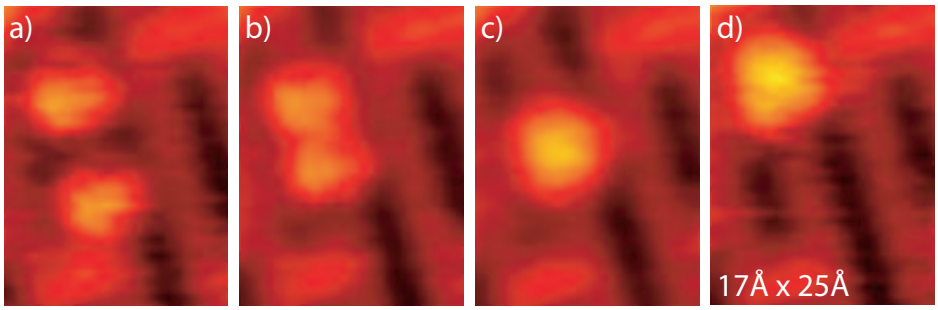

Figure 6.1. *Snapshots from an STM movie acquired on a hydroxylated TiO_2(110) surface with a water coverage of ∼6.0 % ML at ∼179 K. From (a) to (b) two single water molecules are observed to diffuse towards each other and merge to form a water dimer in (c). From (c) to (d) the water dimer is seen to move two lattice sites along the [001] direction.*

cules are seen to have moved towards each other. In image (c) the two species have disappeared and a single larger protrusion has appeared. Again by fixing a grid this protrusion is observed to be centered in between two fivefold coordinated Ti atoms. Since we do not find any changes in the surroundings when comparing (c) to (b), we will assign the species seen in (c) to the collection of two single water molecules, i.e. a water dimer. Comparing (d) to (c) the dimer is found to have moved two lattice sites in between the two images indicating that it moves as a single entity. Following many different dimers for extended periods of time on hydroxylated TiO_2(110) surfaces we found that they are very stable, i.e. they do not split into single water molecules again after formation. In the gas-phase the oxygen-oxygen distance for the water dimer has been found to be ∼2.96 Å [119–121], so the distance of 2.96 Å between fivefold coordinated Ti atoms should be favorable for water dimer formation, although the surface-water interaction might change the ideal oxygen-oxygen distance on the TiO_2(110) surface away from that of the gas-phase. Another oxide surface where water clustering has been observed is the MgO(100) surface, where the Mg-Mg distance is 2.98 Å [62]. However, on this surface it was argued that the H_2O molecules were displaced slightly from the on top Mg positions to shorten the oxygen-oxygen distance and thereby maximize the strength of the hydrogen bonding interactions.

The creation of larger water species is also possible. In Fig. 6.2 four additional snapshots from the same experiment as in Fig. 6.1 are shown. In Fig. 6.2(a) two species ascribed to a water monomer and dimer as seen in Fig. 6.1 are in close proximity. In Fig. 6.2(b) only one larger species is seen. This new species is found to be centered on-top a fivefold Ti atom, and since we do not see any other changes in the proximity we will assign this new species to a water trimer. From image (b) to (c) the water trimer is seen to have moved one lattice spacing in the [001] direction while in image (d) the water trimer is seen to have split spontaneously into two species, a water dimer and monomer. Notice that the dimer and monomer in (d) have switched positions as compared to (a).

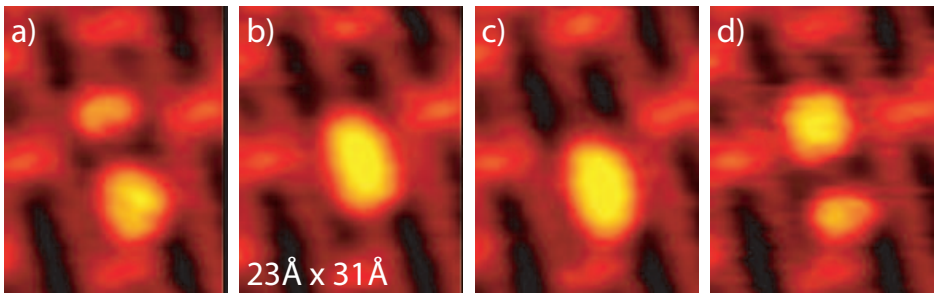

Figure 6.2. *Snapshots from an STM movie acquired at ∼186 K from the same experiment as the images shown in Fig. 6.1. (a) A water monomer and dimer is seen on the same row of fivefold coordinated Ti atoms. In (b) the two species in (a) are seen to have formed a single species. From (b) to (c) the single species is seen to have moved one lattice site along the [001] direction. (d) The single species has split into a water dimer and monomer. Notice that the monomer and dimer have switched positions as compared to (a).*

The STM movie from which the images in Fig. 6.1 and 6.2 are selected spans a temperature range from 176 K to 194 K. Within this temperature interval the lifetime of the water trimers, i.e. the time they could be followed before splitting into a water monomer and dimer again, changed from 6-7 min to less than a minute. Species resembling quadromers and pentamers could also be observed under the investigated conditions. However, these species do not diffuse around as single entities, but seem to split after the formation.

The fact that water dimers are very stable, whereas trimers and larger clusters seem to be less stable, could be a possible explanation for the observed shift in peak temperature of the first layer water TPD peak mentioned in the introduction. Monomers bind together quite strongly to form dimers, thereby stabilizing them on TiO_2(110) surfaces, however, the energy gained by additional water molecules in the creation of larger complexes is smaller, thus making them less stable on the surface and more prone to desorb.

The line profiles shown in Fig. 6.3 show a large difference in the height and width of the three species seen in Fig. 6.1 and 6.2. So by determining whether the species is centered on top Ti or on a bridge site and looking at the size of the protrusion it should be possible to distinguish between the three species. However, in chapter 5 we saw how single water molecules can interact with bridging hydroxyls resulting in diffusion along the $[1\bar{1}0]$ direction of the water monomer, the bridging hydroxyl or both. The water dimer and trimer can also interact with the bridging hydroxyls on the hydroxylated TiO_2(110) surface, and on quasi-stoichiometric[1] surfaces they can donate protons to the bridging oxygen rows, thereby creating a whole zoo of species. In the following only the dimer will be considered as this is the most predominant species under the investigated

[1] A quasi-stoichiometric surface is produced by exposing a hydroxylated TiO_2(110) surface to a metered amount of O_2 at RT. This treatment removes most of the bridging hydroxyls. For details see chapter 8.

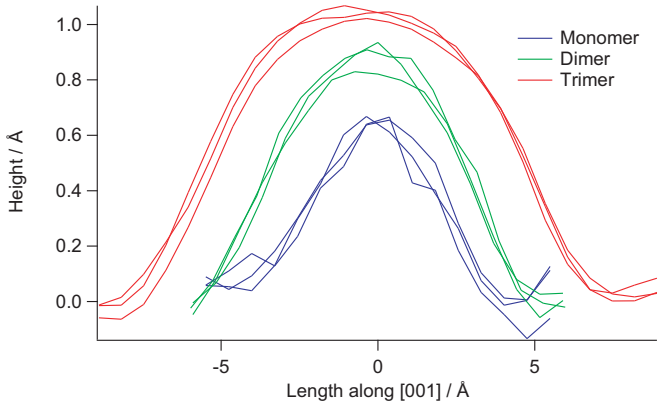

Figure 6.3. *Line profiles of a water monomer, dimer and trimer from the same experiment as the images shown in Fig. 6.1 and 6.2. For each species three line profiles taken from different STM images of the same protrusion are shown. All line profiles are along the [001] direction, which corresponds to the slow scanning direction in this experiment. Zero height for all the line profiles is equal to the height of the rows of fivefold coordinated Ti atoms.*

conditions with water coverages from ∼5 % ML up to ∼10 % ML.

6.2.2 Interaction of water dimers with bridging oxygen rows

6.2.2.1 Water dimers on hydroxylated TiO_2(110) surfaces

On hydroxylated TiO_2(110) surfaces water dimers interact readily with bridging hydroxyls. An example of such an interaction is shown in Fig. 6.4. Here a dimer is seen to diffuse from the bottom in Fig. 6.4(a) along a row of fivefold coordinated Ti atoms to the top in Fig. 6.4(d). When the dimer moves next to the bridging hydroxyl on the adjacent bridging oxygen row the bridging hydroxyl is seen to disappear and the protrusion associated with the water dimer appears slightly larger (Fig. 6.4(c)). In Fig. 6.4(d) the bridging hydroxyl has reappeared and the dimer is seen to have moved further. Comparing images (d) with (a) and (b) the bridging hydroxyl is seen to have moved one lattice site along the bridging oxygen row in the direction opposite of the water dimer movement. The protrusion seen in (c) is assigned to a water dimer that has accepted one proton or hydrogen atom from a bridging hydroxyl, i.e. an $H_5O_2^+$ or H_5O_2 complex (for simplicity we will term this complex $H_5O_2^{\delta+}$ in the following).

The example of the interaction between a water dimer and the bridging hydroxyl shown in Fig. 6.4 illustrates nicely the typical interaction picture. In the temperature interval where we can track the water dimers on hydroxylated surfaces (up to ∼195 K), whenever a water dimer comes next to a bridging hydroxyl the reaction shown in Fig. 6.4 occurs. When the bridging hydroxyl reappears it always does so on one of the two bridging oxygen rows adjacent to the Ti-row on which the water dimer was adsorbed, and the

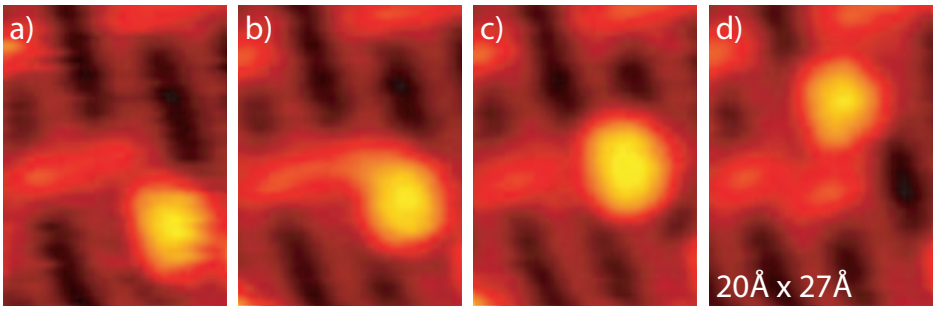

Figure 6.4. *Four snapshots from an STM movie acquired at ∼184 K on a hydroxylated TiO_2(110) surface with a bridging hydroxyl coverage of 11.6 % ML. From (a) to (d) the water dimer is seen to move along the [001] direction from the bottom to the top of the image. As the water dimer comes next to the bridging hydroxyl on the adjacent bridging oxygen row in (c), the bridging hydroxyl disappears and the protrusion associated with the water dimer appears slightly larger. In (d) the bridging hydroxyl has reappeared and the protrusion associated with the dimer has the same size as in (b). Comparing (d) with (a) or (b) the bridging hydroxyl missing in (c) is seen to have moved one lattice site in the opposite direction of the dimer.*

position along the [001] direction depends on the direction in which the water dimer moved. If the water dimer effectively moved past the bridging hydroxyl (comparing before and after the creation of $H_5O_2{}^{\delta+}$) the bridging hydroxyl will effectively have moved one lattice site in the [001] direction (as the example shown in Fig. 6.4). If the water dimer moved back in the same direction as it came from the position of the bridging hydroxyl will be the same along the [001] direction before and after the interaction. However, the position along the $[1\bar{1}0]$ direction might have changed, as the changes in the two directions seem to be independent. The four possible outcomes with respect to the position of the bridging hydroxyl after interaction with a water dimer compared to before the interaction are illustrated in Fig. 6.5.

The lifetime of the $H_5O_2{}^{\delta+}$ species before it turns again into a bridging hydroxyl and water dimer is also an interesting point. If the $H_5O_2{}^{\delta+}$ species is much more stable than a bridging hydroxyl plus water dimer, then the bridging hydroxyls would effectively bind the water dimers and prevent them from diffusing on the TiO_2(110) surface, since the mobility of $H_5O_2{}^{\delta+}$ is very low. At the lowest temperatures where we have followed the dimers (∼150 K) the $H_5O_2{}^{\delta+}$ species has a lifetime of several minutes, while at temperatures around 184 K (the example shown in Fig. 6.4) the average lifetime was on the order of 30 sec. For example, at room temperature the lifetime of this species would be too short to be observed with STM at the present scanning speeds.

When water is coadsorbed with hydrogen on metal surfaces, evidence for hydronium (H_3O^+) have been found [62]. The hydronium species were found to be stabilized by forming $(H_3O^+)(H_2O)_n$ clusters in line with our observations [122]. However, we are not aware of similar findings on oxide surfaces. This might be due to the very small

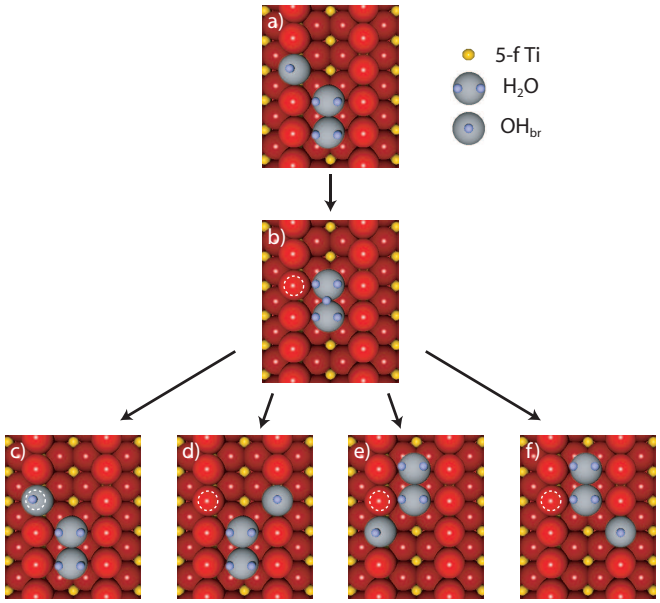

Figure 6.5. *Ball model showing the possible outcomes of the interaction between a water dimer and a bridging hydroxyl. (a) is the starting configuration from which the water dimer moves next to the bridging hydroxyl to create the* $H_5O_2{}^{\delta+}$ *complex in (b). The white dashed circle marks the position of the initial bridging hydroxyl in images (b) to (f). (c - d) The water dimer moves back in the direction from which is came. The bridging hydroxyl does not change its position along the [001] direction. (e - f) The water dimer continues to move upwards, thereby moving past the bridging hydroxyl. The bridging hydroxyl moves effectively one lattice site in the [001] direction.*

concentration of the $H_5O_2{}^{\delta+}$ species, rendering its detection with averaging techniques extremely difficult. And even using a local probe like STM it would be very difficult to assign the species from static images, i.e. without doing time-resolved STM movies.

6.2.2.2 Water dimers on quasi-stoichiometric TiO_2(110) surfaces

In another experiment we prepared a quasi-stoichiometric TiO_2(110) surface by exposing a hydroxylated TiO_2(110) surface to 20 L O_2 at ∼300 K (see chapter 8 for details). Subsequently, the quasi-stoichiometric surface was exposed to water giving a water coverage of ∼9 % ML. On this surface an STM movie was recorded to follow the reactions and diffusion of the water molecules at temperatures around 205 K. An image of the surface area scanned in the STM movie can be seen in Fig. 6.6. The water dimers were observed to interact with the bare bridging oxygen rows. An example of such an interaction is shown in Fig. 6.7. From (a) to (b) the water dimer has jumped one lattice site along the [001] direction. From (b) to (c) a bridging hydroxyl has appeared one

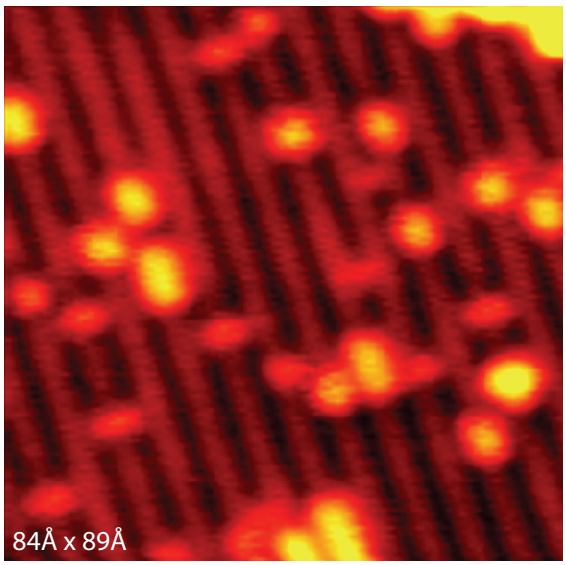

Figure 6.6. *STM image of the water exposed quasi-stoichiometric TiO_2(110) surface scanned in the STM movie. The image was acquired at 205 K and the water coverage is ∼9.0 % ML.*

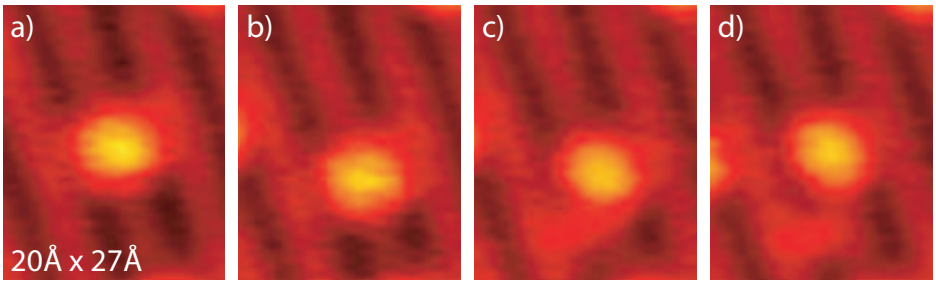

Figure 6.7. *Four snapshots from an STM movie acquired after water exposure on a quasi-stoichiometric TiO_2(110) surface at ∼205 K. (a - b) A water dimer adsorbed on a row of fivefold coordinated Ti atoms is seen to move one lattice site along the [001] direction. (b - c) A bridging hydroxyl appears one lattice site away from the the water dimer. (c - d) The protrusion is seen to move away one lattice site from the created bridging hydroxyl.*

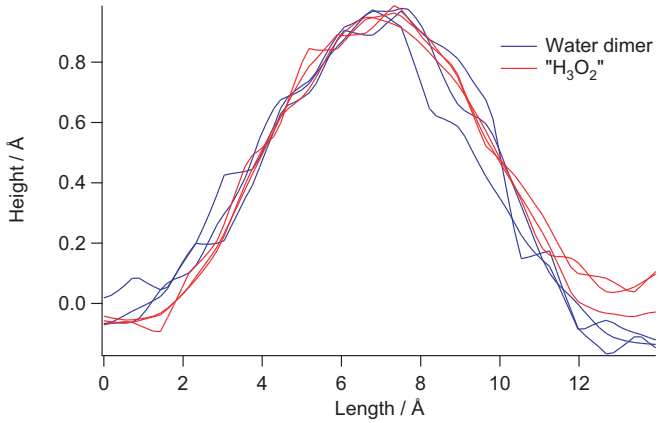

Figure 6.8. *Line profiles of the water dimer seen in Fig. 6.7(a) and (b), and H_3O_2 species seen in (c) and (d). For both species three line profiles were taken from three different STM images. All heights are with respect to the height of the fivefold coordinated Ti atom rows.*

lattice site from the protrusion associated with the water dimer in (b). Since nothing else changed in the near surroundings and since the diffusion properties of the protrusion associated with the water dimer were clearly different after this event, we attribute the appearance of the bridging hydroxyl to the following reaction:

$$H_4O_2 + O_{br} \rightarrow H_3O_2 + OH_{br} \tag{6.1}$$

The new species, H_3O_2, was much less mobile than the water dimers under the investigated conditions, which along with the observation of the creation of a new bridging hydroxyl was the best way to assign the new species. The hopping rate for the H_3O_2 species was $\sim$0.01 s^{-1} compared to the hopping rate of the water dimer which was $\sim$0.3 s^{-1}. Line profiles of the H_3O_2 species compared with the water dimer are shown in Fig. 6.8. From the line profiles it is obvious that comparing sizes of the protrusions seen in STM is not a reliable way of distinguishing the water dimer from the H_3O_2 species.

The exact charge state of the H_3O_2 species, could not be determined from the STM measurements, i.e. the new species might very well be negatively charged instead of neutral as the labeling suggests.

6.2.3 Comparison with DFT calculations

Regarding adsorption of water on TiO_2(110) surfaces there is a considerable disagreement between theoretical calculations and experimental results. While theory usually predicts dissociative adsorption as favorable on the stoichiometric TiO_2(110) surface, experiment only shows water dissociation at vacancies (see discussion in e.g. [10, 62,

75]). In chapter 5 we argued that the discrepancy for single water molecules could be due to the fact that the terminal hydroxyl left on the row of fivefold coordinated Ti atoms after dissociation is not mobile and hence not able to move away from the split of proton. In a recent paper by Lindan and Zhang [75] the adsorption properties of water dimers on the stoichiometric TiO_2(110) surface were also investigated. And in good agreement with the observations presented here, these authors found a mixed state with one water molecule in a molecular state and the other in a dissociated state to be the most stable configuration. The difference from the monomer case is then that we find the H_3O_2 species to be mobile under the investigated conditions. However, as we very seldom observe the reaction in Eq. (6.1) on the hydroxylated TiO_2(110) surface there seems also to be an effect of the surface state on the energetics of this reaction. As most theoretical calculations have been performed on stoichiometric surfaces this could be another contributing factor to the discrepancy between theoretical calculations and findings in surface science experiments on hydroxylated TiO_2(110) surfaces.

6.3 Conclusions

We have presented results showing that water molecules adsorbed on TiO_2(110) surfaces form stable water dimers and trimers. The water dimers are stable in large temperature and time intervals, while trimers have lifetimes of a few minutes at the investigated temperatures of $\sim$176 K to $\sim$194 K. On a hydroxylated TiO_2(110) surface the water dimer readily interacts with a bridging hydroxyl to form what we propose is a $H_5O_2{}^+$ or maybe H_5O_2 species. The lifetime of this new species was on order of 30 sec at $\sim$184 K. Through the formation of this complex the water dimer can mediate the diffusion of bridging hydroxyls in both the [001] and $[1\bar{1}0]$ direction.

On the quasi-stoichiometric TiO_2(110) surface the water dimer was found to interact with the bare bridging oxygen rows by creating a bridging hydroxyl:

$$H_4O_2 + O_{br} \rightarrow H_3O_2 + OH_{br} \tag{6.2}$$

in good agreement with recent theoretical calculations. The H_3O_2 species formed in the reaction was found to have a hopping rate of $\sim$0.01 s^{-1} at the investigated temperatures around 205 K.

CHAPTER 7

Diffusion of water monomers and dimers on TiO_2(110) surfaces

Fast scanning STM was utilized to follow the diffusion of water monomers and dimers on rows of 5f-Ti atoms on hydroxylated and quasi-stoichiometric TiO_2(110) surfaces. The energy barrier for water monomer diffusion was found to be 0.50 eV on the hydroxylated surface and 0.04 eV higher on the quasi-stoichiometric surface. For water dimer diffusion on hydroxylated TiO_2(110) surfaces the energy barrier and the prefactor were found to be $\sim$0.2 eV and 10^5-10^6, respectively. The very low prefactor suggests influence of tunneling in the diffusion process. However, when comparing the diffusion of D_2O and H_2O dimers, we did not detect a significant isotope effect. On the quasi-stoichiometric TiO_2(110) surface water dimer diffusion was found to have an energy barrier > 0.5 eV and a prefactor consistent with pure thermally activated diffusion.

7.1 Introduction

Diffusion of adsorbed species is one of the fundamental aspects of surface processes like chemical reactions and the growth of clusters and epitaxial films. For example, in surface catalyzed reactions a general prerequisite is diffusion of the adsorbed species.

Studies of adsorbate diffusion on metal surfaces have been pursued by many groups utilizing a number of different techniques (see e.g. [123]). However, on oxide surfaces and TiO_2(110) in particular only very few investigations of diffusion have been carried out. In chapter 5 we showed how water molecules can mediate the diffusion of bridging hydroxyls on TiO_2(110) surfaces and in Ref. [81] the thermally activated bridging hydroxyl diffusion on TiO_2(110) was investigated.

Previously we have identified the single water molecule from its dissociation in a bridging oxygen vacancy thereby creating a pair of bridging hydroxyls (chapter 5). Furthermore, we tracked the formation of water dimers from these water monomers in chapter 6. Here, utilizing fast scanning STM, we follow the diffusion of water monomers and dimers on hydroxylated TiO_2(110) surfaces and quasi-stoichiometric TiO_2(110) surfaces, i.e. surfaces with no oxygen vacancies and no or very few bridging hydroxyls (see chapter 8 for details). From Arrhenius plots of the extracted hopping rates we estimate prefactors and energy barriers for the diffusion of the two species and discuss possible mechanisms for the water dimer diffusion.

7.2 Basics of diffusion analysis

Adsorbates diffuse on the surface by moving from one potential energy surface minimum to another through an activated state called the transition state. The energy of the

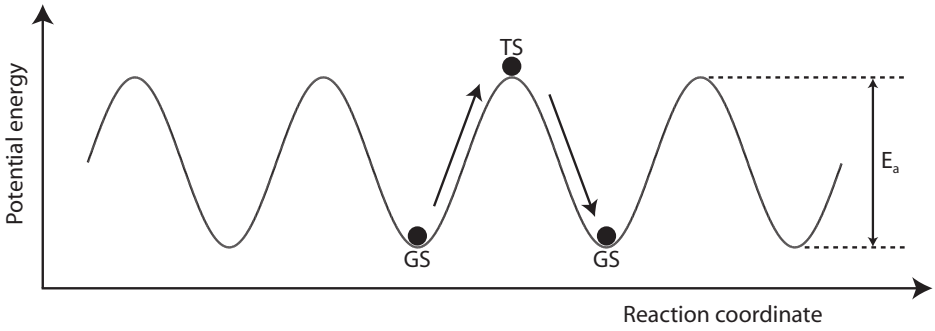

Figure 7.1. *A one-dimensional potential energy surface for an adsorbate. The adsorbate spends almost all its time in the energy minimum or ground state (GS). To diffuse from one energy minimum to another the adsorbate has to go through the activated state called the transition state (TS). The energy difference between the energy minimum and the transition state is called the activation energy (E_a).*

transition state is E_a higher than the energy minimum as illustrated in Fig. 7.1. If the thermal energy is much smaller than the diffusion barrier, $k_B T \ll E_a$, we can assume that individual diffusion events are uncorrelated, since the adsorbate remains most of the time in the adsorption well and only rarely attains enough energy to overcome the diffusion barrier. For such cases, the diffusion is well-described by a random walk process, which can be modeled mathematically by a Poisson process with a mean hopping rate h [124]. The probability that an adsorbate will perform N jumps during a period of time t, is then given by:

$$p(N) = \frac{(ht)^N e^{-ht}}{N!} \tag{7.1}$$

The mean hopping rate h is closely connected to the energy barrier the adsorbate has to overcome and the nature of the diffusion process through the so-called Arrhenius equation:

$$h = h_0 e^{-E_a/k_B T}, \tag{7.2}$$

which generally holds for thermally activated processes. A theoretical foundation for the Arrhenius equation (Eq. 7.2) is provided by transition state theory [123]. Transition state theory also allows us to estimate the prefactor or attempt frequency h_0. For processes where there is no difference in entropy between the ground state and the transition state h_0 will typically be in the range 10^{12} to 10^{13} [123].

7.2.1 Extracting diffusion parameters from STM experiments

STM movies are discrete samples in time of the same area of the surface. This means that we are not tracking an adsorbate continuously but only sampling its position at fixed time intervals determined by the scanning speed and the size of the scanned area. From these discrete samples we can deduce the probability for an adsorbate to move a specific number of sites between two STM images. The probabilities are plotted as displacement distributions as the one shown in Fig. 7.2. Inherently, we are not necessarily sensitive to all diffusion events. Between two STM images, an adsorbate could, for example, jump to a neighboring site and jump back to its origin. In the displacement distribution this "event" contributes to the zero displacement probability. Therefore it is a non-trivial task to extract the true hopping rate from STM measurements, because one can not simply calculate the number of jumps made by an adsorbate by adding the measured displacements.

The correct statistical analysis of displacement distributions for one-dimensional diffusion obtained from discrete samples of adsorbate positions was developed by Ehrlich and co-workers [124, 125]. In general one has to consider both jumps between nearest neighbour sites and longer jumps [125], however, here we will only consider jumps between nearest neighbour sites as it was done in [124].

The probability $p(N)$ for making N jumps in a time interval t is given by the Poisson distribution (Eq. 7.1) and the probability of reaching a point x (in units of the nearest

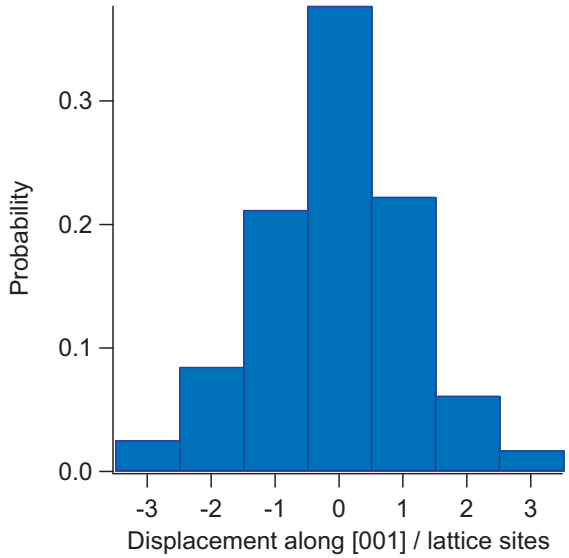

Figure 7.2. *Example of a displacement distribution made by tracking several single water molecules at 204 K. The displacement distribution is made by comparing the positions of the adsorbates in consecutive images. A total of 479 events have been used to make the shown displacement distribution. Only the probabilities for zero, one, two and three jumps are shown, since these were the only ones used for checking for long jumps.*

neighbour distance) after N jumps on a one-dimensional grid is given by the binomial expression

$$p_x(N) = \left(\frac{1}{2}\right)^N \frac{N!}{\left(\frac{N+x}{2}\right)!\left(\frac{N-x}{2}\right)!} \tag{7.3}$$

The displacement probability $P_x(h,t)$ for finding the adsorbate at a distance x from its origin after a time interval t is then given by

$$\begin{aligned} P_x(h,t) &= \sum_{N=0}^{\infty} p_x(N)p(N) && (7.4)\\ &= \sum_{N=0}^{\infty} \left(\frac{1}{2}\right)^N \frac{N!}{\left(\frac{N+x}{2}\right)!\left(\frac{N-x}{2}\right)!} \frac{(ht)^N e^{-ht}}{N!} && (7.5)\\ &= e^{-ht}\left(\frac{ht}{2}\right)^x \sum_{k=0}^{\infty} \frac{\left(\frac{ht}{2}\right)^{2k}}{(k+x)!k!} && (7.6)\\ &= e^{-ht} I_x(ht) && (7.7) \end{aligned}$$

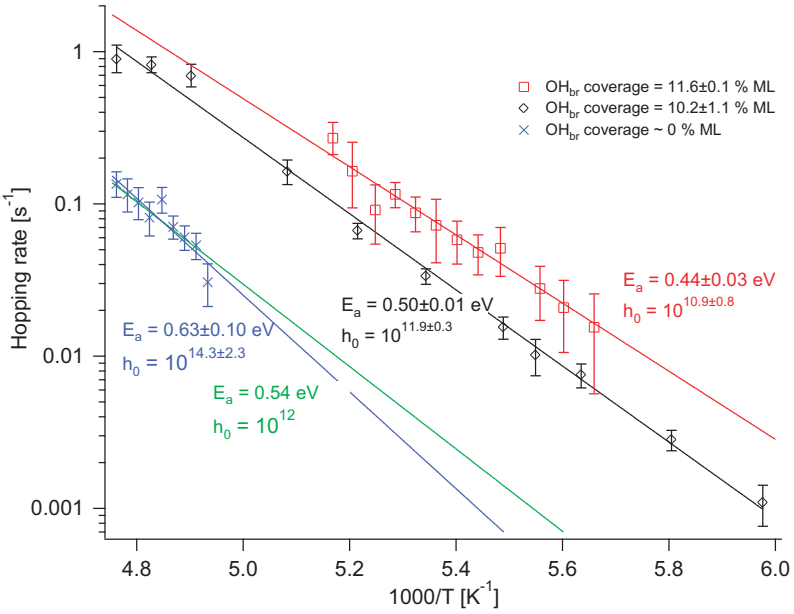

Figure 7.3. *Three Arrhenius plots for the diffusion of water monomers along the [001] direction. The water molecules were only tracked when no bridging hydroxyls were on neighboring sites. The two upper data sets (red squares and black diamonds) are from two hydroxylated TiO_2(110) surfaces, having different bridging hydroxyl concentrations. While the lowest data set is from a quasi-stoichiometric TiO_2(110) surface. Activation barriers and prefactors from the fits to the three sets of data are also shown including the standard deviations. For the data from the quasi-stoichiometric surface a fit was also done keeping the prefactor fixed at 10^{12} (green curve).*

where the substitution $N = 2k + x$ has been used to simplify the expression. I_x is the modified Bessel function of the first kind of the order x, and a closed analytical expression relating the displacement distribution $P_x(h, t)$ to the mean hopping rate h has thus been obtained.

From Eq. 7.7 the hopping rate can be obtained. By comparing hopping rates obtained from P_0, P_1, P_2 and P_3 it is possible to check whether long jumps are involved in the diffusion process [126].

7.3 Results and discussion

7.3.1 Diffusion of water monomers

In Fig. 7.3 three Arrhenius plots for the diffusion of water monomers along the [001] direction are presented. The water molecules were only tracked when no bridging hy-

droxyls were present on neighboring sites. The two upper data sets are from two hydroxylated TiO_2(110) surfaces, having different bridging hydroxyl concentrations. The data points marked with red squares are all from one very long STM movie (4000 images) taken on the same area of the TiO_2(110) surface in a temperature interval from 176 K to 194 K. The water coverage and bridging hydroxyl coverage in the surface area scanned were $\sim$6.0 % ML and 11.6 % ML, respectively. The shown diffusion parameters were found by fitting to the logarithmic form of the Arrhenius equation (Eq. (7.2)). The data points marked with black diamonds are from several shorter STM movies acquired on another TiO_2(110) crystal in a range of different temperatures. All movies were acquired on surface areas with similar bridging hydroxyl and water coverages, which on average were 10.2 % ML and $\sim$5 % ML, respectively. The diffusion parameters are again from a fit to the logarithmic form of Eq. (7.2). The third set of data points (blue crosses) are from one long STM movie (1730 images) made on a quasi-stoichiometric surface, which was prepared by exposing a hydroxylated TiO_2(110) surface to 20 L O_2 at $\sim$300 K. This treatment removes the bridging hydroxyls from the surface without re-oxidizing the bulk of the sample. The details of the reaction between the O_2 and the bridging hydroxyls will be accounted for in chapter 8. After the O_2 exposure the quasi-stoichiometric surface was exposed to a small amount of water at 147 K giving a water coverage of $\sim$9.0 % ML. The data points were like the two other data sets fitted to the logarithmic form of Eq. (7.2) (blue curve).

The energy barriers derived from the data on the hydroxylated surfaces are in relatively good agreement with the barrier of 0.4 eV found from DFT for H_2O hopping from one 5f-Ti to the next (see Fig. 5.6). The prefactors are also in good agreement with what one would expect from transition state theory, i.e. 10^{12} to 10^{13} [123]. Comparing the two sets of data acquired on the hydroxylated surfaces with the data from the quasi-stoichiometric surface it is clear that on the latter hopping rates are significantly lower at the investigated temperatures. Taking into account the standard deviations, prefactors for the three fits are virtually identical. However, there is a significant difference between the energy barriers found, the barrier being higher for the quasi-stoichiometric surface than for the hydroxylated surfaces. To be able to better compare the difference between energy barriers a fit was made to the data set from the quasi-stoichiometric surface with the prefactor fixed at 10^{12} (green curve). The justification for comparing in this way is that we do not expect a significant difference for the hopping rate prefactors from the different samples because the transition state for the diffusion on the quasi-stoichiometric and hydroxylated surfaces are probably very similar, since we only follow the diffusion on hydroxylated surfaces where there are no neighboring bridging hydroxyls. Comparing the energy barrier found from the fit with the fixed prefactor and the energy barrier for diffusion on the surface with 10.2 % ML bridging hydroxyl coverage, there is a difference of $\sim$0.04 eV. An explanation for this difference could be the "pseudo-dissociated" state of the water molecule, a term that was introduced in chapter 5. From DFT we found that the most stable configuration for water monomers is a dissociated state. On the stoichiometric surface water molecules gain $\sim$0.13 eV by transferring one proton to an adjacent bridging oxygen row (Fig. 4.8). However, on a hydroxylated surface the energy gain from transferring a proton to an adjacent bridging oxygen row will depend on whether other bridging hydroxyls are already present on

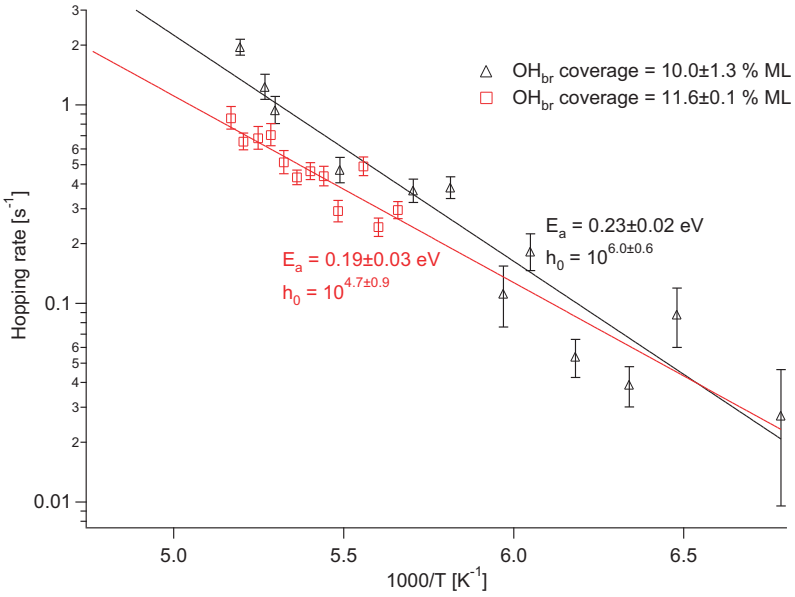

Figure 7.4. *Arrhenius plots for the diffusion of water dimers along the [001] direction including fits of the shown data sets to the logarithmic form of the Arrhenius equation. The hopping rates are for water dimers not interacting with bridging hydroxyls, i.e. water dimers were only tracked when bridging hydroxyls were not on neighboring sites.*

the oxygen row in question. From Fig. 4.8(e) and (f) it is clear that neighboring bridging hydroxyls repel each other and the energy gained by completely separating such a pair is ∼0.15 eV. The effect that bridging hydroxyls repel each other will cause the "pseudo-dissociated" state to become less stable on hydroxylated surfaces compared to stoichiometric surfaces, i.e. the energy difference between the dissociated and molecular state will be smaller. Because this energy difference contributes directly to the barrier for water diffusion the barrier should be lowered on hydroxylated surfaces.

The observation that hopping rates for water monomer diffusion depend on the bridging hydroxyl coverage has been reported previously [127]. However, at the time Ref. [127] was written the assignment of the protrusions on the bridging oxygen rows was not correct, i.e. the protrusions we now assign to bridging hydroxyls were erroneously assigned to bridging oxygen vacancies. Also, the protrusions seen on the rows of fivefold coordinated Ti atoms were assigned to O_2 molecules instead of water molecules (see Erratum for Ref. [110]).

7.3.2 Anomalous water dimer diffusion on TiO_2(110) surfaces

In chapter 6 we showed that water monomers can form stable water dimers that diffuse along the rows of fivefold coordinated Ti atoms. In two sets of experiments we have

followed the diffusion of these water dimers at different temperatures to be able to extract prefactors and energy barriers for their diffusion. The data set in Fig. 7.4 marked with red squares is extracted from the same long STM movie as the red squares in Fig. 7.3 for the monomer diffusion. As for the monomers we conducted an additional experiment by acquiring several STM movies at different temperatures on the same hydroxylated TiO_2(110) crystal (black triangles in Fig. 7.4). However, the movies were acquired on different areas of the crystal surface giving a slightly larger spread in bridging hydroxyl and water coverages for this data set than for the data set from the one long STM movie of the same area on a TiO_2(110) surface. The fits to both data sets show energy barriers around 0.2 eV and prefactors in the order of $\sim 10^5$ to 10^6. Thus, both the energy barriers as well as the prefactors are very different from the ones observed for water monomer diffusion on hydroxylated TiO_2(110) surfaces. The low energy barrier could indicate that the path the water molecules follow in their diffusion from one 5f-Ti to the next is very different for the dimer than for the monomer and that the second water molecule stabilizes the water molecule that is diffusing. We have previously encountered a barrier of $\sim$0.2 eV for diffusion of water molecules in the $[1\bar{1}0]$ direction over the bridging oxygen row at a bridging hydroxyl group (see Fig. 5.7). The water molecule diffusing was in this case stabilized by a strong hydrogen bond between the bridging hydroxyl and the water molecule. A similar mechanism could be at play for the water dimer diffusion. In the low-energy configuration of a water dimer one water molecule acts as a donor in the hydrogen bonding interaction and one molecule acts as an acceptor, i.e. an oxygen-hydrogen bond from one water molecule points towards one of the two lone-pairs on the other water molecule. Thus, inspired by the water molecule diffusion over the bridging hydroxyl, we envisage the acceptor in the water dimer rolling over the donor water molecule stabilized by the hydrogen bond from the donor. In this way the water dimer can move one lattice site along the [001] direction. By switching roles, i.e. the donor becomes the acceptor and vice versa, the dimer can move another site. In the gas phase the donor-acceptor interchange occurs through tunneling at a rate of 10^9 s^{-1} [121]. On TiO_2(110) surfaces the tunneling barrier is probably modified compared to the gas phase. However, through a kinetic Monte Carlo simulation we found that at the investigated temperatures the observed diffusion of the water dimers is possible with donor-acceptor interchange rates as low as 20 s^{-1}.

Another difference with respect to diffusion of monomers is the very low prefactor of $\sim 10^5$ to 10^6 (Fig. 7.4). As previously mentioned, a prefactor of 10^{12} to 10^{13} is usually anticipated for thermally activated diffusion [123]. In a recent STM study of the diffusion and clustering of water molecules on Pd(111) an unusually high diffusion rate for water dimers at low temperature was found [86]. Subsequently, a mechanism for the water dimer diffusion on Pd(110) has been proposed on the basis of DFT calculations [87]. The suggested model is consistent with a very low energy barrier for the diffusion and included a step which proceeded through tunneling of hydrogen atoms. This step modified the apparent prefactor by a factor of $\sim 10^{-8}$, i.e. the prefactor for the model was found to be $\sim 10^4$. A similar effect could be anticipated in case of water dimer diffusion on TiO_2(110) as the acceptor molecule probably has to change the lone pair involved in the hydrogen bond when rolling over the donor water molecule. This process can occur through tunneling of the hydrogen atoms on the acceptor molecule, so-called

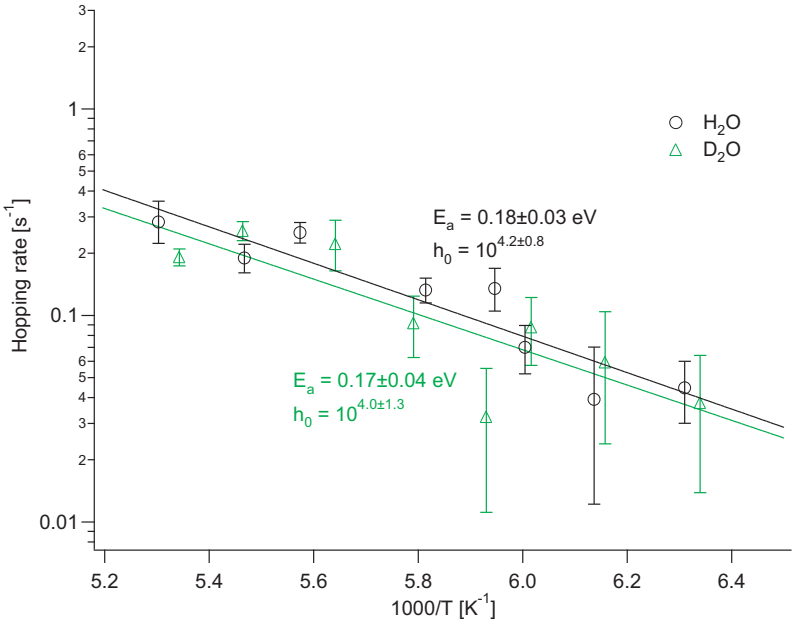

Figure 7.5. *Arrhenius plots of D_2O dimer hopping rates (green triangles) and hopping rates from control experiment with H_2O dimers (black circles) on the same TiO_2(110) crystal. Fits of the data sets to the logarithmic form of the Arrhenius equation are also shown, including prefactors and energy barriers obtained from the fits.*

"acceptor switching" [121, 128]. If this were indeed the case one would expect that the dimer diffusion exhibits an isotope effect, i.e. that D_2O dimers diffuse slower than H_2O dimers because the tunneling probability for ^2H is lower than for ^1H. For water dimer diffusion on Pd(111) D_2O should diffuse a factor of 10 slower than H_2O according to the suggested model [87]. However, in the present case it is not possible to assess how large the effect will be without an exact quantitative model for the hopping rate.

7.3.2.1 Isotope effect - D_2O dimer diffusion

To test for the anticipated isotope effect we performed an experiment tracking D_2O dimers on a hydroxylated TiO_2(110) surface with OD_{br} groups. To ensure we had pure D_2O and OD_{br} on the TiO_2(110) surface the sample was flashed at 623 K for two minutes to desorb all molecular water and all bridging hydroxyls [64] directly before cooling down to $\sim$230 K at which temperature the D_2O was dosed. Cooling down took $\sim$10 min during which the background pressure was $\sim 3 \times 10^{-11}$ Torr. D_2O was dosed through a directional doser to avoid exchange reactions between D_2O and H_2O adsorbed on the chamber walls. D_2O corresponding to $\sim$10 % ML was dosed, enough to fill all bridging oxygen vacancies and give a water coverage of $\sim$5 % ML on the 5f-Ti

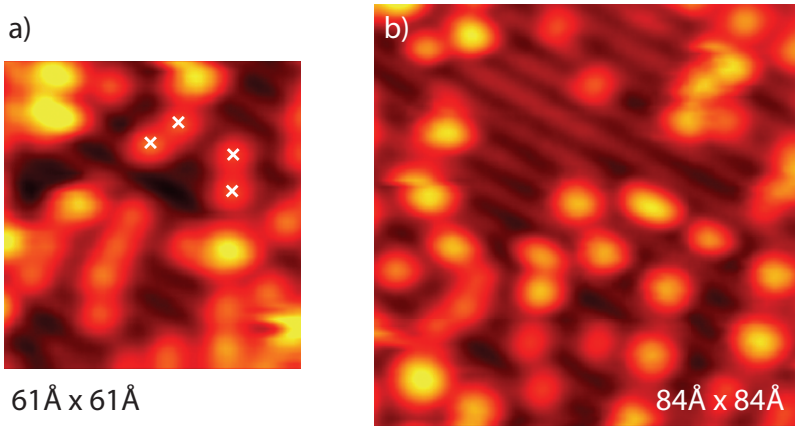

Figure 7.6. *(a) Snapshot from STM movie of water dimer diffusion on a hydroxylated TiO_2(110) surface at 193 K. Four bridging hydroxyls are marked with white crosses. The bridging hydroxyl coverage is 12.8 % ML. (b) Snapshot from STM movie where the bridging hydroxyls have been desorbed from the central part of the area (notice there are no protrusions on the dark rows in the central part of the image).*

atom rows. The sample was subsequently transferred to the STM at a temperature of 180 K. The procedure of flashing and again dosing D_2O was performed every 3-4 hours to ensure that adsorption of H_2O from the residual gas in the UHV chamber did not contaminate the adsorbed D_2O significantly. The hopping rates found for the D_2O dimers at different temperatures are shown in Fig. 7.5. Also shown are the results from a control experiment with H_2O. In this experiment the same TiO_2(110) crystal used for the D_2O dimer experiment was after flashing dosed with H_2O by backfilling the UHV chamber giving a H_2O coverage of $\sim$12 % ML, enough to fill all bridging vacancies and give a water coverage of $\sim$7 % ML on the 5f-Ti atom rows. The sample was then transferred to the STM at a temperature of 180 K and a number of STM movies at different temperatures were acquired.

Comparing the data set from the D_2O diffusion with the data set from the H_2O control experiment in Fig. 7.5 there is no clear difference. Prefactor and energy barrier for D_2O diffusion show no significant difference compared with the parameters extracted from H_2O diffusion. However, without a quantitative model for the water dimer diffusion it is not possible to distinguish whether the experimental data are at odds with a model incorporating hydrogen atom tunneling.

7.3.2.2 Dimer diffusion on quasi-stoichiometric TiO_2(110) surfaces

We have previously shown that it is possible to remove bridging hydroxyls locally by applying voltage pulses with $U_{pulse} \geq +2.5$ V (see section 4.2.3), thereby creating small quasi-stoichiometric TiO_2(110) surface areas. After acquiring a STM movie of water

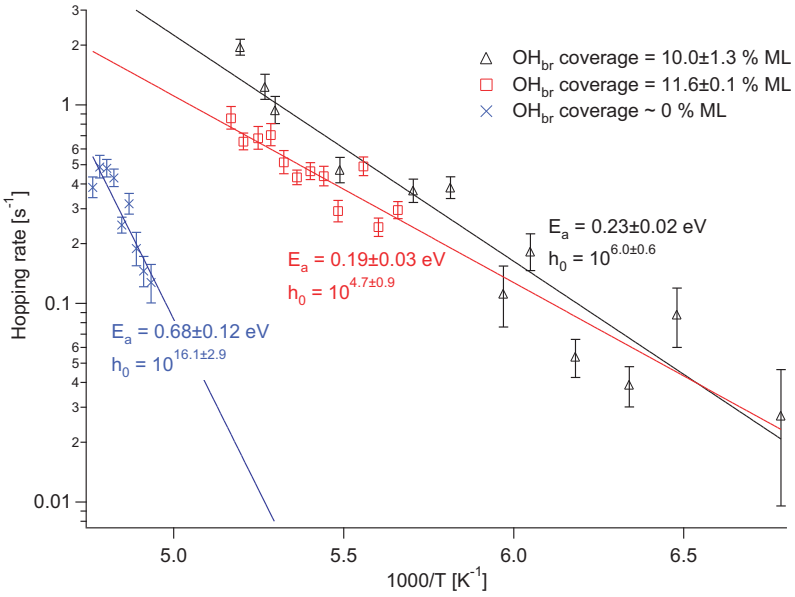

Figure 7.7. *Arrhenius plot for dimer diffusion on a quasi-stoichiometric TiO_2(110) surface (blue crosses). The dimer diffusion data from the hydroxylated surfaces are shown for comparison.*

dimers diffusing at a temperature of ∼193 K on a hydroxylated TiO_2(110) surface we desorbed bridging hydroxyls from a small area on the hydroxylated TiO_2(110) surface and followed the diffusion of water dimers in this small area (Fig. 7.6). When desorbing the bridging hydroxyls we were very cautious not to give pulses near water dimers. The water dimer hopping rate on the hydroxylated surface was found to be ∼1.9 s^{-1} (black triangle at the highest temperature in Fig. 7.7). In the area where the bridging hydroxyls had been desorbed the hopping rate was found to be ∼0.18 s^{-1}, i.e. a factor of ten lower than on the surface with hydroxyls.

In the experiment for water monomer diffusion on a quasi-stoichiometric TiO_2(110) surface previously described (section 7.3.1) we were also able to follow the diffusion of water dimers. The extracted hopping rates are plotted in Fig. 7.7 (blue crosses) along with the hopping rates for water dimers on hydroxylated TiO_2(110) surfaces previously presented in Fig. 7.4. Two features are quite obvious from the water dimer hopping rates on the quasi-stoichiometric surface: (1) water dimer diffusion is slower on the quasi-stoichiometric surface than on the hydroxylated surfaces; (2) the inclination is much larger on the quasi-stoichiometric surface than on hydroxylated TiO_2(110) surfaces, i.e. the barrier for diffusion is much larger. Because of the relatively small temperature interval investigated in this experiment the diffusion parameters obtained from the fit have relatively large uncertainties. Taking the lower limit for the prefactor ($h_0 = 10^{13.2}$), which is in the range of what one would expect for thermally activated diffusion, the

corresponding energy barrier is $E_a \approx 0.56$ eV.

It is clear from both of the above experiments that removing the bridging hydroxyls from the TiO_2(110) surface has a large effect on the diffusion of the water dimers, and the Arrhenius plot in Fig. 7.7 indicates that possibly a different diffusion mechanism is at play on the quasi-stoichiometric surface than on a hydroxylated surface. The lower limit for the prefactor on the quasi-stoichiometric surface is very close to the value expected from transition state theory for thermally activated diffusion [123]. There can be several reasons for this altered behavior. One reason could be that the data from the quasi-stoichiometric surface were acquired at a higher temperature than the data on the hydroxylated surfaces. Tunneling processes in thermally activated diffusion is a low temperature phenomenon and their will be a temperature at which a thermally activated pathway becomes faster than the tunneling process, because the tunneling probability does not depend on temperature. Another possibility is, that the barrier for the water dimer diffusion on the quasi-stoichiometric surface is linked to another process than the dimer diffusion itself. Preliminary DFT calculations have shown that water dimers favor to reside directly above Ti-interstitials which are located in the subsurface region. The binding between the two species is relatively strong and the rationale is that it is not favorable for the water dimer to diffuse without the Ti-interstitial and the Ti-interstitial is much too heavy to diffuse through tunneling. However, one then has to explain why the Ti-interstitials are not controlling the water dimer diffusion on the hydroxylated TiO_2(110) surface. Clearly there are still open questions to be answered in this regard.

7.4 Conclusions

We have investigated the diffusion of water monomers and dimers on the rows of 5f-Ti atoms on hydroxylated and quasi-stoichiometric TiO_2(110) surfaces by fast scanning STM. Water monomers diffuse with an energy barrier of $\sim$0.5 eV. The barrier was found to be 0.04 eV lower on the hydroxylated surface than on the quasi-stoichiometric surface, which was explained by the difference in stability of the pseudo-dissociated water monomer state.

The water dimer was found to diffuse with a low energy barrier of $\sim$0.2 eV and a very low prefactor of $\sim 10^5$-10^6. We suggest a model for the water dimer diffusion where the acceptor of the hydrogen bond in the water dimer rolls over the donor of the hydrogen bond. The low barrier for the diffusion is due to the stabilizing effect of the hydrogen bond as the acceptor rolls over the donor water molecule. The very low prefactor could be due to tunneling of the hydrogen atoms on the acceptor molecule during the diffusion, so-called acceptor switching. However, no significant isotope effect was detected in diffusion experiments using D_2O dimers instead of H_2O dimers.

CHAPTER 8

Interaction of oxygen with hydroxylated TiO_2(110) surfaces

This chapter reports a detailed STM study of the interaction between O_2 and bridging hydroxyls on the TiO_2(110) surface. O_2 is observed to initially react with a bridging hydroxyl to form a stable intermediate assigned to HO_2 adsorbed on the rows of fivefold coordinated Ti atoms. Through the interaction with water dimers adsorbed on the rows of fivefold coordinated Ti atoms the HO_2 species formed initially is found to evolve in a number of steps to a water dimer by extraction of hydrogen atoms from the bridging hydroxyl groups. Furthermore, we show that by exposing the hydroxylated TiO_2(110) surface to a metered amount of O_2 at RT, it is possible to form a quasi-stoichiometric TiO_2(110) surface.

8.1 Introduction

The interaction between oxygen and the hydroxylated TiO_2(110) surface has previously been studied in detail experimentally by Henderson *et al.* [46] and theoretically by Tilocca *et al.* [129] and Liu *et al.* [130]. Henderson *et al.* used EELS, HREELS and TPD to study the electronic and chemical state of the hydroxylated surface before and after oxygen exposure at different temperatures, and to get an idea of the reaction dynamics, e.g. what intermediates were involved. Water TPD on the hydroxylated TiO_2(110) surface showed a peak at 520 K associated with the recombination of two bridging hydroxyls to form a desorbing water molecule and an oxygen vacancy. When the surface was exposed to increasing amounts of oxygen the water TPD state at 520 K was progressively removed and replaced by a sharper water peak at 300-320 K. This water TPD peak was assigned on the basis of previous work [44, 131] to the combination of two terminal hydroxyls adsorbed at fivefold coordinated Ti sites. The combination of the two terminal hydroxyls to form water would leave behind an oxygen adatom at a fivefold coordinated Ti site. From the HREELS measurements it was found that the reaction between the adsorbed oxygen and the bridging hydroxyls was almost complete at 230 K.

The theoretical investigations by Tilocca *et al.* showed that O_2 can react with a pair of bridging hydroxyls without prior chemisorption of the O_2 molecule to form different intermediates, an H_2O_2 molecule adsorbed on a fivefold coordinated Ti site being the most stable. They did not find it feasible for the H_2O_2 to dissociate into two terminal hydroxyls as suggested by Henderson [46]. Liu *et al.* investigated in detail the adsorption and diffusion of O_2 on the hydroxylated TiO_2(110) surface. They found a strong dependence of the adsorption energy of O_2 on the coverage of bridging hydroxyl groups. A dependence which they could correlate to the amount of charge transferred to the adsorbed oxygen molecule - increasing the number of defects on the surface would increase the amount of negative charge transferred to the adsorbed O_2, thereby increasing the adsorption energy. Furthermore, they found that the distance between the adsorbed oxygen molecule and bridging hydroxyl did only have a small effect on the adsorption energy of O_2.

In this study we have examined the interaction between O_2 and the hydroxylated TiO_2(110) surface using STM. The results show that O_2 can react with a single bridging hydroxyl to form a stable intermediate ascribed to HO_2[1] on an adjacent Ti-row. This intermediate does not diffuse at the investigated temperatures. Further protons are transferred to the intermediate through interaction with mobile water dimers adsorbed on the rows of fivefold coordinated Ti atoms to finally create a water dimer which desorbs at a temperature around 300 K. We also demonstrate a feasible way of creating an almost stoichiometric TiO_2(110) surface by dosing O_2 at 300 K. Using DFT results from the literature a schematic of the energetics involved in the oxidation of the hydroxylated TiO_2(110) surface will finally be discussed.

[1] This should only be thought of as keeping track of how many oxygen and hydrogen atoms this species contains and not as a claim that we actually observe an HO_2 molecule.

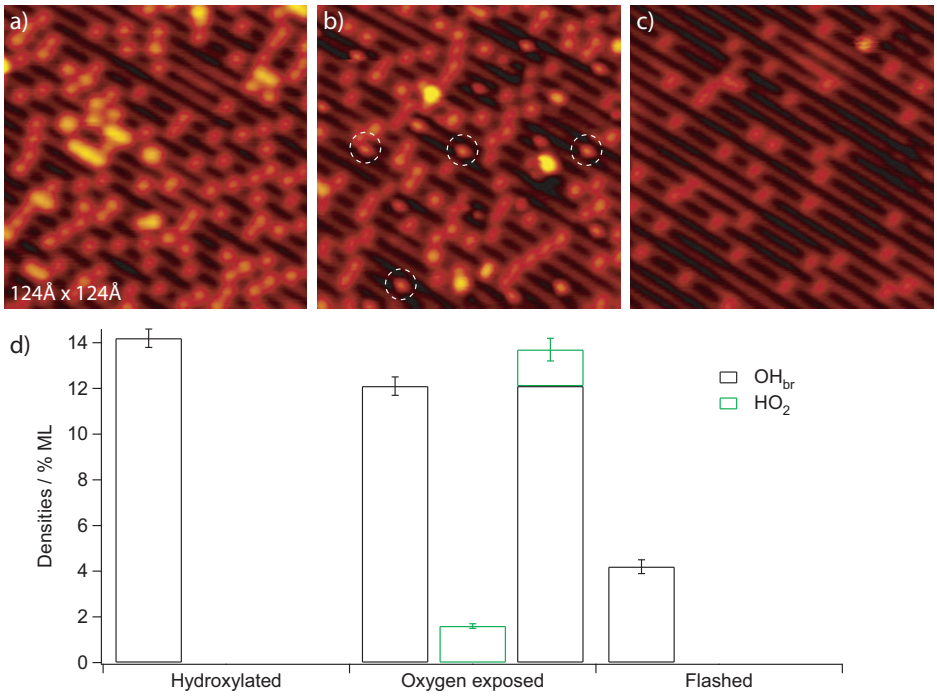

Figure 8.1. *STM images acquired at ∼110 K. (a) An image of the hydroxylated TiO_2(110) surface. The bridging hydroxyl concentration was 14.2±0.4 % ML. (b) The sample in (a) exposed to 4 L O_2 at 165 K. Examples of the predominant new species are marked with white rings. (c) The oxygen exposed sample in (b) flashed to 376 K for 2 min. The only major defect observed on this surface are bridging hydroxyl groups at a concentration of 4.2±0.3 % ML. (d) Bar-graph with coverages of bridging hydroxyls (OH_{br}), the new species seen in image (b) (HO_2), and the sum of the two species on the three surfaces*

8.2 Results and discussion

8.2.1 Initial reaction between O_2 and a bridging hydroxyl

In Fig. 8.1(a) an image of the hydroxylated TiO_2(110) surface is presented. This surface was prepared by exposing a clean reduced TiO_2(110) surface to ∼0.2 L of water at 168 K and subsequently flashing the surface to 373 K. As presented in detail in chapters 4 and 5 this procedure turns a reduced surface having predominantly oxygen vacancies into a surface having exclusively bridging hydroxyls. The hydroxylated surface was then exposed to 4 L O_2 at 165 K and subsequently quenched in the STM to the measuring temperature of ∼110 K. After this procedure the predominant species was still the bridging hydroxyls. However, a new species had appeared on the Ti-rows at a concentration

of 1.6±0.1 % ML. In Fig. 8.1(b) an STM image of the oxygen exposed surface is shown with the new species marked with white rings. The new species was stable at the investigated temperatures (∼110 K) and by fixing a grid using the surrounding bridging hydroxyls as anchor points the new species was seen to be centered in between two fivefold coordinated Ti sites. Importantly, we know from previous measurements that molecularly adsorbed oxygen is not observed in STM. The decrease in density of the bridging hydroxyls after the oxygen exposure as compared to the density on the freshly hydroxylated surface was 2.1±0.6 % ML, which is comparable to the density of the new species, indicating that the new species may simply be the reaction product between O_2 and a hydrogen atom from a bridging hydroxyl, i.e. HO_2 (Fig. 8.1(d)).

After flashing the oxygen exposed surface to 376 K for 2 min, the concentration of bridging hydroxyls on the surface dropped to 4.2±0.3 % ML, and the new species seen directly after oxygen exposure had disappeared (see Fig. 8.1(c)). According to the measurements of Henderson *et al.* [46] what desorbs during such a flash are water molecules and they do so around 300 K, indicating that mobility is induced on the surface during the flash and that further protons are transferred to the intermediate to transform it from what is likely HO_2 to surface species having the stoichiometry of H_2O. The bridging hydroxyls have very low mobility even at 300 K (see chapter 4 or Ref. [81]) meaning that the species adsorbed on the Ti-rows are responsible for the mobility on the surface. We will discuss this further in the following when we look at STM movies made during O_2 exposure of a hydroxylated TiO_2(110) surface.

Doing the math, one quickly realizes that the 1.6 % ML coverage of the new species assigned to HO_2 can only account for ∼6-7 % ML of the ∼10 % ML change in the coverage of bridging hydroxyls on the flashed oxygen exposed surface compared to the freshly prepared hydroxylated surface. However, at the sample temperature at which the O_2 exposure was performed, its likely that O_2 can adsorb molecularly without reacting with the bridging hydroxyls [45, 46]. During the flash the molecularly adsorbed O_2 can then react with the bridging hydroxyls.

8.2.2 Direct observation of the initial reaction between O_2 and a bridging hydroxyl

We will now discuss an STM movie acquired during O_2 exposure of a hydroxylated TiO_2(110) surface at temperatures around 190 K. The measurement was performed by backfilling the UHV chamber with O_2 after starting to record an STM movie. The background O_2 pressure was kept at $\sim 10^{-8}$ Torr, however, the pressure at the surface where the tip is scanning was probably a factor of five to ten lower than the measured pressure. Before the oxygen exposure was initiated, the concentration of water molecules on the surface was ∼6 %. As we will see in the following these water molecules play an important role in the further oxidation of the surface after the initial reaction between O_2 and a bridging hydroxyl.

Upon O_2 exposure we observed that bridging hydroxyls were consumed concomitant with the appearance of new protrusions on the adjacent Ti-rows. Two examples of such events can be seen in Fig. 8.2. In the first event (Fig. 8.2(a)-(b)) one bridging hydroxyl disappears and a new protrusion appears on the adjacent Ti-row. By fixing

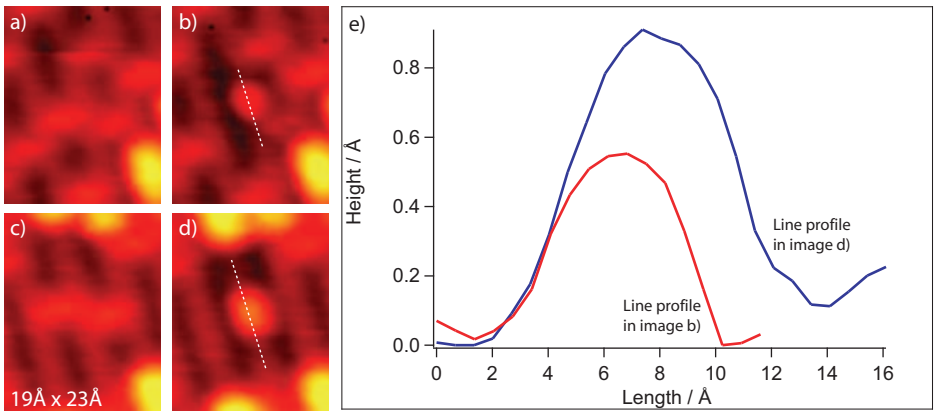

Figure 8.2. *Two sets of consecutive images from the STM movie made during O_2 exposure of a hydroxylated TiO_2(110) surface at ∼190 K together with line profiles of two of the observed species. (a)-(b) One bridging hydroxyl disappears concomitant with the appearance of a new species on the Ti-row next to the position of the disappeared bridging hydroxyl. (c)-(d) Two bridging hydroxyls disappear concomitant with the appearance of a new protrusion on the Ti-row between the two disappeared bridging hydroxyls. (e) Line profiles of the two new protrusions seen in image (b) and (d).*

a grid using the surrounding bridging hydroxyls as anchor points it can be seen that the new protrusion is centered in between two fivefold coordinated Ti atoms with the one Ti atom being next to the position of the former bridging hydroxyl. In the second event (Fig. 8.2(c)-(d)), two bridging hydroxyls disappear at the same time and one protrusion appears on the Ti-row between the positions of the two bridging hydroxyls that disappeared. Importantly, we did not observe the disappearance of bridging hydroxyls without at the same time observing the creation of a new protrusion on the adjacent Ti-row, or through the interaction of the bridging hydroxyl with the adsorbed species on the Ti-rows (the latter will be discussed further below). Therefore we will assign the protrusion in Fig. 8.2(b) to the initial reaction product between O_2 and a single hydrogen, i.e. HO_2, and the protrusion in Fig. 8.2(d) to the reaction product between O_2 and two hydrogen atoms, i.e. H_2O_2 in line with the assignment of the new protrusions seen after O_2 exposure in Fig. 8.1(b). From the line profiles in Fig. 8.2(e) it is clear that the reaction product containing two hydrogen atoms appears much larger in the STM images than the product containing only one hydrogen atom. This observation will be used in the following when looking at the interaction between the initial reaction product (HO_2) and the diffusing water species on the surface.

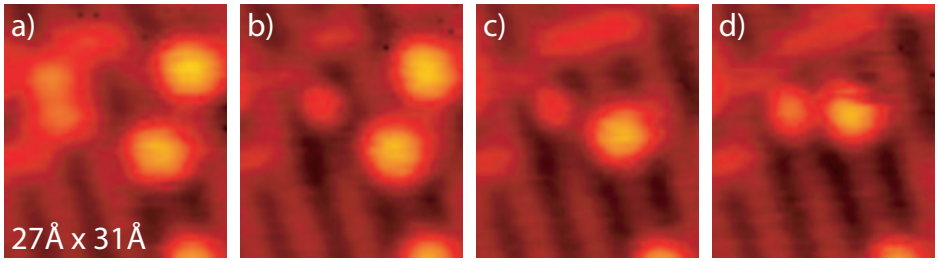

Figure 8.3. *(a)-(b) Initial reaction between O_2 and bridging hydroxyl produces initial reaction product on Ti-row (c)-(d) Water dimer jumps next to the initial reaction product resulting in a clearly enlarged appearance of the initial reaction product indicating that a proton transfer has occurred.*

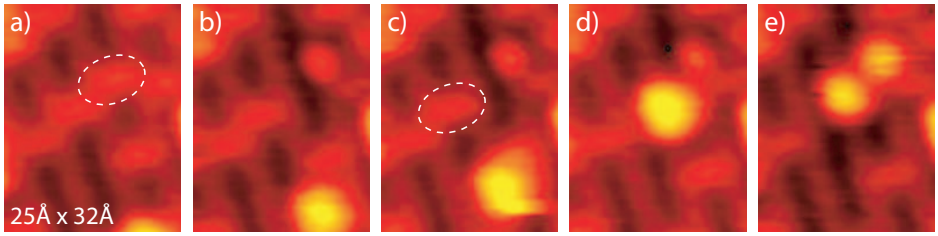

Figure 8.4. *(a)-(b) Bridging hydroxyl removed concomitant with the appearance of a protrusion on the adjacent Ti-row. (c)-(d) Water dimer diffuses to the bridging hydroxyl marked in (c) to form the H_5O_2 species which was assigned in chapter 6. (d)-(e) The H_5O_2 species jumps one lattice site towards the protrusion created (a)-(b) and a clear change in size of the two protrusions involved is observed indicating a proton transfer.*

8.2.3 Further steps in the oxidation of hydroxylated TiO_2(110) surfaces

None of the initial reaction products seen in Fig. 8.2(b) and (d) were observed to diffuse on the timescale in which they could be followed in the STM movie (up to 5-10 minutes). However, through the interaction with the water dimers adsorbed on the Ti-rows they evolved in to species that were mobile at the investigated temperatures. A first example of such an interaction is shown in Fig. 8.3. The initial reaction between O_2 and a bridging hydroxyl takes place between images (a) and (b) in Fig. 8.3 forming the HO_2 species assigned previously. From image (c) to (d) in Fig. 8.3 a water dimer is seen to diffuse next to the HO_2 species and a clear change in size of the protrusion is observed. A second example of how the water dimers adsorbed on the surface can interact with the initial reaction products is shown in Fig. 8.4. Again the initial reaction between O_2 and a bridging hydroxyl is seen to have occurred between image (a) and (b). From image (c) to (d) a water dimer is seen to move next to the bridging hydroxyl marked in (c),

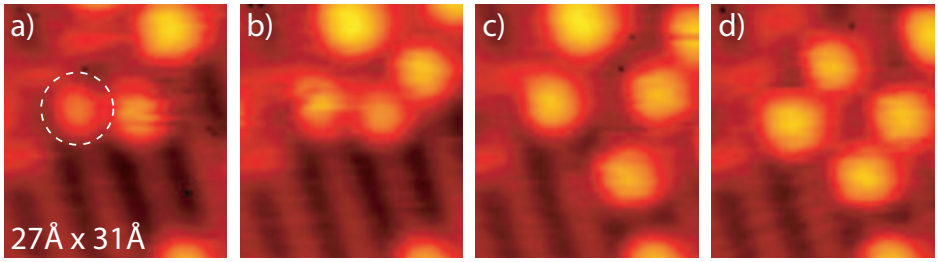

Figure 8.5. *STM images following the snapshots shown in Fig. 8.3. Several dimers interact with the protrusion created in the initial reaction (marked in (a)). Finally the protrusion becomes mobile and the first diffusion event is observed when comparing images (c) and (d).*

thereby forming the H_5O_2 species discussed in chapter 6. From image (d) to (e) the H_5O_2 species has moved one lattice site towards the HO_2 protrusion and a clear change in the measured size of both protrusions is observed.

The interpretation of the events presented above in Fig. 8.3 and 8.4 is based on proton transfers between the species adsorbed on Ti-rows. In chapter 6 water dimers and their ability to donate and accept protons depending on the surroundings were discussed in detail (sections 6.2.2.1 and 6.2.2.2). Here we will continue along the same lines to try to explain the reactions seen in the STM images so far. The size change between images (c) and (d) in Fig. 8.3 of the protrusion from the initial reaction (HO_2) indicates that one or more protons are transferred to this species. Taking into account the stoichiometry of the two species interacting the reaction is most likely:

$$HO_2 + H_4O_2 \rightarrow H_2O_2 + H_3O_2 \tag{8.1}$$

The second series of events (Fig. 8.4) is quite similar to the first one. The difference being that an H_5O_2 species is formed which then interacts with the HO_2 group created in the initial reaction between O_2 and a bridging hydroxyl. The interaction takes place between image (d) and (e) in Fig. 8.4 and given that we end up with two identical species on adjacent Ti-rows in image (e), we ascribe the reaction to:

$$HO_2 + H_5O_2 \rightarrow 2H_3O_2 \tag{8.2}$$

Interestingly, as discussed in section 6.2.2.2, the H_3O_2 species were found to be mobile at temperatures around 210 K meaning that at slightly higher temperatures than this movie was recorded at, this species would diffuse around and be able to pick up an additional proton from the remaining bridging hydroxyls to form a water dimer.

The images in Fig. 8.3 show only the first of a series of proton transfers. In Fig. 8.5 snapshots following the further development can be seen. Due to the very similar appearance of H_3O_2 and the water dimer (see Fig. 6.8) the subsequent proton transfers from other water dimers are, however, difficult to follow with certainty. On the other hand, the mobility of the different species is relatively easy to assess and from this it is

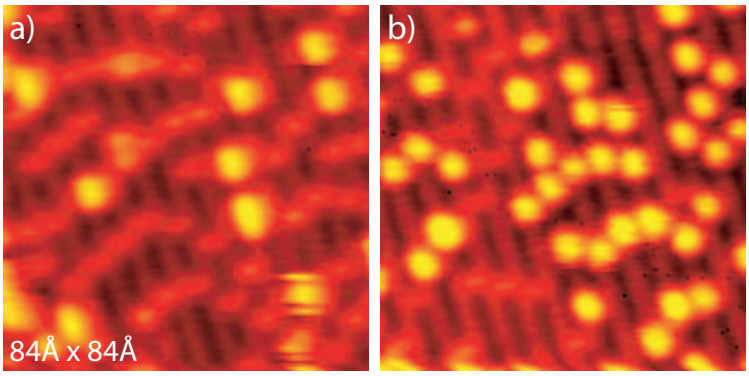

Figure 8.6. *(a) STM image acquired at ∼190 K of the surface area scanned in the movie before backfilling the UHV chamber with O_2. The number of bridging hydroxyls is ∼46. (b) The same area of the surface as in (a) after exposing it to O_2 for ∼56 min. The number of bridging hydroxyls is ∼15.*

clear that the initial reaction product evolves to a water dimer during the course of the STM movie. The first observed jump is seen when comparing images (c) and (d), and several jumps follow in the STM movie.

To further validate the point that the species created initially in the reaction between O_2 and a bridging hydroxyl are finally turned into water dimers, Fig. 8.6 shows STM images of the whole area scanned in the STM movie. Fig. 8.6(a) is an STM image from the STM movie acquired before backfilling the UHV chamber with O_2. The STM image in Fig. 8.6(b) was acquired after scanning in an O_2 background for ∼56 min. During the period of time between the two images, an event like the one shown in Fig. 8.2(a)-(b) was observed six times and an event like the one in Fig. 8.2(c)-(d) was observed one time, i.e. a total of seven events where O_2 reacts with one or two bridging hydroxyls. In the same time the number of bridging hydroxyls had dropped from ∼46 in Fig. 8.6(a) to ∼15 in Fig. 8.6(b). Thus, for every reaction as the ones shown in Fig. 8.2 an average number of 4.4 bridging hydroxyls disappear from the surface, in good agreement with the suggested model that O_2 initially reacting with a bridging hydroxyl is finally reduced to a water dimer.

The model which has been presented here is very different from the one proposed by Henderson *et al.* [46] in which water was formed through the combination of two terminal hydroxyls leaving behind an oxygen adatom as the water desorbed. However, a large difference between this study and the study by Henderson is the ratio between the number of oxygen molecules that stick to and react with the bridging hydroxyls, and the number of hydroxyls. In the experiments shown here, the ratio between bridging hydroxyls and O_2 has always been higher than four to one, thus making it possible to form water from all the oxygen molecules. In the study by Henderson *et al.* this ratio was far from always higher than four to one. So for example at a ratio of two to one it might be more favorable for two oxygen molecules to share four protons to form two

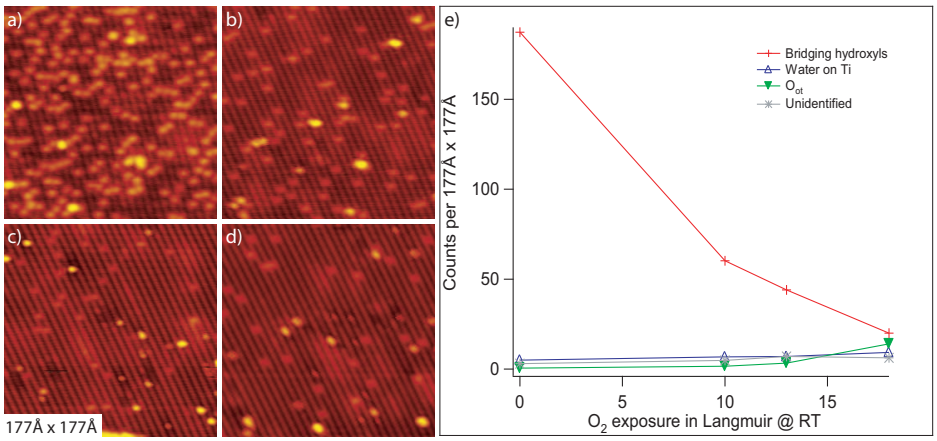

Figure 8.7. *STM images acquired at 100-120 K of the hydroxylated TiO_2(110) surface after different O_2 exposures at ∼300 K. (a) Before O_2 exposure. (b)-(d) After exposure to 10, 13 and 18 L O_2, respectively. (e) The average number of defects and adsorbates found in the STM images acquired after each exposure. The average is made from five or more images for each exposure (0-18 L).*

H_2O_2 species than to form a water dimer and one adsorbed oxygen molecule, making the model suggested by Henderson plausible for certain ratios between the number of bridging hydroxyls and O_2.

8.2.4 Forming almost stoichiometric TiO_2(110) surfaces

In section 4.2.3 we showed how it is possible to remove selected bridging hydroxyl groups by giving a voltage pulse when the tip is directly above the selected defect. Defect free areas can also be produced by scanning the surface with tunneling voltages of $V_T \geq 2.5$ V. However, this is not a feasible way to remove defects from very large areas or entire crystal surfaces, and it also only works for STM. A simpler way to remove almost all surface defects from hydroxylated TiO_2(110) is to expose the surface to O_2 at ∼300 K. In Fig. 8.7 STM images acquired after exposing the sample to increasing amounts of O_2 at ∼300 K and subsequently keeping the sample at ∼300 K for five minutes are shown along with the average counts for all the STM images acquired after the different exposures. From the plot of the average counts of the defects and adsorbates found on the surface it is clear that the main effect of exposing the hydroxylated TiO_2(110) surface to O_2 is to remove the bridging hydroxyls. After a total exposure of 18 L of O_2 the concentration of bridging hydroxyls had dropped to ∼1/10 of the initial concentration, while the concentration of new adsorbates on the surface is still only comparable to the final bridging hydroxyl concentration.

The mechanism proposed here for the removal of the bridging hydroxyls at 300 K consists of several steps as suggested by the measurements at lower temperatures. The

different steps are listed below with comments to the different steps following the list:

1. Initial reaction between O_2 and a bridging hydroxyl forms a stable HO_2 species adsorbed on a row of fivefold coordinated Ti atoms:

$$O_2 + OH_{br} \rightarrow HO_2 + O_{br} \tag{8.3}$$

2. A water dimer adsorbed on the Ti-row transfers a proton to the HO_2 species:

$$HO_2 + H_4O_2 \rightarrow H_2O_2 + H_3O_2 \tag{8.4}$$

3. The H_3O_2 species was found to be mobile at temperatures as low as $\sim$210 K (see section 6.2.2.2) meaning that it will diffuse very fast at $\sim$300 K and quickly be able to pick up a proton from a bridging hydroxyl group thereby again forming a water dimer

$$H_3O_2 + OH_{br} \rightarrow H_4O_2 + O_{br} \tag{8.5}$$

4. By interacting with a second water dimer or by interacting with the same water dimer a second time the initial reaction product is turned into a mobile H_3O_2 species:

$$H_2O_2 + H_4O_2 \rightarrow H_3O_2 + H_3O_2 \tag{8.6}$$

5. The mobile H_3O_2 species can pick up a proton from a bridging hydroxyl and participate in further interactions with HO_2 species or it can desorb from the surface.

6. When O_2 is no longer supplied to the surface reactions 8.4 and 8.6 will eventually stop and the concentration of water on the TiO_2(110) surface will reach an equilibrium with the background pressure of water in the chamber.

In the first step it is not clear whether the oxygen molecule that reacts with the bridging hydroxyl is first adsorbed on the surface or reacts directly from the gas phase. According to the molecular dynamics simulations of Tilocca *et al.* [129] O_2 does not need to chemisorb on the hydroxylated TiO_2(110) surface before reacting with the bridging hydroxyl. However, in the measurements by Henderson *et al.* [46] it was clear that O_2 could chemisorb at low temperatures (in their case $\sim$120 K) without reacting with the bridging hydroxyls. When heating up the sample they then found the reaction between chemisorbed O_2 and the bridging hydroxyls to be complete at $\sim$230 K. Using STM it is difficult in a direct way to give insight to this point, since O_2 chemisorbed on TiO_2(110) is not visible in STM and the reaction between O_2 and a bridging hydroxyl probably takes places on a timescale not accessible with STM. Following the evolution in the bridging hydroxyl concentration (Fig. 8.7(e)) some qualitative statements can be made about the initial reaction between O_2 and the bridging hydroxyls. It is clear from the slope of the bridging hydroxyl concentration curve that the probability for an oxygen molecule to be involved in a reaction with a bridging hydroxyl decreases with decreasing bridging hydroxyl concentration. Two possible explanations for this could be: (1) O_2

reacts directly from the gas phase with a bridging hydroxyl on the surface giving a reaction probability proportional to the bridging hydroxyl concentration, or (2) O_2 adsorbs on the TiO_2(110) surface before reacting with a bridging hydroxyl, but the adsorption of O_2 is very dependent on the bridging hydroxyl concentration. In connection to the second explanation, Liu *et al.* have calculated the adsorption energy of O_2 as a function of bridging hydroxyl concentration [130]. They found the adsorption energy of O_2 to be a monotonous increasing function as a function of bridging hydroxyl concentration. Additionally, they report a linear correlation between the amount of negative charge that had been transferred to the oxygen molecule and the adsorption energy. In their model the only electronic defects were the bridging hydroxyls. However, in a reduced TiO_2(110) sample other defects like Ti^{3+}-interstitials can donate charge to adsorbed oxygen making the adsorption energy of O_2 less dependent on the bridging hydroxyl concentration than reported in the work by Liu *et al.* [130].

In relation to steps two, five and six the coverage and desorption kinetics of water at a temperature of 300 K are key points. One might think that no water is present on the surface since the first-layer desorption feature in water TPD spectra has its maximum at $\sim$270 K [38,46,63,65]. However, it is difficult to determine based on TPD results the net coverage of water on the TiO_2(110) surface at RT. To date, no conclusive model is available which explains the TPD results comprehensively [65,73]. In addition, the tail of the first layer feature spans temperatures higher than 300 K and shifts towards higher temperatures as the initial coverage is lowered (Fig. 1 in Ref. [46] and Fig. 3 in Ref. [63]). Thus, trace amounts of water cannot be ruled out based on TPD results. Note that for the thermal equilibrium, Brinkley *et al.* reported a water coverage of 0.01 ML (upper limit) at 350 K [65], and Pan *et al.* 0.07 ML (lower limit) at 300 K [37], respectively. These values are based on studies using modulated molecular beam scattering [65] and low-energy ion scattering [37], respectively.

8.2.5 Energetics for forming stoichiometric TiO_2(110) surfaces

In the following an overview is given of the energetics involved in two possible ways that one could think of re-oxidizing the reduced TiO_2(110) surface at 300 K to create a TiO_2(110) surface without oxygen vacancies. Starting from a bulk-reduced TiO_2(110) sample, i.e. a sample with oxygen vacancies at the surface as well as bulk electron donors in the form of subsurface vacancies or Ti^{3+}-interstitials, two possible pathways are sketched in Fig. 8.8. The starting point for both pathways is the dark blue block with two "oxygen vacancies" at the top of the figure and this is also taken as the zero-point for the potential energy scale.

The pathway on the left side, which was also considered in section 4.2.6.2 is simply the oxidation of the reduced TiO_2(110) surface by dissociation of an oxygen molecule in an oxygen vacancy followed by the diffusion of the oxygen adatom created in the dissociation of O_2 to the second oxygen vacancy. The energy barrier for the diffusion of the oxygen adatom was found to be $\sim$1.14 eV, i.e. too high to be accessible at 300 K. Thus this is not a feasible way to form a TiO_2(110) surface without oxygen vacancies.

The pathway on the right side is the pathway following the explanation of the STM results presented in the previous sections. By dissociating two water molecules in the

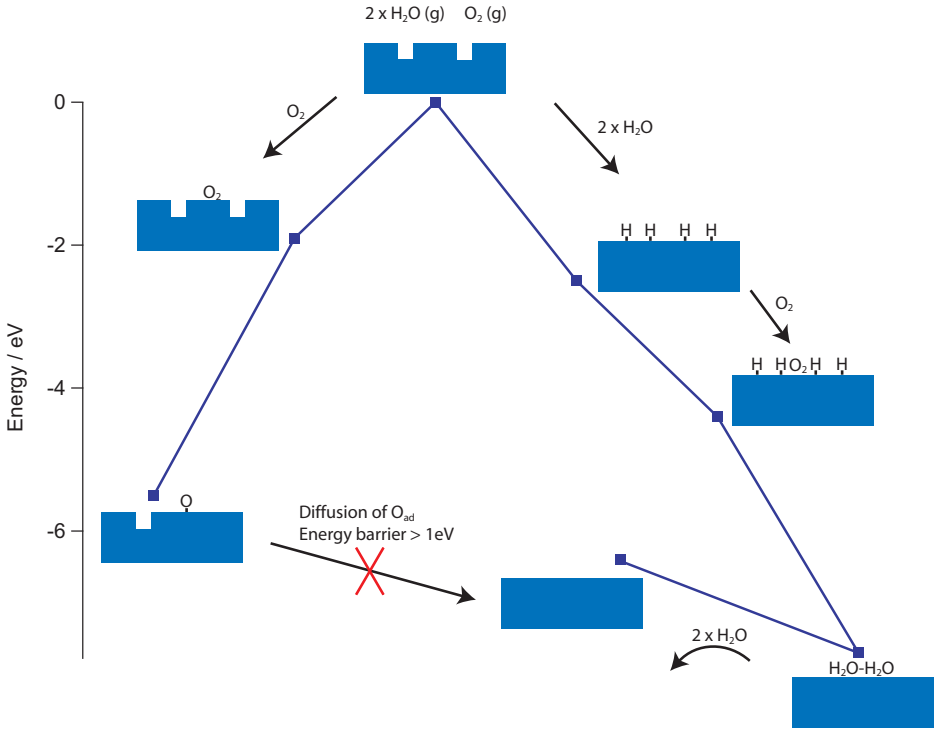

Figure 8.8. *Schematic showing configurations and DFT based energies (see text for references) for two different pathways for filling the oxygen vacancies on the reduced TiO_2(110) surface. The potential energies are given with respect to the reduced TiO_2(110) surface with two oxygen vacancies and O_2 and two H_2O in the gas phase at 0 K (no entropy contribution). This configuration is symbolized at the top of the figure as a dark blue block with two "oxygen vacancies" and the three molecules in the gas phase. The left pathway is oxidation of the surface by dissociating O_2 in an oxygen vacancy followed by diffusion of the oxygen adatom to the second vacancy. The diffusion of the oxygen adatom is hindered by a large barrier of ∼1.14 eV (see Fig. 4.9). The right pathway consists of several steps - the initial step being the filling of the oxygen vacancies with water molecules. In the next steps O_2 is adsorbed and reacts with the protons on the bridging hydroxyls to form two water molecules which finally are desorbed from the stoichiometric TiO_2(110) surface.*

two vacancies and subsequently splitting the pairs of bridging hydroxyls into single bridging hydroxyls an energy gain of 2.5 eV is obtained (see section 4.2.6.1). To show all possible steps we will assume that O_2 is first chemisorbed on the TiO_2(110) surface before reacting with the bridging hydroxyls. Another possibility would be that the oxygen molecule reacts directly from the gas phase to form an HO_2 species adsorbed on the surface. The maximum adsorption energy for an oxygen molecule provided in the work by Liu *et al.* [130] is $\sim$2 eV (for a 1 ML coverage of bridging hydroxyls) and the adsorption energy given in the work by Tilocca *et al.* [129] is 2.38 eV for O_2 adsorbed next to a pair of bridging hydroxyls. Both of the values are relatively close to values for O_2 adsorbed next to an oxygen vacancy which is given in the pathway on the left. The adsorbed O_2 can now react with the bridging hydroxyls forming two water molecules (or a water dimer). Following this pathway, there is a large energy gain as we end up in the lowest energy state with a TiO_2(110) surface with no oxygen vacancies and two adsorbed water molecules. The energy of this state compared to the starting point can be calculated from the energy we gain by filling the two oxygen vacancies with oxygen atoms, $\sim$6.5 eV (see Fig. 4.9), plus the energy gained by adsorbing two water molecules on the stoichiometric surface, $\sim$1.3 eV (see Fig. 4.8), giving a total energy gain of $\sim$7.8 eV. Desorbing the two water molecules in the last step will cost $\sim$1.3 eV yielding a total energy gain of $\sim$6.5 eV.

The schematic in Fig. 8.8 is relatively simplistic and only shows energies of some of the configurations in the processes. None of the intermediates in the oxidation of the hydroxylated TiO_2(110) surface, e.g. HO_2 and H_2O_2, discussed in relation to the STM results presented have been included as well as any barriers between the different configurations shown, except for the diffusion of O_{ad}. Tilocca *et al.* [129] calculated the adsorption energies of HO_2 and H_2O_2 and found these to be slightly lower than the adsorption energy of O_2 (less than 0.15 eV difference). The calculations were done without including subsurface electron donors like Ti^{3+}-interstitials. Preliminary DFT results show that the incorporation of Ti^{3+}-interstitials has a significant impact on the adsorption energies of the intermediate species making them more stable when the interstitial is included [132].

8.3 Conclusions

In summary, this chapter represents a detailed STM study of the interaction between O_2 and bridging hydroxyls on the TiO_2(110) surface. Utilizing the unique capabilities of the fast scanning STM we have been able follow the oxidation of a hydroxylated TiO_2(110) surface or equivalent the reduction of O_2 to water on this surface in detail. Our key findings are:

1. O_2 reacts initially with a bridging hydroxyl to form a stable intermediate assigned to HO_2 adsorbed on the rows of fivefold coordinated Ti atoms.

2. Through the interaction with water dimers adsorbed on the rows of fivefold coordinated Ti atoms the HO_2 species formed initially evolve in a number of steps to a water dimer.

3. Exposing the hydroxylated TiO_2(110) surface to O_2 at $\sim$300 K we showed that it is possible to form a quasi-stoichiometric TiO_2(110) surface.

CHAPTER 9

Bonding of gold nanoparticles on TiO_2(110) surfaces

We studied the nucleation of gold clusters on TiO_2(110) surfaces in three different oxidation states by high-resolution STM. The three TiO_2(110) supports chosen were (i) reduced having bridging oxygen vacancies, (ii) hydroxylated having bridging hydroxyl groups, and (iii) oxidized having oxygen ad-atoms. At room temperature, gold nanoclusters nucleate homogeneously on the terraces of the reduced and oxidized supports, while on the hydroxylated TiO_2(110) surface clusters form preferentially at the step edges. From interplay with DFT calculations, we identified two different gold-TiO_2(110) adhesion mechanisms for the reduced and oxidized supports. The adhesion of gold clusters is strongest on the oxidized support, and the implications of this finding for catalytic applications are discussed.

9.1 Introduction

Finding of distinctive catalytic properties of dispersed gold nanoparticles on oxide supports [90, 91] has stimulated extensive research activities [10, 91, 92, 94], and a general consensus now exists on several aspects of this system. The size of the gold particles substantially affects the catalytic activity, and the gold clusters must be smaller than 5 nm for high catalytic activity [8, 95, 96]. The choice of the oxide support influences the catalytic activity, so there is a strong "support effect" in addition to the "size effect" [91, 94, 99], and reducible oxides are advantageous compared to non-reducible ones [99, 133]. However, the relation of the adhesion properties of nanosized gold with catalytic activity is still unresolved. A number of studies (mainly catalysis work done on high area support materials) have reported that slightly oxidized gold ($Au^{+\delta}$), in addition to metallic gold (Au^0), is important to achieve high activity of dispersed Au catalysts [58, 91, 94, 103–105, 134, 135]. In parallel, several surface science studies of model systems preferred an interpretation where oxygen vacancies have been invoked as being responsible for the stabilization and activity of Au clusters on the support [100–102, 136].

We studied the fundamental mechanisms of metal oxide-support adhesion by means of STM and DFT calculations. We compare the nucleation of Au clusters on one support material that had been prepared in different oxidation states. We chose rutile TiO_2(110) as the model support, because numerous studies exist on the Au/TiO_2 model system, and Au/TiO_2 is a good catalysts for CO oxidation at low temperatures as shown in the pioneering studies by Haruta [90, 95], Goodman [8, 136] and the work of others [137–139].

9.2 Results and discussion

9.2.1 TiO_2(110) surface preparation and Au exposure at RT

Clean, reduced TiO_2(110) (*r*-TiO_2(110)) surfaces with 5-8 % ML bridging oxygen vacancies were prepared as described in chapter 2 (Fig. 9.1(a)). By applying a short flash to 600 K when the sample had reached RT after annealing, we could produce surfaces with almost exclusively bridging oxygen vacancies and only very few bridging hydroxyls (see chapter 4). Starting with a *r*-TiO_2(110) surface, we prepared two further well-defined TiO_2(110) surfaces under UHV conditions. First, we produced a hydroxylated TiO_2(110) (*h*-TiO_2(110)) surface with bridging hydroxyls by exposing the *r*-TiO_2(110) surface to water at 120 K, followed by slowly warming the crystal up to 400 K. In this way we ended up with a TiO_2(110) surface having only single bridging hydroxyls and no bridging oxygen vacancies (Fig. 9.1(b)). Second, we prepared an oxidized TiO_2(110) (*o*-TiO_2(110)) surface via O_2 exposure (1.5-6 L depending on bridging oxygen vacancy concentration) of the *r*-TiO_2(110) surface at 120 K, followed by a short flash up to RT. The O_2 exposure was chosen as small as possible to avoid the formation of suboxides on the *o*-TiO_2(110) surface [8, 49, 140]. The O_2 molecules dissociate in the bridging oxygen vacancies (chapter 4 and [44]), resulting in an *o*-TiO_2(110) surface characterized

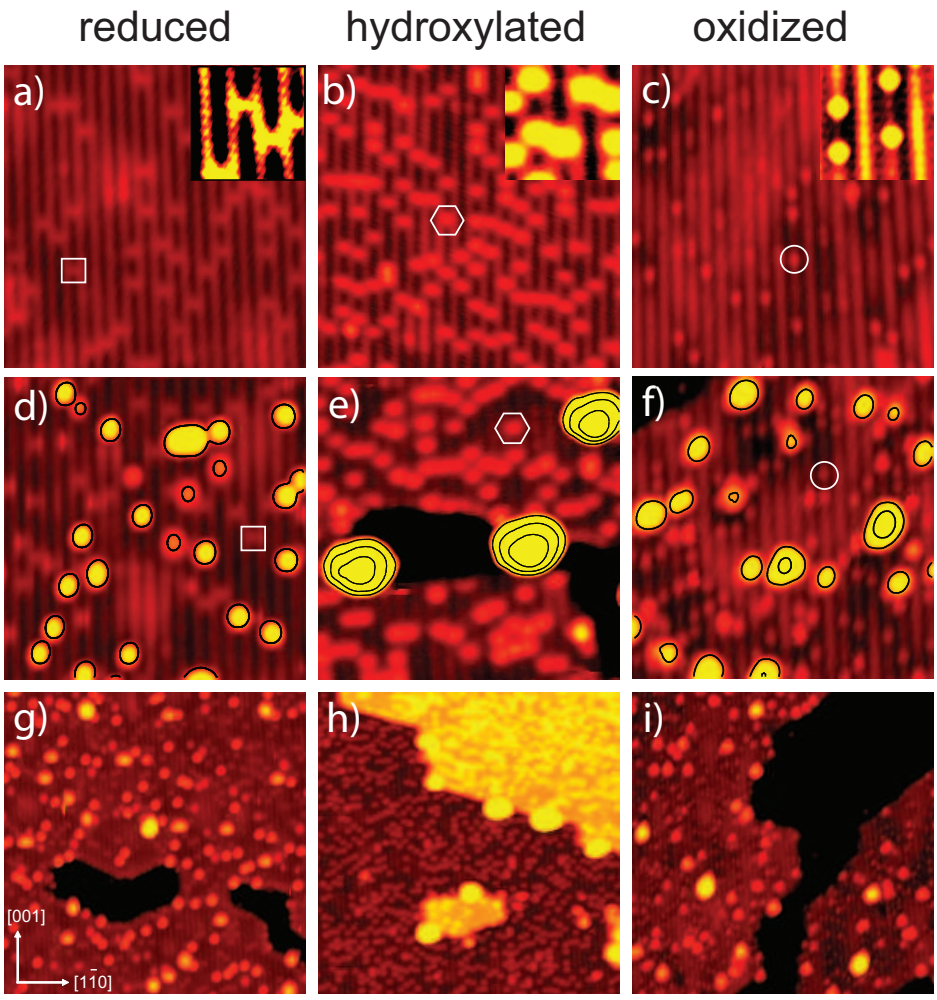

Figure 9.1. *STM images of (a)* r-TiO_2*(110) , (b)* h-TiO_2*(110) and (c)* o-TiO_2*(110) surfaces prior to Au exposure (*130×130 $Å^2$*). Symbols indicate bridging oxygen vacancies (square), bridging hydroxyls (hexagon) and oxygen adatoms in the Ti troughs (circle). Insets (*30×30 $Å^2$*) show the point defects of interest enlarged. The preparation recipes for the different surfaces are described in the text. (d - i) STM images after 3 % ML Au exposure at RT. The size of the images is* 130×130 $Å^2$ *(d - f) and* 350×350 $Å^2$ *(g - i), respectively. In (d - f) the heights of the Au clusters are given by contour lines at 1.2 Å, 3.2 Å and 5.2 Å above the terrace. Directions as indicated in (g). All STM images were acquired at* $120 - 140$ *K.*

by perfect bridging oxygen rows and by a number of oxygen adatoms located in the Ti troughs (Fig. 9.1(c)).

After exposing these three different $TiO_2(110)$ surfaces to 3 % ML Au at RT (1 ML is defined as 1.39×10^{15} atoms per cm^2 corresponding to the density of un-reconstructed Au(111)), we observed quite different Au cluster morphologies. In case of the *r*-$TiO_2(110)$ surface, numerous rather small Au clusters are distributed homogeneously on the terraces (Fig. 9.1(d) and (g)). In contrast, on the *h*-$TiO_2(110)$ surface, we found fairly large Au clusters that decorate preferentially the step edges of the substrate, and no small Au clusters on the terraces are seen (Fig. 9.1(e) and (h)). However, on the oxidized *o*-$TiO_2(110)$ surface we again found Au clusters to nucleate homogeneously on the terraces (Fig. 9.1(f) and (i)).

9.2.2 Influence of sample temperature on Au cluster morphology

The absence of homogeneously distributed small Au nanoclusters on the *h*-$TiO_2(110)$ surface implies that monomeric Au (Au_1) and small Au nanoclusters diffuse readily at RT on this surface. This finding is in agreement with previous RT-STM studies addressing Au/$TiO_2(110)$ [8, 100, 141], where sintering of incoming Au_1 has been reported. In the present work we found homogeneously distributed small Au clusters also on the terraces of the *h*-$TiO_2(110)$ surface when we cooled the substrate down to $-57\,^{\circ}C$ prior to exposure (Fig. 9.2(a) and (b)). According to these results we infer that the interaction between Au clusters and the *h*-$TiO_2(110)$ surface is fairly weak [142]. On the contrary, both for the *r*-$TiO_2(110)$ surface (with bridging oxygen vacancies), and the *o*-$TiO_2(110)$ surface (with oxygen adatoms), the results presented in Fig. 9.1 imply that on these two $TiO_2(110)$ surfaces stronger Au-TiO_2 interactions occur than on the *h*-$TiO_2(110)$ surface. When we compared the herein-presented comprehensive data set with previous data from our group [100], it became apparent that, in Ref. [100], Au was evaporated onto $TiO_2(110)$ surfaces of various character. For the low-temperature experiments in Ref. [100], the starting point was a clean *r*-$TiO_2(110)$ surface. For the Au exposures at higher temperatures, however, unintentionally *h*-$TiO_2(110)$ surfaces were used. Taking this into account, there is full agreement between the STM results in Ref. [100] and the present work. In both data sets, $\sim$80 % of the Au clusters were found at the step edges after Au exposure onto *h*-$TiO_2(110)$ at RT.

Given the stronger interactions with the *r*- and the *o*-$TiO_2(110)$ surfaces, we explored the effect of heating on the Au cluster morphologies on these two TiO_2 surfaces (Fig. 9.2(c) to (f)). Starting points in these experiments were *r*- and *o*-$TiO_2(110)$ surfaces that we exposed to 3 % ML Au at RT, (Fig. 9.1(d) and (g), and Fig. 9.1(f) and (i), respectively). After subsequent heating of the samples to $68\,^{\circ}C$, Au sintering is clearly evident for Au/*r*-$TiO_2(110)$ (Fig. 9.2(c)), but not for Au/*o*-$TiO_2(110)$ (Fig. 9.2(e)). The different stabilities of the Au clusters against sintering on the two $TiO_2(110)$ surfaces considered are even more obvious when looking at the corresponding Au height histograms (Fig. 9.2(d) and (f)). The Au cluster height histograms were deduced from areas of $\sim 10^4$ nm^2 Au exposed $TiO_2(110)$ surface. Au clusters were distinguished from smaller protrusions on the $TiO_2(110)$ surfaces by applying a threshold of 1.2 Å above the terrace when counting Au clusters. For reference, we also show the height histograms

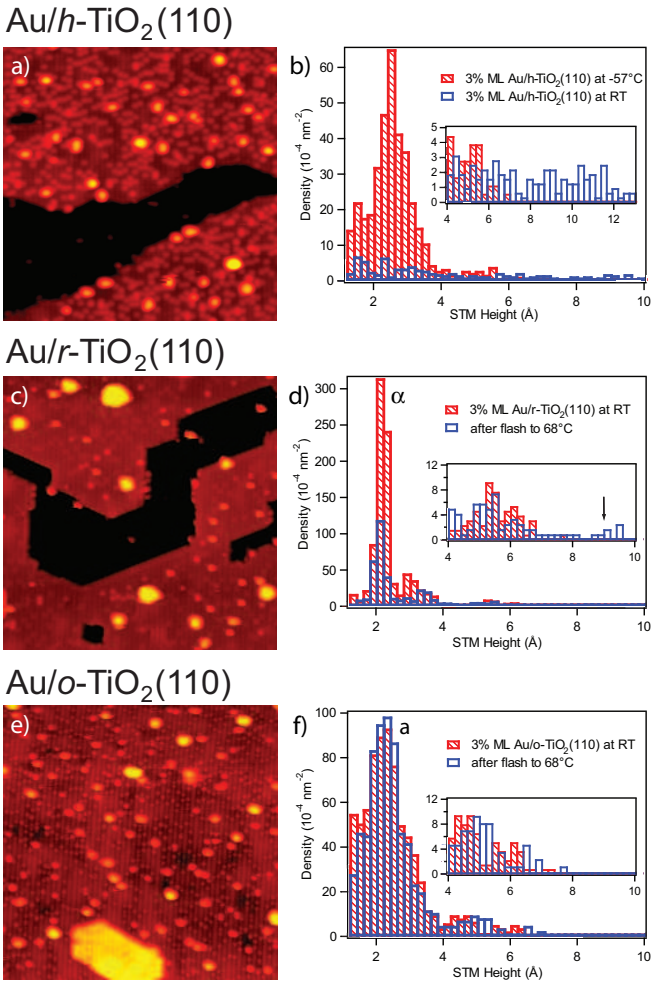

Figure 9.2. *(a) STM image of the* h-TiO_2*(110) surface after 3 % ML Au exposure at* $-57\,^{\circ}\mathrm{C}$ *(*$350 \times 350\,\mathring{A}^2$*), and (b) Au height histograms corresponding to Au/*h-TiO_2*(110) surfaces for substrate temperatures of* $-57\,^{\circ}\mathrm{C}$ *(hatched red bars) and RT (blue bars). The histograms rely on scanned areas of* $\sim 10^4$ *nm*^{2} *each (*$\sim$*1000 Au clusters per histogram). A threshold of 1.2 Å above the terrace was chosen to ensure that exclusively Au clusters are considered for the histograms. (c) STM image of the Au/*r-TiO_2*(110) surface (*$350 \times 350\,\mathring{A}^2$*) prepared by 3 % ML Au deposition at RT followed by heating up to* $68\,^{\circ}\mathrm{C}$*. (d) Au height histograms corresponding to Au/*r-TiO_2*(110) prior (hatched red bars) and after (blue bars) heating of the sample. In (d), the peaks indicated by "*α*" corresponds to* Au_1 *trapped in bridging oxygen vacancies. The arrow in the inset indicates large* Au_n *clusters that are the result of sintering. (e - f) Like (c) and (d) but for the Au/*o-TiO_2*(110) surface. In (f), the peaks indicated by "a" correspond to* Au_n *clusters of one layer height. No sintering was observed. All STM images were acquired at* $120 - 140$ *K.*

obtained on the Au exposed surfaces prior to heating (the red hatched bars). After heating of the Au/*r*-TiO_2(110) surface (the blue bars in Fig. 9.2(d)), the sharp feature at Au cluster heights of 1.8 to 2.6 Å (labeled "α") is almost three times less intense than before. Because the "α"-peak corresponds to Au_1 trapped in bridging oxygen vacancies (see below), this result indicates that about two-thirds of the Au_1 clusters have coalesced with other Au_n clusters. The sintering of Au_1/Au_n clusters on the *r*-TiO_2(110) surface leads to the formation of large Au_n clusters with STM heights up to 10 Å (Fig. 9.2(d), inset). Nothing in the STM data points to the occurrence of a ripening mechanism. Instead, our data are consistent with coalescence of Au_n clusters as the prevailing sintering mechanism.

On the *o*-TiO_2(110) surface the Au height histograms (Fig. 9.2(f)) show pronounced peaks of identical intensities at STM heights between 1.2 and 3.4 Å (labeled "a") both prior and after heating of the sample. The characteristic a-peak found for the Au/*o*-TiO_2(110) surface is less intense, but broader than the narrow α peak typical for Au_1 on the *r*-TiO_2(110) surface. This result can be explained by the existence of many stable Au_n cluster configurations on the *o*-TiO_2(110) surface, while only few stable Au_n cluster configurations seem to exist on the *r*-TiO_2(110) surface. The clear dependence of the Au height distribution on *r*-TiO_2(110) as opposed to the invariance of the distribution on *o*-TiO_2(110) upon heating to $68\,^{\circ}\mathrm{C}$ reveals that the Au_n clusters bind stronger to the O-rich oxide support.

9.2.3 DFT calculations and comparison with STM measurements

To rationalize the obtained Au cluster distributions after Au exposure at RT, we compared the diffusion of Au_1 on the three different TiO_2(110) surfaces of interest by means of DFT calculations (31). The Au_n adhesion potential energies (APEs) on the various TiO_2(110) supports were calculated according to

$$APE = E_{tot}(Au_n + support) - E_{tot}(Au_n) - E_{tot}(support), \tag{9.1}$$

where $E_{tot}(Au_n + support)$, $E_{tot}(Au_n)$, and $E_{tot}(support)$ are the total energies of the combined systems, the most stable gas phase Au_n 2D clusters, and the TiO_2(110) surface in a certain oxidation state, respectively. Negative APEs indicate stable adhesion of the Au_n clusters. In some distance of the point defects, all three surfaces can be considered as being stoichiometric (*s*-TiO_2(110)). In this case the diffusion barriers are found to be very low, i.e. Au_1 readily diffuses at RT. Diffusion of Au_1 on *s*-TiO_2(110) is possible in the [001] direction, but also in the $[1\bar{1}0]$ direction (Fig. 9.3(a)). Previous DFT calculations likewise indicate facile diffusion of small Au particles on stoichiometric oxide surfaces [102, 143–145].

For the *h*-TiO_2(110) surface we reached identical conclusions, as the diffusion barriers are almost unchanged (Fig. 9.3(b)). However, the Au monomers can be trapped at point defects on the terraces of the *r*- and *o*-TiO_2(110) surfaces (right side of Fig. 9.3(c) and (d), respectively). In these cases the barriers are high enough to prevent diffusion events at RT. These calculations are fully in line with our STM observations of homogeneously distributed small Au nanoclusters exclusively on the *r*- and *o*-TiO_2(110)

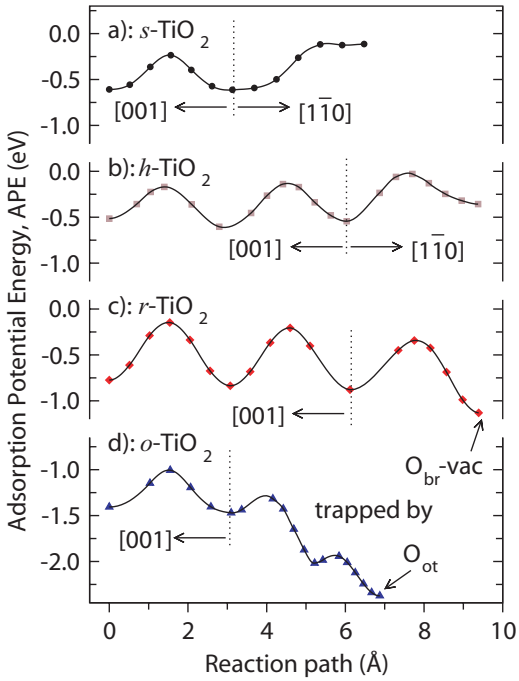

Figure 9.3. *Potential energy profiles for Au_1 diffusion on* s- *(a),* h- *(b),* r- *(c), and* o-*TiO_2(110) (d). The minima at which Au_1 are trapped at the point defects on* r- *and* o-*TiO_2(110) are indicated (arrows; vac means vacancy, O_{ot} means oxygen adatom). On* s- *and* o-*TiO_2(110), Au_1 diffuses along the bridging oxygen rows, whereas, on* h- *and* r-*TiO_2(110), Au_1 diffuses along the Ti troughs.*

surfaces and sintering of Au clusters on the *h*-TiO_2(110) surface after Au exposure at RT (Fig. 9.1).

In Fig. 9.4 we compare the energetically most favorable Au structures found in DFT calculations with the high-resolution STM images of most abundant small Au_n clusters. On *r*-TiO_2(110), the smallest Au related protrusions (Fig. 9.4(d)) arise from Au_1 in bridging oxygen vacancies, as the density of these smallest protrusions increases upon Au exposure at the expense of the density of the faint protrusions arising from bridging oxygen vacancies [100]. The second smallest protrusions found (Fig. 9.4(e) and (f)) originate from linear Au trimers (Au_3). This assignment relies on the following: (i) Au dimers (Au_2) are calculated to adhere less strongly to the support than Au_3 clusters (Fig. 9.6), and (ii) DFT calculations of two Au_3 configurations, either symmetrically (Fig. 9.4(b)) or asymmetrically (Fig. 9.4(c)) attached to the bridging oxygen vacancy, precisely reproduce the two most abundant protrusions in this size range revealed in the STM measurements.

On the *o*-TiO_2(110) surface we observed a different distribution of protrusions of

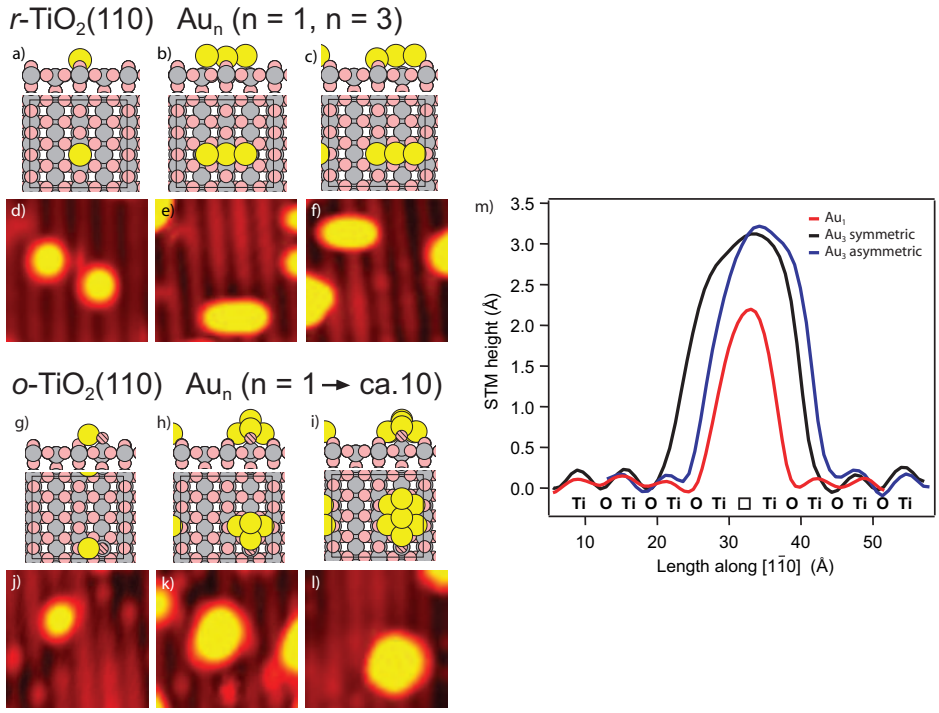

Figure 9.4. *(Top panel) Most favorable structures found in DFT calculations for Au_1 trapped in an bridging oxygen vacancy (a), Au_3 symmetrically attached on an bridging oxygen vacancy (b), and asymmetrically attached Au_3 (c). (d - f) Zoom-in STM images (40×40 Å^2) showing Au_n clusters that are ascribed to the calculated Au_n cluster configurations. Corresponding line profiles to these measurements are shown in (m) (Bottom panel) Most favorable structures found in DFT calculations for Au_1 (g), Au_4 (h), and Au_7 (i) on o-TiO_2(110). (j to l) Zoom-in STM images (40×40 Å^2) of Au_n clusters attached in the vicinity of oxygen adatoms that are tentatively assigned to the calculated Au_n cluster configurations.*

Au_n clusters, as shown in Fig. 9.4(j) to (l), where some of the smallest Au topographies are depicted. As the oxygen adatoms serve as nucleation sites for incoming Au_1 (Fig. 9.3(d)), the oxygen adatoms are probably incorporated into the Au_n clusters. A one-to-one assignment of measured protrusions to certain Au_n-O_{ot} clusters is not trivial, but the distinct height distribution of the Au clusters on the *o*-TiO_2(110) surface allows us to distinguish between Au_n clusters consisting of one, two or even three Au layers (Fig. 9.5).

The DFT results of a more complete survey for stable Au_n clusters with $1 \leq n \leq 5$ and $n = 7$ on the three TiO_2(110) surfaces of interest are summarized in Fig. 9.6. As reference, we also considered *s*-TiO_2(110), although this surface was not studied ex-

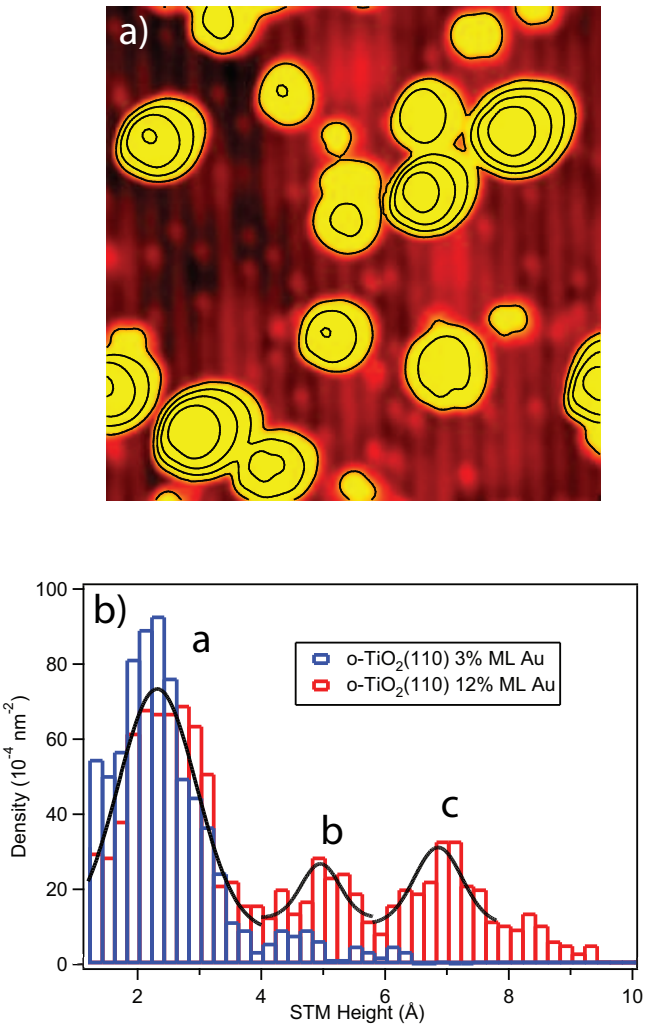

Figure 9.5. *(a) STM image of the* o-TiO_2*(110) after 12 % ML Au exposure at RT* (130×130 $Å^2$*). The STM heights of the Au clusters are given by contour lines at 1.2 Å, 3.2 Å and 5.2 Å above the terrace. (b) Height histograms obtained for 3 % and 12 % ML Au exposure onto* o-TiO_2*(110). The histograms rely on scanned areas of* $\sim 10^4$ nm^2 *each (*$\sim$*1000 Au clusters per histogram). Solid lines are Gaussian fits to the peaks in the histogram corresponding to the 12 % ML Au exposure. The height differences between neighboring peaks a and b and peaks b and c of 2.6 Å and 2.1 Å, respectively, are close to the Au(100) (2.04 Å) and Au(111) (2.35 Å) interlayer spacings. Therefore, we ascribe peaks a, b, and c to Au clusters consisting of one, two and three Au layers, respectively*

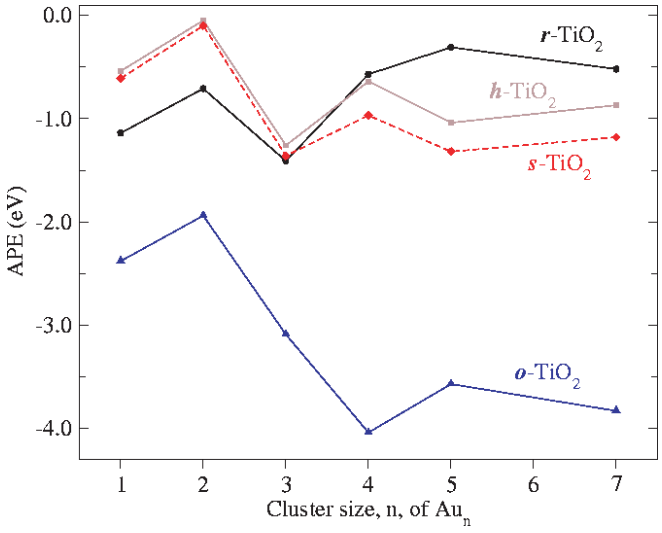

Figure 9.6. *Plots of the DFT-based APEs (per Au_n cluster) of the most stable Au_n clusters with $1 \leq n \leq 5$ and $n = 7$ on* r-, h-, s- *and* o-*TiO_2(110) surfaces, respectively.*

perimentally. The most stable configurations on s-TiO_2(110) are 2D structures that are attached via the bridging oxygen atoms and thus are aligned in the [001] direction. As reported previously, these structures adhere only weakly [50]. On the h-TiO_2(110) surface, we found even smaller APEs for the most stable configurations. In contrast, on the r-TiO_2(110) surface Au_1 and Au_3 bind relatively strongly in bridging oxygen vacancies, while Au_2, Au_4, Au_5 and Au_7 bind very weakly. Importantly, for the o-TiO_2(110) surface we found extraordinarily strong bonding of all Au_n clusters considered.

According to the DFT results addressing r- and o-TiO_2(110), the energy for Au_n cluster detachment from the defects on the r-TiO_2(110) surfaces decreases rapidly with cluster size, but not on the o-TiO_2(110), where the detachment energy remains high. This means that for a given Au dispersion a higher persistence against sintering upon heating is likely to exist on the o-TiO_2(110) surface compared to the situation on the r-TiO_2(110) surface. Thus, the DFT results presented in Fig. 9.6 corroborate the STM findings shown in Fig. 9.2(c) to (f).

9.2.4 Charge transfer and bond mechanisms for Au clusters

To gain insight into why the Au_n clusters bind much stronger on the o-TiO_2(110) surface than on the r-TiO_2(110) surface, we compared electron charge density difference maps for two selected Au_n clusters (Fig. 9.7(a) and (c)). For the r-TiO_2(110) surface, we chose an Au_3 cluster symmetrically attached in an bridging oxygen vacancy, because this cluster we observed with the STM (Fig. 9.4(e)). Analyzing the bonding qualitatively in three dimensions (Fig. 9.7(a)), we found that electron charge accumulates (red iso-

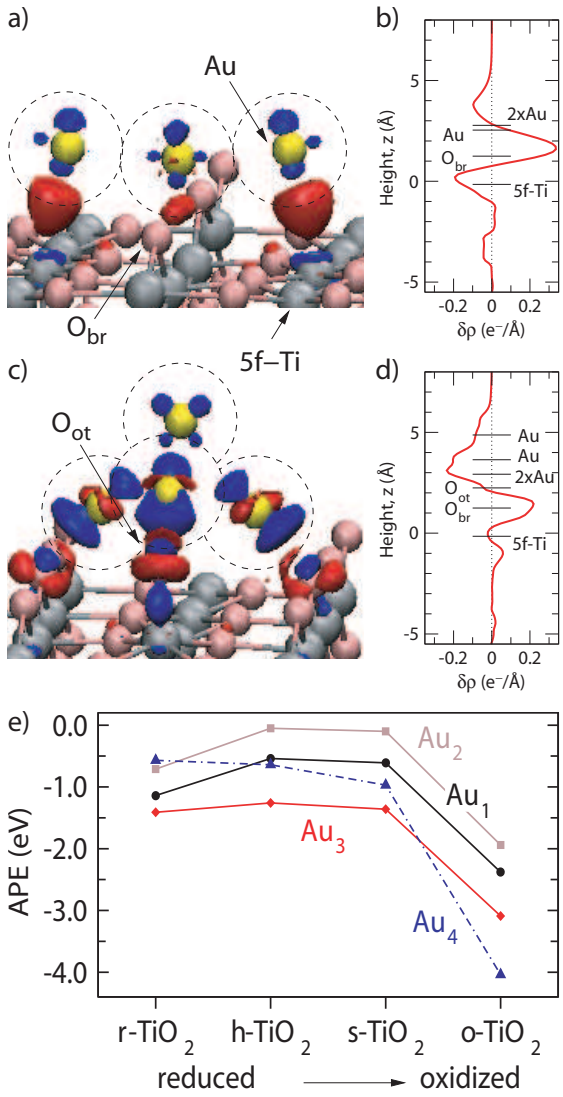

Figure 9.7. *(a) Charge density difference map of an Au_3 cluster attached to an bridging oxygen vacancy. Yellow spheres and dashed circles mark positions of Au atoms. Blue and red isosurfaces indicate depletion and addition, respectively, of 0.05 e^- per $Å^3$. (c) Charge density difference map of Au_4 attached on o-TiO_2(110). Isosurfaces are defined as in (a). (b) and (d) Electron charge density difference ($\delta\rho$) for the same systems as in (a) and (c), respectively, but integrated over the x and y dimensions of the super cell. The z positions of O and Au atoms are given with respect to the 5f-Ti atoms ($z = 0$), whereby the label "2×Au" is used to indicate the z positions of the two Au atoms that have identical z values in the two Au_n clusters considered. (e) Plot of the calculated APEs for the most stable small Au_n clusters ($n = 1$ to 4) as a function of the "TiO_2(110) oxidation state" (compare with Fig. 9.6).*

surfaces) between the Au atoms and the substrate 5f-Ti upon adsorption, indicating the formation of covalent bonds. A more quantitative analysis where we only considered the charge redistribution perpendicular to the support shows that the Au atoms primarily experience charge polarization upon adsorption (Fig. 9.7(b)).

On the *o*-TiO_2(110) surface, we studied the extraordinarily stable Au_4 cluster in the vicinity of an oxygen adatom. In this case charge redistribution is seen along the Au-O bond axes (Fig. 9.7(c)), indicating that the Au-O bonds contribute to the attachment of the Au_4 cluster. The quantitative analysis (Fig. 9.7(d)) reveals that electron charge has indeed been transferred to the surface O atoms, whereby the Au_4 cluster has become cationic. This means that the bonding of Au_4 on the *o*-TiO_2(110) surface is partially ionic.

Contribution of ionic bonding in case of Au_4 on *o*-TiO_2(110) is consistent with the calculated atomic Au 5d-populations upon adsorption of Au_3 and Au_4 on the *r*- and *o*-TiO_2(110) surfaces, respectively. Compared to Au_3 and Au_4 in the gas phase, the total 5d-population is reduced by 0.24 e^- and 0.56 e^- for Au_3/*r*-TiO_2(110) and Au_4/*o*-TiO_2(110), respectively. Changes in the Au 6s and 6p populations also occur and must be in the order of 0.25 e^- accumulation per Au cluster for Au_3/*r*-TiO_2(110) in order to conform with Fig. 9.7(d), where only charge polarization and no net charging is shown. The changes in the Au 6s and 6p populations cannot be quantified because these orbitals overlap substantially with other orbitals originating from neighboring atoms. The larger reduction of the 5d-populations for Au_4/*o*-TiO_2(110) can be traced back mainly to the single Au atom that binds directly to the oxygen adatom, as this Au atom contributes by 0.22 e^- of the 0.56 e^-.

The different bond mechanisms of the considered Au_n clusters (Fig. 9.7(a) to (d)) reflect that the reduced *r*- and *h*-TiO_2(110) surfaces are electron rich (formally having two and one excess electrons per bridging oxygen vacancy and OH_{br} species, respectively), while the oxidized TiO_2(110) surface is electron deficient (formally missing two electrons per oxygen adatom). As a function of the surface oxidation state, the Au_n - TiO_2(110) adhesion is non-monotonic for n = 1, 2 and 3 with the lowest adhesion strengths on the *h*- and *s*-TiO_2(110) surfaces (Fig. 9.7(e)). For these small Au_n clusters the adhesion strength increases on *r*-TiO_2(110), because the covalent bonds between Ti and Au form more readily when not all of the Ti are in their fully oxidized state. However, an adhesion mechanism involving cationic Au occurs when the surface is oxidized (*o*-TiO_2(110)), which leads to a much stronger Au_n-support bonding than on the *r*-TiO_2(110) surface.

9.3 Conclusions and implications for model studies of supported Au clusters

In light of the presented experimental and computational results, we doubt that O vacancies on oxide surfaces are relevant at all for the stabilization of dispersed Au particles under real reaction conditions with usually high oxygen pressures. Instead, our results suggest that even under slightly oxidizing conditions as used here the Au particles are stabilized via Au-O-M bonds (where M represents a metal atom of the supporting ox-

ide). This interpretation is in line with recent reports on cationic Au species for Au supported on magnesia [103], ceria [104, 134] and iron oxide [105].

In all of the model studies addressing Au supported on titania where the catalytic activity of the systems considered was shown, very high oxygen exposures had been used to prepare or to "activate" the catalysts [8, 96, 136, 139]. This observation is an additional reason why we question previously proposed structure models, including our own [50, 100], where it was implied that in oxygen vacancies attached Au clusters cause the catalytic activity in "real" catalysts (i.e., at high pressure). We propose that Au dispersed on reducible oxides are better catalysts than those supported on non-reducible ones, because reducible oxides are more capable of forming of O-rich Au-support interfaces. Note that O-rich surface terminations have been identified not only for titania (chapter 4 and [146]), but also for several other reducible oxides including vanadium and iron oxide [147].

A much stronger Au oxide-support adhesion exists on O-rich Au-support interfaces than on O-poor oxide-support surfaces. For catalytic applications, this result suggests the occurrence of cationic gold at the Au-support interface as a general feature. For the reduced TiO_2(110) surface we found that bridging oxygen vacancies allow for the stabilization of gold monomers and gold trimers, but larger gold clusters cannot be sufficiently stabilized. We emphasize that the presented new approach of studying the oxide support in a range of oxidation states is applicable to numerous other model systems.

CHAPTER 10

Summary and outlook

A number of studies of the TiO_2(110) surface has been presented in this thesis. The main approach in the presented studies has been the use of fast-scanning and high-resolution scanning tunneling microscopy (STM) measurements in conjunction with density functional theory (DFT) calculations. Here we will give a brief summary of the scientific findings in this work.

In chapter 4 we assigned different features observed in STM images to bridging oxygen vacancies, oxygen atoms adsorbed on fivefold Ti atoms, and single as well as pairs of bridging hydroxyl groups. The assignment was performed by means of adsorption and desorption experiments using water and oxygen as probe molecules. DFT calculations compared the interaction of oxygen and water with TiO_2(110) surfaces having oxygen vacancies with the situation when these molecules encounter a stoichiometric TiO_2(110) surface. The DFT calculations strongly supported the assignments of the features observed experimentally with STM.

The findings of chapter 4 were elaborated further in chapter 5 in which we followed the dissociation of water molecules at bridging oxygen vacancies. The product of the water dissociation at an oxygen vacancy is the formation of a paired hydroxyl group. These pairs were found to be stable and immobile unless they interact with adsorbed water molecules. As the result of the interaction with a water molecule a proton is transferred to an adjacent oxygen row, and two single hydroxyls are formed. Additionally, we showed that bridging hydroxyl groups facilitate the diffusion of water molecules over bridging oxygen rows.

By means of high-resolution STM movies we observed the formation of stable water dimers and trimers on the rows of fivefold coordinated Ti atoms as reported in chapter 6. The water dimers were observed to readily interact with bridging hydroxyl groups to

form a species assigned to $H_5O_2^+$ or H_5O_2. Through the interaction with bridging hydroxyl groups the water dimers were found to be able to mediate the diffusion of bridging hydroxyls along both the [001] and the $[1\bar{1}0]$ direction. On quasi-stoichiometric surfaces, i.e. surfaces with no oxygen vacancies and only very few bridging hydroxyls, the water dimers were observed to interact directly with the bare bridging oxygen rows, resulting in the dissociation of one of the two water molecules in the water dimer in good agreement with recent DFT calculations.

In chapter 7 we compared the diffusion of water monomers and water dimers on both hydroxylated and quasi-stoichiometric TiO_2(110) surfaces. The energy barrier for water monomer diffusion was found to be 0.5 eV on the hydroxylated surface, and slightly higher on the quasi-stoichiometric surface. The water dimer was observed to have a low energy barrier for diffusion equal to $\sim$0.2 eV and a low prefactor in the range of 10^5-10^6 on the hydroxylated surface. The very low prefactor suggested influence of tunneling in the diffusion process. However, when comparing the diffusion of D_2O and H_2O dimers, we did not detect a significant isotope effect. On the quasi-stoichiometric surface water dimer diffusion was found to have an energy barrier $>$0.5 eV and a prefactor consistent with pure thermally activated diffusion.

A detailed STM study of the interaction between O_2 and bridging hydroxyls on the TiO_2(110) surface was reported in chapter 8. O_2 was observed to initially react with a bridging hydroxyl to form a stable intermediate assigned to HO_2 adsorbed on the rows of fivefold coordinated Ti atoms. Through the interaction with water dimers adsorbed on the rows of fivefold coordinated Ti atoms, the HO_2 species formed initially was found to evolve into a water dimer in a number of steps involving the extraction of hydrogen atoms from bridging hydroxyl groups. Furthermore, by exposing the hydroxylated TiO_2(110) surface to a metered amount of O_2 at RT, we showed that it is possible to form a quasi-stoichiometric TiO_2(110) surface.

The last study presented in this thesis concerns the bonding of gold nanoclusters on differently prepared TiO_2(110) surfaces: A reduced TiO_2(110) surface having bridging oxygen vacancies, a hydroxylated TiO_2(110) surface having bridging hydroxyl groups, and an oxidized TiO_2(110) surface with oxygen adatoms on the fivefold coordinated Ti atom rows. At RT small gold nanoclusters were observed to nucleate on the terraces of both the reduced and the oxidized supports, whereas on the hydroxylated surface, clusters formed preferentially at the step edges. From DFT calculations two different adhesion mechanisms for the reduced and the oxidized support were identified. The adhesion was found to be strongest on the oxidized support. We proposed that gold nanoclusters supported on oxidized surfaces mimic better the properties of real catalysts than gold nanoclusters on reduced supports.

The work presented in this thesis illustrates nicely the capabilities of the STM technique for studying properties of TiO_2(110) surfaces related to point defects. Besides providing new insight into this fascinating material, the present works also leaves open questions which calls for a continuation of the work. One of the natural directions to pursue is the combination of the characterization of the gold nanoclusters on differently prepared TiO_2(110) surfaces with reactivity measurements. A setup for such a purpose has been developed in our group. It would be very informative to test the activity of the differently prepared samples for CO oxidation, and to evaluate the effect of exposing the

samples to reaction conditions on, for example, the morphology of the gold nanoclusters, because one of the main factors believed to be responsible for the deactivation of such catalysts, is sintering of the gold nanoclusters. It should be mentioned, however, that detecting the production of CO_2 is difficult, because CO_2 is one of the residual gases present under UHV conditions.

The mechanism for the water dimer diffusion is still not fully solved. At the time of the measurements it was not possible to extend the temperature range in which the water dimers could be followed reliably. However, a new set of electronics have recently been developed for the control of our STM. With this set of electronics it is possible to acquire STM images with atomic resolution at rates up to 50 frames per second, thus enabling us to expand the range of temperatures, at which diffusion can be followed. In this way we might be able to detect a change to purely thermally activated diffusion at higher temperatures.

By far, the most actively pursued applied research on TiO_2 is its use for photo-assisted degradation of organic molecules. A very interesting extension of our studies on TiO_2(110) surfaces, would therefore be to investigate the influence of UV-light on the behavior of different adsorbates on TiO_2 surfaces. As a first step we have equipped our UHV chamber with a UV-lamp, which enables us to expose our samples to UV-light in-situ, and do post-exposure measurements. A second step will be to modify the STM itself, making it possible to expose the sample to UV-light while scanning. In this way valuable information on reactive sites during irradiation can be gained. Another direction in which to expand our presented studies is to investigate other surfaces of rutile TiO_2, or to investigate the surfaces of anatase TiO_2. The latter is especially interesting from a photo-catalysis point of view, since the nanoparticles used for photocatalysis consist mainly of anatase TiO_2.

CHAPTER 11

Dansk resumé

Dette afsnit er et kort dansk resumé henvendt til ikke-specialister, dvs. personer som ikke til daglig arbejder med videnskabelige undersøgelser af forskellige materialers overflader. Afsnittet vil først give en kort motivation for de undersøgelser, der er beskrevet i denne afhandling og derefter vil nogle af de mest interessante resultater blive forsøgt forklaret på en måde som forhåbentlig vil være forståelig for de fleste. Skulle dette mod hensigten ikke være tilfældet skyldes det selvfølgelig udelukkende forfatterens manglende pædagogiske evner.

Mange ikke ædle metaller kan reagere med ilten i luften og danne såkaldte metaloxider, f.eks. jernoxid (rust), aluminiumoxid og titandioxid. Sådanne metaloxider har mange interessante egenskaber og bruges i mange forskellige anvendelser. Denne afhandling omhandler kun et metaloxid – titandioxid (TiO_2) – og mere specifikt overfladen af titandioxid. Jeg vil derfor i det følgende udelukkende koncentrere mig om anvendelserne af TiO_2, samt forsøge at understrege hvorfor det er specielt interessant at undersøge overfladen af dette materiale.

En af de egenskaber, der gør TiO_2 interessant at studere ud fra et videnskabeligt synspunkt, er dets evne til at optage energi fra sollyset og bruge denne energi til f.eks. at nedbryde organiske molekyler, som skidt og snavs, der sidder på overfladen af titandioxiden. Dette kaldes fotokatalytisk nedbrydning af organiske molekyler, da titandioxiden hjælper eller katalyserer lysets nedbrydning af molekylerne. Denne egenskab har man bl.a. udnyttet til at lave selvrensende overflader. Et eksempel på denne anvendelse kan ses i Fig. 11.1, hvor man kan se forskellen på to dele af en ydermur, hvor den øverste del er coatet med TiO_2 og den nederste del bare er malet med almindelig maling.

Selve nedbrydningen af de organiske molekyler sker som nævnt på overfladen. Derfor vil vi meget gerne følge enkelte molekyler på overfladen og se hvordan de bliver

Figure 11.1. *Billede af en ydermur på en bygning i Tokyos centrum. Den øverste del er dækket af en selvrensende TiO_2 coating, mens den nederste halvdel bare er malet med almindelig maling.*

påvirket af overfladen og hinanden, og ultimativt også hvordan sollyset påvirker molekylerne på overfladen for på bedst mulig måde at kunne udnytte titandioxidens egenskaber.

Bilkatalysatoren omdanner bl.a. kulmonoxid (CO), der bliver dannet under motorens forbrænding af brændstoffet, til den langt mindre skadelige kuldioxid (CO_2). Denne reaktion sker dog først når katalysatoren er varmet op til flere hundrede grader. Så de første 5-10 min. bilen kører bliver CO'en ledt lige ud i den luft vi indånder. I alt stammer cirka 50 % af den samlede mængde CO der kommer fra bilernes udstødning fra koldstarterne, altså de første 5-10 minutters kørsel inden katalysatoren bliver varm. Derfor har en opdagelse gjort af en japansk gruppe ledet af Masatake Haruta skabt stor opmærksomhed. De opdagede, at guldøer i nanostørrelse, som sidder på overfladen af TiO_2, er gode katalysatorer for at omdanne CO til CO_2. Og det helt ekstraordinære fantatiske i denne sammenhæng er, at guldnanoøerne på TiO_2 kan få reaktionen til at ske allerede ved temperaturer lavere end stuetemperatur. Så potentielt kan guldnanoøerne være med til at forbedre nutidens katalysatorer.

Et af de store spørgsmål er hvorfor guld i nanostørrelse på TiO_2 er en god katalysator, for guld kendes normalt som et ædelt og inert metal som ikke reagerer med noget. Endvidere er man meget interesseret i at vide præcis hvor på overfladen af katalysatoren reaktionen sker. Om det hele sker på de små guldøer eller om det sker i et samspil mellem TiO_2-overfladen og guldøerne.

Et af problemerne med at bruge guldnanoøer på TiO_2 som katalysator er, at de små guldøer har en tendens til at smelte sammen når katalysatoren bruges og dermed bliver varm. De store guldøer duer ikke til at omdanne CO til CO_2, så når dette sker "dør" katalysatoren. Det er derfor vigtigt at undersøge hvordan man bedst muligt kan forankre

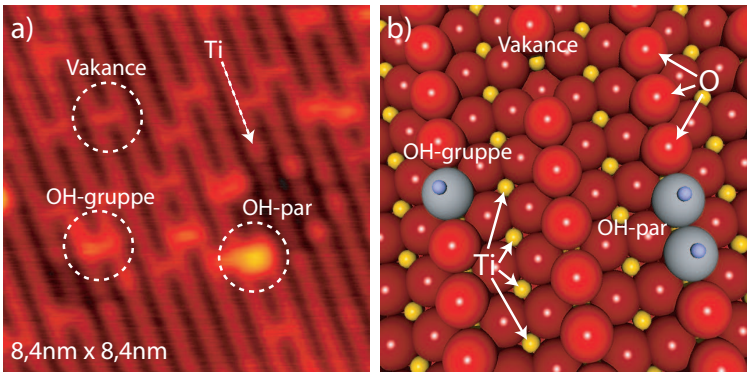

Figure 11.2. *STM-billede (a) og boldemodel (b) af TiO_2-overflade. De lyse rækker på STM-billedet er rækkerne med titanatomer (Ti), mens rækkerne med iltatomer (O) fremstår mørke i STM-billedet. Overfladen er ikke perfekt og enkelte iltatomer mangler. Et sådant manglende iltatom kaldes en vakance. Vakancer viser sig som lysende pletter på de mørke rækker i STM-billedet. Hvis et vandmolekyle (H_2O) "fylder" en sådan vakance dannes et OH-par. Sådanne OH-par kan skilles og danne to enkelte OH-grupper. OH-gruppernes iltatomer i boldemodellen er grå-blå, for at markere, at de er anderledes end de iltatomer (røde), hvorpå der ikke sidder et brintatom.*

guldøerne til titandioxiden.

Alle de eksperimentelle undersøgelser der er præsenteret i denne afhandling er lavet med et såkaldt skanning tunnelmikroskop (STM). Populært fortalt kan et sådant mikroskop føle de enkelte atomer på en overflade og ud fra dette laver en computer billeder af overfladen. Desværre fortæller mikroskopet os ikke, hvad det er for atomer det føler. Når vi kigger eller skanner på en TiO_2 overflade kan vi derfor ikke umiddelbart se hvilke atomer der er ilt og hvilke der er titan. For nogle år siden fandt en forskningsgruppe dog ud af, at de lyse rækker man ser i STM-billeder af en TiO_2-overflade er titanatomer og de mørke rækker er iltatomer (se Fig. 11.2). Men det har været meget vanskeligt at identificere de forskellige lysende pletter man kan se på de mørke ilt-rækker. Vi har fundet ud af, at hvis man er meget påpasselig med at gøre TiO_2-overfladen ren, så kan man få en overflade, som kun har de mindst lyse af de tre typer pletter, der er vist i Fig. 11.2(a), altså vakancerne. Det skal i denne forbindelse nævnes, at for at kunne studere TiO_2-overfladen, så er vi nødt til arbejde under såkaldt ultrahøjt vakuum. Det betyder, at vi har TiO_2-prøven i en beholder, som vi har pumpet al luften ud af, da der ellers lynhurtigt vil sætte sig så meget ilt, vand og hvad der ellers er i luften, på prøvens overflade, at vi ikke kan se selve TiO_2-overfladen. Det viser sig dog, at det er uhyre vanskeligt at komme af med al den vanddamp som naturligt findes i luften medmindre man er meget opmærksom på problemet. Vandmolekylerne omdanner så efterhånden vakancerne til de to andre typer lyse pletter som kan ses i Fig. 11.2(a). Den største og lyseste af de to pletter er et hydroxyl-par (OH-par). Det dannes, når et vandmolekyle (H_2O) fylder vakancen, ved, at iltatomet i vandmolekylet udfylder pladsen for det manglende iltatom.

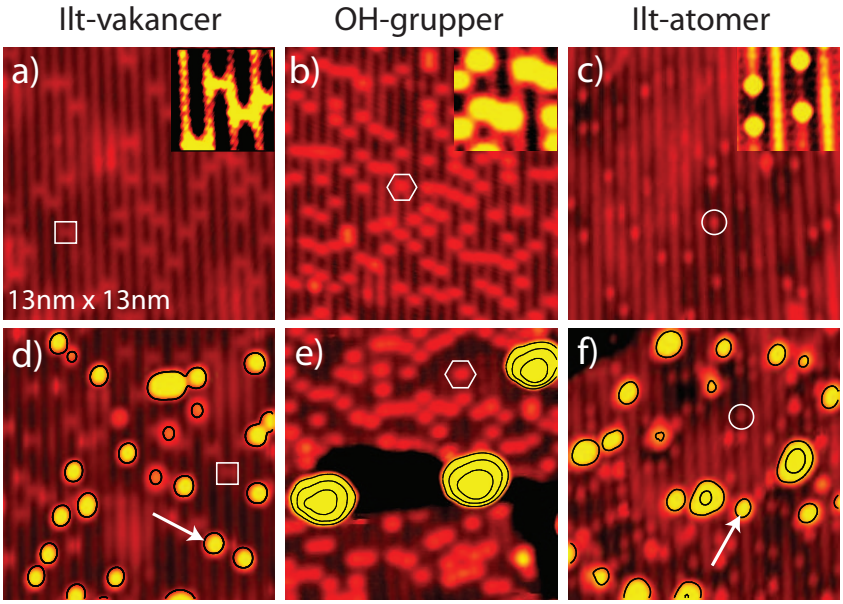

Figure 11.3. *STM-billeder af tre forskellige TiO_2-overflader med og uden guldnanoøer. Alle billederne er 13 nm × 13 nm. (a) Ren TiO_2-overflade med vakancer. (b) TiO_2-overflade med enkelt OH-grupper og (c) TiO_2-overflade med iltatomer på titanrækkerne. (d-f) Samme overflader efter fordampning af guld. Der er den samme mængde guld på alle tre overflader. En hvid pil markerer et enkelt iltatom bundet henholdsvis i en vakance (d) og til et iltatom (f).*

Når det sker vil det ene brintatom (H) fra vandmolekylet hoppe over på et af de to iltatomer, der sidder lige ved siden af vakancen. Et sådant OH-par kan så senere deles ved at et vandmolekyle flytter et brintatom fra en række af iltatomer til rækken af iltatomer overfor. Hvis man varmer på prøven kan man også få brintatomerne og dermed OH-grupperne til at hoppe langs iltrækkerne.

Det kan måske lyde lidt banalt og ikke så relevant sådan at identificere, hvad forskellige lysende pletter er på et STM-billede. Men for at man kan studere mere avancerede systemer, som f.eks. det næste studie jeg vil præsentere, så er det helt essentielt, at vi kan identificere, hvad der er på TiO_2-overfladen.

I dette studie undersøgte vi, hvordan guldnanoøer dannes på tre forskellige TiO_2-overflader. De tre overflader kan ses i Fig. 11.3(a-c). Den første er den rene TiO_2-overflade, hvor der kun er ilt-vakancer på overfladen. Overflade nummer to har vi dannet ved at udsætte den rene overflade for en lille smule vand. På den måde får vi fyldt vakancerne med vandmolekyler og får dannet enkelt OH-grupper på overfladen (OH-grupperne i et par frastøder hinanden en lille smule, så efter et stykke tid har man kun enkelt OH-grupper). Den tredje overflade (Fig. 11.3(c)) er ikke blevet omtalt før. Den har vi dannet ved at lukke iltmolekyler (O_2) ind på TiO_2-overfladen med ilt-vakancerne.

Så fylder det ene af de to iltatomer i iltmolekylet ilt-vakancen, mens det overskydende iltatom sætter sig på et titanatom ved siden af vakancen. Så man får det samme antal ekstra iltatomer på overfladen, som man havde ilt-vakancer inden man lukkede iltmolekyler ind på overfladen.

Efter at have fordampet lidt guldatomer på overfladerne ser vi små guldøer på TiO_2-overfladen med ilt-vakancer og på overfladen med de ekstra iltatomer, mens vi på overfladen med OH-grupper kun ser få store guldøer (Fig. 11.3(d-f) – der er den samme mængde guld på alle overfladerne). På overfladen med vakancer kan vi se, at vakancerne kan binde enkelte guldatomer (hvid pil i Fig. 11.3(d)), ligesom iltatomerne også binder guldet til sig (Fig. 11.3(e)). Derimod virker det ikke som om OH-grupperne kan binde guldatomerne, hvorfor disse løber sammen til få store øer.

For at finde ud af om vakancerne eller iltatomerne var de bedste forankringspunkter for guldet varmede vi de to overflader op. På overfladen med vakancer løb guldatomerne meget hurtigt sammen til store øer, mens guldet på overfladen med iltatomer ikke løb sammen når overfladen blev varmet. Vi kunne derfor konkludere at iltatomerne er de bedste forankringspunkter for guldet.

Håbet er, at sådanne fundamentale undersøgelser kan være med til at udvikle fremtidige katalysatorer som kan udnytte de fantastiske egenskaber guldøer i nanostørrelse på TiO_2 har, uden at katalysatoren "dør" efter kort tids brug.

Acknowledgements

The work presented in this thesis is the result of a collaboration with a number of co-workers. At this point it is therefore a great pleasure to acknowledge all the persons that have contributed to the presented work and with whom I have interacted.

First of all I would like to thank my supervisor Flemming Besenbacher for his enthusiastic support and guidance. His never ending pursuit for new scientific areas to explore is what have made this thesis possible. The postdocs with whom I have worked on this project have also worked as guides for me on this PhD journey. Stefan Wendt is greatly acknowledged for scrutiny of scientific details which played the major part in unravelling the basics of the $TiO_2(110)$ surface. His willingness to always help out in the lab as well as with issues concerning scientific writing is also greatly appreciated. Renald Schaub presented the details of the experimental setup to me and have made STM movie analysis easy with his professional programming skills. His enthusiasm for science and life as such has been highly appreciated both inside and outside the university walls. Stefan Wendt and Renald Schaub are also greatly acknowledged for suggestions and comments during the making of this thesis. I have also very much enjoyed working with Daniel Matthey and Erik Wahlström. A special thanks goes to Erik Lægsgaard who created the magnificent Aarhus STM, and whose invaluable help keeps them running. His endless efforts to improve the capabilities of the STM are greatly appreciated.

Concerning theoretical investigations I have enjoyed many long discussions with Bjørk Hammer and learned a lot from his input. Also theoreticians Jianguo Wang and Maria Dall Rasmussen are acknowledged for their contributions.

The many PhD students of the scanning probe microscopy group at iNANO have contributed greatly to make everyday life at the institute a pleasant experience. I would especially like to thank Jan Knudsen, Jakob Kibsgaard, Jonas Ørbæk Hansen and Richard Lindsay Merte for good and helpful company in the lab. Former PhD students Ebbe Kruse Vestergaard and Ronnie Vang are remembered for introducing me to scanning tunneling microscopy. Help from Esben R. Andresen regarding our optical setup has been much appreciated. A special thanks also goes to Martin Lorentzen, Georg Olesen, Sigrid Weigelt and Mads Hovgaard, with whom I have had many scientific as well non-scientific discussions. Annette Riisberg and Jeanette Dandanell are thanked for proof-reading manuscripts.

Bibliography

[1] V. E. Henrich and P. A. Cox, *The surface science of metal oxides* (Cambridge University Press, Cambridge, 1996).

[2] B. Kasemo, "Biological Surface Science", *Surf. Sci.* **500**, 656 (2002).

[3] B. O'Regan and M. Grätzel, "A low-cost, high efficiency solar cell based on dye-sensitized colloidal TiO_2 films", *Nature* **353**, 737 (1991).

[4] M. K. Nazeeruddin, A. Kay, I. Rodicio, R. Humpbry-Baker, E. Müller, P. Liska, N. Vlachopoulos, and M. Grätzel, "Conversion of Light to Electricity by cis-X_2Bis(2,2'-bipyridyl-4,4'-dicarboxylate)ruthenium(II) Charge-Transfer Sensitizers (X = Cl^-, Br^-, I^-, CN^-, and SCN^-) on Nanocrystalline TiO_2 Electrodes", *J. Am. Chem. Soc.* **115**, 6382 (1993).

[5] M. Haruta, S. Tsubota, T. Kobayashi, H. Kageyama, M. J. Genet, and B. Delmon, "Low-Temperature Oxidation of CO over Gold Supported on TiO_2, α-Fe_2O_3 and Co_3O_4", *J. Catal.* **144**, 175 (1993).

[6] C. J. H. Jacobsen, I. Schmidt, A. Boisen, and K. Johannsen, *Katalytisk kemi - et spørgsmål om miljø og ressourcer* (Haldor Topsøe A/S, Lyngby, Denmark, 2002).

[7] B. Hammer and J. K. Nørskov, "Why gold is the noblest of all the metals", *Nature* **376**, 238 (1995).

[8] M. Valden, X. Lai, and D. W. Goodman, "Onset of Catalytic Activity of gold Clusters on Titania with the Appearance of Nonmetallic Properties", *Science* **281**, 1647 (1998).

[9] A. Fujishima and K. Honda, "Electrochemical Photolysis of Water at a Semiconductor Electrode", *Nature* **238**, 37 (1972).

[10] U. Diebold, "The surface science of titanium dioxide", *Surf. Sci. Rep.* **48**, 53 (2003).

[11] http://www.pilkingtonselfcleaningglass.co.uk/.

[12] R. Wang, K. Hashimoto, A. Fujishima, M. Chikuni, E. Kojima, A. Kitamura, M. Shimohigoshi, and T. Watanabe, "Light-induced amphiphilic surfaces", *Nature* **388**, 431 (1997).

[13] G. Binnig, H. Rohrer, C. Gerber, and E. Weibel, "Surface Studies by Scanning Tunneling Microscopy", *Phys. Rev. Lett.* **49**, 57 (1982).

[14] "The official website of The Nobel Foundation",, http://nobelprize.org/physics/laureates/1986/index.html.

[15] J. Tersoff and D. R. Hamann, "Theory and Application for the Scanning Tunneling Microscope", *Phys. Rev. Lett.* **50**, 1998 (1983).

[16] J. Bardeen, "Tunneling from a Many-Particle Point of View", *Phys. Rev. Lett.* **6**, 57 (1961).

[17] E. Lægsgaard, F. Besenbacher, K. Mortensen, and I. Stensgaard, "A fully automated, 'thimble-size' scanning tunnelling microscope", *J. Microscop.* **152**, 663 (1988).

[18] U. Diebold, J. Lehman, T. Mahmoud, M. Kuhn, G. Leonardelli, W. Hebenstreit, M. Schmid, and P. Varga, "Intrinsic defects on a $TiO_2(110)(1\times1)$ surface and their reaction with oxygen: a scanning tunneling microscopy study", *Surf. Sci.* **411**, 137 (1998).

[19] P. Hohenberg and W. Kohn, "Inhomogeneous Electron Gas", *Phys. Rev.* **136**, B864 (1964).

[20] W. Kohn and L. J. Sham, "Self-Consistent Equations Including Exchange and Correlation Effects", *Phys. Rev.* **140**, A1133 (1965).

[21] B. Hammer, L. B. Hansen, and J. K. Nørskov, "Improved adsorption energetics within density-functional theory using revised Perdew-Burke-Ernzerhof functionals", *Phys. Rev. B* **59**, 7413 (1999).

[22] L. A. Harris and A. A. Quong, "Molecular Chemisorption as the Theoretically Preferred Pathway for Water Adsorption on Ideal Rutile TiO_2(110)", *Phys. Rev. Lett.* **93**, 086105 (2004).

[23] http://ruby.colorado.edu/ smyth/min/tio2.html.

[24] S. Munnix and M. Schmeits, "Electronic structure of ideal TiO_2(110), TiO_2(001), and TiO_2(100) surfaces", *Phys. Rev. B* **30**, 2207 (1984).

[25] U. Diebold, M. Li, O. Dulub, E. L. D. Hebenstreit, and W. Hebenstreit, "The relationship between bulk and surface properties of rutile TiO_2(110)", *Surf. Rev. Lett.* **7**, 613 (2000).

[26] D. C. Cronemeyer, "Electrical and Optical Properties of Rutile Single Crystals", *Phys. Rev.* **87**, 876 (1952).

[27] D. C. Cronemeyer, "Infrared Absorption of Reduced Rutile TiO_2 Single Crystals", *Phys. Rev.* **113**, 1222 (1959).

[28] R. R. Hasiguti and E. Yagi, "Electrical conductivity below 3 K of slightly reduced oxygen-deficient rutile TiO_{2-x}", *Phys. Rev. B* **49**, 7251 (1994).

[29] E. Yagi, R. R. Hasiguti, and M. Aono, "Electronic conduction above 4 K of slightly reduced oxygen-deficient rutile TiO_{2-x}", *Phys. Rev. B* **54**, 7945 (1996).

[30] M. A. Henderson, "Mechanism for the bulk-assisted reoxidation of ion sputtered TiO_2 surfaces: diffusion of oxygen to the surface or titanium to the bulk?", *Surf. Sci.* **343**, L1156 (1995).

[31] M. A. Henderson, "A surface perspective on self-diffusion in rutile TiO_2", *Surf. Sci.* **419**, 174 (1999).

[32] H. B. Huntington and G. A. Sullivan, "Interstitial Diffusion Mechanism in Rutile", *Phys. Rev. Lett.* **14**, 177 (1965).

[33] H. Iddir, S. Ogut, P. Zapol, and N. D. Browning, "Diffusion mechanisms of native point defects in rutile TiO_2: Ab initio total-energy calculations", *Phys. Rev. B* **75**, 073203 (2007).

[34] M. Ramamoorthy, D. Vanderbilt, and R. D. King-Smith, "First-principles calculations of the energetics of stoichiometric TiO_2 surfaces", *Phys. Rev. B* **49**, 16721 (1994).

[35] A. Linsebigler, G. Lu, and J. T. J. Yates, "Photocatalysis on TiO_2 Surfaces: Principles, Mechanisms, and Selected Results", *Chem. Rev.* **95**, 735 (1995).

[36] M. A. Barteau, "Organic Reactions at Well-Defined Oxide Surfaces", *Chem. Rev.* **96**, 1413 (1996).

[37] J.-M. Pan, B. L. Maschhoff, U. Diebold, and T. E. Madey, "Interaction of water, oxygen, and hydrogen with TiO_2(110) surfaces having different defect densities", *J. Vac. Sci. Technol. A* **10**, 2470 (1992).

[38] M. B. Hugenschmidt, L. Gamble, and C. T. Campbell, "The interaction of H_2O with a TiO_2(110) surface", *Surf. Sci.* **302**, 329 (1994).

[39] W. Göpel, J. Anderson, D. Frankel, M. Jaehnig, K. Phillips, J. Schafer, and G. Rocker, "Surface-Defects Of TiO_2(110) - A Combined XPS, XAES And ELS Study", *Surf. Sci.* **139**, 333 (1984).

[40] L.-Q. Wang, D. R. Baer, M. H. Engelhard, and A. N. Shultz, "The adsorption of liquid and vapor water on TiO_2(110) surfaces: The role of defects", *Surf. Sci.* **344**, 237 (1995).

[41] V. E. Henrich, G. Dresselhaus, and H. J. Zeiger, "Observation Of 2-Dimensional Phases Associated With Defect States On Surface Of TiO_2", *Phys. Rev. Lett.* **36**, 1335 (1976).

[42] R. L. Kurtz, R. Stockbauer, T. E. Madey, E. Román, and J. L. de Segovia, "Synchrotron radiation studies of H_2O adsorption on TiO_2(110)", *Surf. Sci.* **218**, 178 (1989).

[43] G. Rocker, J. A. Schaefer, and W. Göpel, "Localized and delocalized vibrations on TiO_2(110) studied by high-resolution electron-energy-loss spectroscopy", *Phys. Rev. B* **30**, 3704 (1984).

[44] W. S. Epling, C. H. F. Peden, M. A. Henderson, and U. Diebold, "Evidence for oxygen adatoms on TiO_2(110) resulting from O_2 dissociation at vacancy sites", *Surf. Sci.* **412/413**, 333 (1998).

[45] M. A. Henderson, W. S. Epling, C. L. Perkins, and C. H. F. Peden, "Interaction of Molecular Oxygen with the Vacuum-Annealed TiO_2(110) Surface: Molecular and Dissociative Channels", *J. Phys. Chem. B* **103**, 5328 (1999).

[46] M. A. Henderson, W. S. Epling, C. H. F. Peden, and C. L. Perkins, "Insights into Photoexcited Electron Scavenging Processes on TiO_2 Obtained from Studies of the Reaction of O_2 with OH Groups Adsorbed at Electronic Defects on TiO_2(110)", *J. Phys. Chem. B* **107**, 534 (2003).

[47] H. Onishi and Y. Iwasawa, "Dynamic Visualization of a Metal-Oxide-Surface/Gas-Phase Reaction: Time-Resolved Observation by Scanning Tunneling Microscopy at 800 K", *Phys. Rev. Lett.* **76**, 791 (1996).

[48] M. Li, W. Hebenstreit, and U. Diebold, "Oxygen-induced restructuring of the rutile TiO_2(110)(1x1) surface", *Surf. Sci.* **414**, L951 (1998).

[49] M. Li, W. Hebenstreit, L. Gross, U. Diebold, M. A. Henderson, D. R. Jennison, P. A. Schultz, and M. P. Sears, "Oxygen-induced restructuring of the TiO_2(110) surface: a comprehensive study", *Surf. Sci.* **437**, 173 (1999).

[50] L. M. Molina, M. D. Rasmussen, and B. Hammer, "Adsorption of O_2 and oxidation of CO at Au nanoparticles supported by TiO_2(110)", *The Journal of Chemical Physics* **120**, 7673 (2004).

[51] L. M. Molina, M. D. Rasmussen, and B. Hammer, "Erratum: "Adsorption of O_2 and oxidation of CO at Au nanoparticles supported by TiO_2(110)" [J. Chem. Phys. **120**, 7673 (2004)]", *The Journal of Chemical Physics* **123**, 029903 (2005).

[52] R. Schaub, P. Thostrup, N. Lopez, E. Lægsgaard, I. Stensgaard, J. K. Nørskov, and F. Besenbacher, "Oxygen vacancies as active sites for water dissociation on rutile TiO_2(110)", *Phys. Rev. Lett.* **87**, 266104 (2001).

[53] M. Ramamoorthy, R. D. King-Smith, and D. Vanderbilt, "Defects on TiO_2(110) surfaces", *Phys. Rev. B* **49**, 7709 (1994).

[54] A. T. Paxton and L. Thiên-Nga, "Electronic structure of reduced titanium dioxide", *Phys. Rev. B* **57**, 1579 (1998).

[55] M. D. Rasmussen, L. M. Molina, and B. Hammer, "Adsorption, diffusion, and dissociation of molecular oxygen at defected TiO_2(110): A density functional theory study", *J. Chem. Phys.* **120**, 988 (2004).

[56] X. Wu, A. Selloni, and S. K. Nayak, "First principles study of CO oxidation on TiO_2(110): The role of surface oxygen vacancies", *The Journal of Chemical Physics* **120**, 4512 (2004).

[57] C. D. Valentin, G. Pacchioni, and A. Selloni, "Electronic Structure of Defect States in Hydroxylated and Reduced Rutile TiO_2(110) Surfaces", *Phys. Rev. Lett.* **97**, 166803 (2006).

[58] J. G. Wang and B. Hammer, "Role of Au^+ in Supporting and Activating Au_7 on TiO_2(110)", *Phys. Rev. Lett.* **97**, 136107 (2006).

[59] U. Diebold, J. F. Anderson, K.-O. Ng, and D. Vanderbilt, "Evidence for the Tunneling Site on Transition-Metal Oxides: TiO_2(110)", *Phys. Rev. Lett.* **77**, 1322 (1996).

[60] S. Suzuki, K. Fukui, H. Onishi, and Y. Iwasawa, "Hydrogen Adatoms on TiO_2(110)-(1×1) Characterized by Scanning Tunneling Microscopy and Electron Stimulated Desorption", *Phys. Rev. Lett.* **84**, 2156 (2000).

[61] J. V. Lauritsen, A. S. Foster, G. H. Olesen, M. C. Christensen, A. Kühnle, S. Helveg, J. R. Rostrup-Nielsen, B. S. Clausen, M. Reichling, and F. Besenbacher, "Chemical identification of point defects and adsorbates on a metal oxide surface by atomic force microscopy", *Nanotech.* **17**, 3436 (2006).

[62] M. A. Henderson, "The interaction of water with solid surfaces: fundamental aspects revisited", *Surf. Sci. Rep.* **46**, 1 (2002).

[63] M. A. Henderson, "An HREELS and TPD study of water on TiO_2(110): The extent of molecular versus dissociative adsorption", *Surf. Sci.* **355**, 151 (1996).

[64] M. A. Henderson, "Structural Sensitivity in the Dissociation of Water on TiO_2 Single-Crystal Surfaces", *Langmuir* **12**, 5093 (1996).

[65] D. Brinkley, M. Dietrich, T. Engel, P. Farrall, G. Gantner, A. Schafer, and A. Szuchmacher, "A modulated molecular beam study of the extent of H_2O dissociation on $TiO_2(110)$", *Surf. Sci.* **395**, 292 (1998).

[66] I. M. Brookes, C. A. Muryn, and G. Thornton, "Imaging Water Dissociation on $TiO_2(110)$", *Phys. Rev. Lett.* **87**, 266103 (2001).

[67] A. Fahmi and C. Minot, "A theoretical investigation of water adsorption on titanium dioxide surfaces", *Surf. Sci.* **304**, 343 (1994).

[68] J. Goniakowski and M. J. Gillan, "The adsorption of H_2O on TiO_2 and $SnO_2(110)$ studied by first-principles calculations", *Surf. Sci.* **350**, 145 (1996).

[69] T. Bredow and K. Jug, "Theoretical investigation of water adsorption at rutile and anatase surfaces", *Surf. Sci.* **327**, 398 (1995).

[70] S. P. Bates, G. Kresse, and M. J. Gillan, "The adsorption and dissociation of ROH molecules on $TiO_2(110)$", *Surf. Sci.* **409**, 336 (1998).

[71] P. J. D. Lindan, N. M. Harrison, J. M. Holender, and M. J. Gillan, "First-principles molecular dynamics simulation of water dissociation on $TiO_2(110)$", *Chem. Phys. Lett.* **261**, 246 (1996).

[72] P. J. D. Lindan, N. M. Harrison, and M. J. Gillan, "Mixed Dissociative and Molecular Adsorption of Water on the Rutile (110) Surface", *Phys. Rev. Lett.* **80**, 762 (1998).

[73] C. Zhang and P. J. D. Lindan, "Multilayer water adsorption on rutile $TiO_2(110)$: A first-principles study", *J. Chem. Phys.* **118**, 4620 (2003).

[74] C. Zhang and P. J. D. Lindan, "A density functional theory study of the coadsorption of water and oxygen on $TiO_2(110)$", *J. Chem. Phys.* **121**, 3811 (2004).

[75] P. J. D. Lindan and C. Zhang, "Exothermic water dissociation on the rutile $TiO_2(110)$ surface", *Phys. Rev. B* **72**, 075439 (2005).

[76] E. V. Stefanovich and T. N. Truong, "Ab initio study of water adsorption on $TiO_2(110)$: molecular adsorption versus dissociative chemisorption", *Chem. Phys. Lett.* **299**, 623 (1999).

[77] P. J. D. Lindan and C. Zhang, "Comment on "Molecular Chemisorption as the Theoretically Preferred Pathway for Water Adsorption on Ideal Rutile $TiO_2(110)$"", *Phys. Rev. Lett.* **95**, 029601 (2005).

[78] L. A. Harris and A. A. Quong, "Harris and Quong Reply", *Phys. Rev. Lett.* **95**, 029602 (2005).

[79] P. J. D. Lindan, J. Muscat, S. Bates, N. M. Harrison, and M. Gillan, "Ab initio simulation of molecular processes on oxide surfaces", *Faraday Discuss.* 135 (1997).

[80] O. Bikondoa, C. L. Pang, R. Ithnin, C. A. Muryn, H. Onishi, and G. Thornton, "Direct visualization of defect-mediated dissociation of water on $TiO_2(110)$", *Nature Mater.* **5**, 189 (2006).

[81] Z. Zhang, O. Bondarchuk, B. D. Kay, J. M. White, and Z. Dohnalek, "Imaging Water Dissociation on $TiO_2(110)$: Evidence for Inequivalent Geminate OH Groups", *J. Phys. Chem. B* **110**, 21840 (2006).

[82] R. Bryl, T. Wysocki, and R. Blaszczyszyn, "Field-induced redistribution and diffusion of water on a Pt field emitter", *Appl. Surf. Sci.* **87-88**, 69 (1995).

[83] R. Bryl, "Diffusion of H_2O on surfaces of clean and Au covered tungsten field emitters", *Vacuum* **48**, 333 (1997).

[84] R. Bryl and R. Blaszczyszyn, "Surface diffusion of water on clean and Au-covered tungsten field emitter tips", *Vacuum* **54**, 103 (1999).

[85] E. Fomin, M. Tatarkhanov, T. Mitsui, M. Rose, D. F. Ogletree, and M. Salmeron, "Vibrationally assisted diffusion of H_2O and D_2O on Pd(111)", *Surf. Sci.* **600**, 542 (2006).

[86] T. Mitsui, M. K. Rose, E. Fomin, D. F. Ogletree, and M. Salmeron, "Water Diffusion and Clustering on Pd(111)", *Science* **297**, 1850 (2002).

[87] V. A. Ranea, A. Michaelides, R. Ramírez, P. L. d. Andres, J. A. Vergés, and D. A. King, "Water Dimer Diffusion on Pd(111) Assisted by an H-Bond Donor-Acceptor Tunneling Exchange", *Phys. Rev. Lett.* **92**, 136104 (2004).

[88] A. Michaelides, "Density functional theory simulations of water-metal interfaces: waltzing waters, a novel 2D ice phase, and more", *Applied Physics A: Materials Science & Processing* **85**, 415 (2006).

[89] M. Akbulut, N. J. Sack, and T. E. Madey, "Adsorption and reaction of water on oxidized tungsten: thermal desorption and electron stimulated desorption measurements", *Surf. Sci.* **351**, 209 (1996).

[90] M. Haruta, N. Yamada, T. Kobayashi, and S. Iljima, "Gold Catalysts Prepared by Coprecipitation for Low-Temperature Oxidation of Hydrogen and of Carbon Monoxide", *J. Catal.* **115**, 301 (1989).

[91] G. C. Bond and D. T. Thompson, "Gold-catalysed oxidation of carbon monoxide", *Gold Bull.* **33**, 41 (2000).

[92] F. Cosandey and T. E. Madey, "Growth, morphology, interfacial effects and catalytic properties of Au on TiO_2", *Surf. Rev. Lett.* **8**, 73 (2001).

[93] M. Haruta, "Catalysis of Gold Nanoparticles Deposited on Metal Oxides", *CATTECH* **6**, 102 (2002).

[94] R. Meyer, C. Lemire, S. K. Shaikhutdinov, and H. Freund, "Surface chemistry of catalysis by gold", *Gold Bull.* **37**, 72 (2004).

[95] G. R. Bamwenda, S. Tsubota, T. Nakamura, and M. Haruta, "The influence of the preparation methods on the catalytic activity of platinum and gold supported on TiO_2 for CO oxidation", *Catal. Lett.* **44**, 83 (1997).

[96] S. Lee, C. Fan, T. Wu, and S. L. Anderson, "CO Oxidation on Au_n/TiO_2 Catalysts Produced by Size-Selected Cluster Deposition", *J. Am. Chem. Soc.* **126**, 5682 (2004).

[97] M. Okumura, S. Nakamura, S. Tsubota, T. Nakamura, M. Azuma, and M. Haruta, "Chemical vapor deposition of gold on Al_2O_3, SiO_2, and TiO_2 for the oxidation of CO and of H_2", *Catal. Lett.* **51**, 53 (1998).

[98] J.-D. Grunwaldt, C. Kiener, C. Wogerbauer, and A. Baiker, "Preparation of Supported Gold Catalysts for Low-Temperature CO Oxidation via "Size-Controlled" Gold Colloids", *J. Catal.* **181**, 223 (1999).

[99] M. M. Schubert, S. Hackenberg, A. C. van Veen, M. Muhler, V. Plzak, and R. J. Behm, "CO Oxidation over Supported Gold Catalysts–"Inert" and "Active" Support Materials and Their Role for the Oxygen Supply during Reaction", *J. Catal.* **197**, 113 (2001).

[100] E.Wahlström, N. Lopez, R. Schaub, P. Thostrup, A. Rønnau, C. Africh, E. Lægsgaard, J. K. Nørskov, and F. Besenbacher, "Bonding of Gold Nanoclusters to Oxygen Vacancies on Rutile TiO_2(110)", *Phys. Rev. Lett.* **90**, 026101 (2003).

[101] I. N. Remediakis, N. Lopez, and J. K. Nørskov, "CO Oxidation on Rutile-Supported Au Nanoparticles", *Angew. Chem. Int. Ed.* **44**, 1824 (2005).

[102] A. S. Wörz, U. Heiz, F. Cinquini, and G. Pacchioni, "Charging of Au Atoms on TiO_2 Thin Films from CO Vibrational Spectroscopy and DFT Calculations", *J. Phys. Chem. B* **109**, 18418 (2005).

[103] J. Guzman and B. C. Gates, "Catalysis by Supported Gold: Correlation between Catalytic Activity for CO Oxidation and Oxidation States of Gold", *J. Am. Chem. Soc.* **126**, 2672 (2004).

[104] J. Guzman, S. Carrettin, and A. Corma, "Spectroscopic Evidence for the Supply of Reactive Oxygen during CO Oxidation Catalyzed by Gold Supported on Nanocrystalline CeO_2", *J. Am. Chem. Soc.* **127**, 3286 (2005).

[105] G. J. Hutchings, M. S. Hall, A. F. Carley, P. Landon, B. E. Solsona, C. J. Kiely, A. Herzing, M. Makkee, J. A. Moulijn, A. Overweg, J. C. Fierro-Gonzalez, J. Guzman, and B. C. Gates, "Role of gold cations in the oxidation of carbon monoxide catalyzed by iron oxide-supported gold", *J. Catal.* **242**, 71 (2006).

[106] J. V. Lauritsen, R. T. Vang, and F. Besenbacher, "From atom-resolved scanning tunneling microscopy (STM) studies to the design of new catalysts", *Catal. Today* **111**, 34 (2006).

[107] G. Lu, A. Linsebigler, and J. T. Yates, "Ti^{3+} Defect Sites on TiO_2(110): Production and Chemical Detection of Active Sites", *J. Phys. Chem.* **98**, 11733 (1994).

[108] C. Xu, X. Lai, G. W. Zajac, and D. W. Goodman, "Scanning tunneling microscopy studies of the TiO_2(110) surface: Structure and the nucleation growth of Pd", *Phys. Rev. B* **56**, 13464 (1997).

[109] R. E. Tanner, M. R. Castell, and G. A. D. Briggs, "High resolution scanning tunnelling microscopy of the rutile TiO_2(110) surface", *Surf. Sci.* **412-413**, 672 (1998).

[110] R. Schaub, E. Wahlström, A. Rønnau, E. Lægsgaard, I. Stensgaard, and F. Besenbacher, "Oxygen-Mediated Diffusion of Oxygen Vacancies on the TiO_2(110) Surface", *Science* **299**, 377 (2003).

[111] S. Mezhenny, P. Maksymovych, T. L. Thompson, O. Diwald, D. Stahl, S. D. Walck, and J. T. Y. Jr., "STM studies of defect production on the TiO_2(110)-(1x1) and TiO_2(110)-(1x2) surfaces induced by UV irradiation", *Chem. Phys. Lett.* **369**, 152 (2003).

[112] M. A. Henderson, J. M. White, H. Uetsuka, and H. Onishi, "Photochemical Charge Transfer and Trapping at the Interface between an Organic Adlayer and an Oxide Semiconductor", *J. Am. Chem. Soc.* **125**, 14974 (2003).

[113] F. Besenbacher, "Scanning tunnelling microscopy studies of metal surfaces", *Rep. Prog. Phys.* **59**, 1737 (1996).

[114] M. L. Knotek, "Characterization of hydrogen species on TiO_2 by electron-stimulated desorption", *Surf. Sci.* **91**, L17 (1980).

[115] Y. D. Kim, A. P. Seitsonen, S. Wendt, J. Wang, C. Fan, K. Jacobi, H. Over, and G. Ertl, "Characterization of Various Oxygen Species on an Oxide Surface: RuO_2(110)", *J. Phys. Chem. B* **105**, 3752 (2001).

[116] H. Over, M. Knapp, E. Lundgren, A. P. Seitsonen, M. Schmid, and P. Varga, "Visualization of Atomic Processes on Ruthenium Dioxide using Scanning Tunneling Microscopy", *ChemPhysChem* **5**, 167 (2004).

[117] P. A. Thiel and T. E. Madey, "The interaction of water with solid surfaces: Fundamental aspects", *Surf. Sci. Rep.* **7**, 211 (1987).

[118] G. E. Brown, V. E. Henrich, W. H. Casey, D. L. Clark, C. Eggleston, A. Felmy, D. W. Goodman, M. Gratzel, G. Maciel, M. I. McCarthy, K. H. Nealson, D. A. Sverjensky, M. F. Toney, and J. M. Zachara, "Metal Oxide Surfaces and Their Interactions with Aqueous Solutions and Microbial Organisms", *Chem. Rev.* **99**, 77 (1999).

[119] S. S. Xantheas and T. H. Dunning, "Ab-Initio Studies Of Cyclic Water Clusters $(H_2O)_N$, N = 1-6.1. Optimal Structures And Vibrational-Spectra", *J. Chem. Phys.* **99**, 8774 (1993).

[120] T. R. Dyke, K. M. Mack, and J. S. Muenter, "The structure of water dimer from molecular beam electric resonance spectroscopy", *The Journal of Chemical Physics* **66**, 498 (1977).

[121] R. S. Fellers, C. Leforestier, L. B. Braly, M. G. Brown, and R. J. Saykally, "Spectroscopic Determination of the Water Pair Potential", *Science* **284**, 945 (1999).

[122] P. P. Olivera, A. Ferral, and E. M. Patrito, "Theoretical Investigation of Hydrated Hydronium Ions on Ag(111)", *J. Phys. Chem. B* **105**, 7227 (2001).

[123] J. V. Barth, "Transport of adsorbates at metal surfaces: from thermal migration to hot precursors", *Surf. Sci. Rep.* **40**, 75 (2000).

[124] G. Ehrlich, "Atomic Displacement in One- and Two-Dimensional Diffusion", *J. Chem. Phys.* **44**, 1050 (1966).

[125] S. C. Wang, J. D. Wrigley, and G. Ehrlich, "Atomic jump lengths in surface diffusion: Re, Mo, Ir, and Rh on W(211)", *The Journal of Chemical Physics* **91**, 5087 (1989).

[126] T. R. Linderoth, S. Horch, E. Lægsgaard, I. Stensgaard, and F. Besenbacher, "Surface Diffusion of Pt on Pt(110): Arrhenius Behavior of Long Jumps", *Phys. Rev. Lett.* **78**, 4978 (1997).

[127] E. Wahlström, E. K. Vestergaard, R. Schaub, A. Rønnau, M. Vestergaard, E. Lægsgaard, I. Stensgaard, and F. Besenbacher, "Electron Transfer-Induced Dynamics of Oxygen Molecules on the TiO_2(110) Surface", *Science* **303**, 511 (2004).

[128] R. S. Fellers, L. B. Braly, R. J. Saykally, and C. Leforestier, "Fully coupled six-dimensional calculations of the water dimer vibration-rotation-tunneling states with split Wigner pseudospectral approach. II. Improvements and tests of additional potentials", *J. Chem. Phys.* **110**, 6306 (1999).

[129] A. Tilocca, C. DiValentin, and A. Selloni, "O_2 Interaction and Reactivity on a Model Hydroxylated Rutile(110) Surface", *J. Phys. Chem. B* **109**, 20963 (2005).

[130] L. M. Liu, B. McAllister, H. Q. Ye, and P. Hu, "Identifying an O_2 Supply Pathway in CO Oxidation on Au/TiO_2(110): A Density Functional Theory Study on the Intrinsic Role of Water", *J. Am. Chem. Soc.* **128**, 4017 (2006).

[131] C. L. Perkins and M. A. Henderson, "Photodesorption and Trapping of Molecular Oxygen at the TiO_2(110)-Water Ice Interface", *J. Phys. Chem. B* **105**, 3856 (2001).

[132] Personal communication with Dr. Bjørk Hammer.

[133] S. H. Overbury, L. Ortiz-Soto, H. Zhu, B. Lee, M. Amiridis, and S. Dai, "Comparison of Au Catalysts Supported on Mesoporous Titania and Silica: Investigation of Au Particle Size Effects and Metal-Support Interactions", *Catal. Lett.* **95**, 99 (2004).

[134] Q. Fu, H. Saltsburg, and M. Flytzani-Stephanopoulos, "Active Nonmetallic Au and Pt Species on Ceria-Based Water-Gas Shift Catalysts", *Science* **301**, 935 (2003).

[135] L. Fu, N. Q. Wu, J. H. Yang, F. Qu, D. L. Johnson, M. C. Kung, H. H. Kung, and V. P. Dravid, "Direct Evidence of Oxidized Gold on Supported Gold Catalysts", *J. Phys. Chem. B* **109**, 3704 (2005).

[136] M. S. Chen and D. W. Goodman, "The Structure of Catalytically Active Gold on Titania", *Science* **306**, 252 (2004).

[137] F. Boccuzzi and A. Chiorino, "FTIR Study of CO Oxidation on Au/TiO_2 at 90 K and Room Temperature. An Insight into the Nature of the Reaction Centers", *J. Phys. Chem. B* **104**, 5414 (2000).

[138] B. Schumacher, V. Plzak, M. Kinne, and R. J. Behm, "Highly active Au/TiO_2 catalysts for low-temperature CO oxidation: preparation, conditioning and stability", *Catal. Lett.* **89**, 109 (2003).

[139] T. S. Kim, J. D. Stiehl, C. T. Reeves, R. J. Meyer, and C. B. Mullins, "Cryogenic CO Oxidation on TiO_2-Supported Gold Nanoclusters Precovered with Atomic Oxygen", *J. Am. Chem. Soc.* **125**, 2018 (2003).

[140] K. T. Park, M. H. Pan, V. Meunier, and E. W. Plummer, "Surface Reconstructions of TiO_2(110) Driven by Suboxides", *Phys. Rev. Lett.* **96**, 226105 (2006).

[141] X. Tong, L. Benz, P. Kemper, H. Metiu, M. T. Bowers, and S. K. Buratto, "Intact Size-Selected Au_n Clusters on a TiO_2(110)-(1 x 1) Surface at Room Temperature", *J. Am. Chem. Soc.* **127**, 13516 (2005).

[142] C. T. Campbell, S. C. Parker, and D. E. Starr, "The Effect of Size-Dependent Nanoparticle Energetics on Catalyst Sintering", *Science* **298**, 811 (2002).

[143] A. D. Vitto, G. Pacchioni, F. Delbecq, and P. Sautet, "Au Atoms and Dimers on the MgO(100) Surface: A DFT Study of Nucleation at Defects", *J. Phys. Chem. B* **109**, 8040 (2005).

[144] H. Iddir, S. Ogut, N. D. Browning, and M. M. Disko, "Adsorption and diffusion of Pt and Au on the stoichiometric and reduced TiO_2 rutile (110) surfaces", *Phys. Rev. B* **72**, 081407 (2005).

[145] H. Iddir, S. Ogut, N. D. Browning, and M. M. Disko, "Erratum: Adsorption and diffusion of Pt and Au on the stoichiometric and reduced TiO_2 rutile (110) surfaces [Phys. Rev. B **72**, 081407(R) (2005)]", *Phys. Rev. B* **73**, 039902 (2006).

[146] T. J. Beck, A. Klust, M. Batzill, U. Diebold, C. D. Valentin, and A. Selloni, "Surface Structure of TiO_2(011) - (2 x 1)", *Phys. Rev. Lett.* **93**, 036104 (2004).

[147] M. A. Haija, S. Guimond, Y. Romanyshyn, A. Uhl, H. Kuhlenbeck, T. K. Todorova, M. V. Ganduglia-Pirovano, J. Dobler, J. Sauer, and H. J. Freund, "Low temperature adsorption of oxygen on reduced V_2O_3(0001) surfaces", *Surf. Sci.* **600**, 1497 (2006).